THEORETICAL STUDIES OF QUANTUM SPIN SYSTEMS.

David Coombes

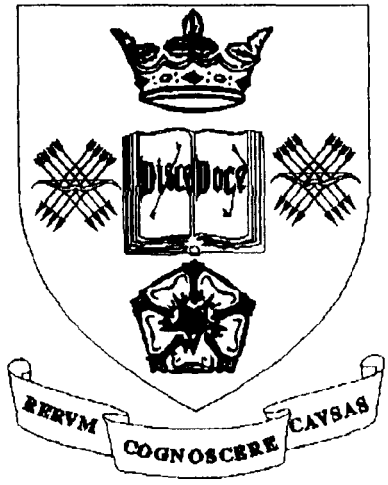

Department of Physics

University of Sheffield

June 1998

Theoretical Studies of Quantum Spin Systems.

David Coombes

A thesis submitted for the degree of Doctor of Philosophy

University of Sheffield, June 1998.

Summary

In this thesis we present the results of calculations of the properties of quantum spin systems. The majority of the work is concerned with one dimensional spin chains and the particular effects that reduced dimensionality produce. The final chapter describes some earlier work on mixed valence manganite compounds.

We demonstrate one derivation of the Heisenberg Hamiltonian and discuss its applicability to modelling magnetic systems both in three and one dimension. We discuss systems that are exactly soluble and the failure of spin wave theory in 1-D. The Density-Matrix Renormalisation Group (DMRG) method is discussed in detail as is the extension to finite temperature (TMRG).

We show results of calculations on a number of S=1/2 and S=1 models and fundamental differences in their excitation spectra is observed. The thermodynamics of these systems have been obtained over a wide temperature range. In addition, excellent agreement with experiment is shown for a number of quasi one dimensional compounds. The DMRG and TMRG are shown to be very competitive and accurate methods of studying such systems, especially in the case of gapped systems.

The final chapter discusses the role of correlated magnetic clusters in determining the magnetic properties of mixed valence manganites at temperatures near the Curie temperature. Our results are supported by recent direct experimental observation of the formation of these clusters. We also briefly discuss some preliminary results regarding the effect of an interface on the electronic and magnetic properties of these compounds.

Acknowledgements

There are many people who have helped me during my time in Sheffield both scientifically and socially. It is a pleasure and a privilege to be able to extend my thanks to them all.

Firstly, my supervisor Professor Gillian Gehring, for all the knowledge she has shared with me over last three (or nearer four, sorry Gillian) years and her patience in explaining things to me, usually more than once. Thanks to Dr Tao Xiang at the IRC in Superconductivity at Cambridge, a truly inspirational physicist, and to Dr Robert Bursill for showing me the wonders of the DMRG and Miss Backpacker '97 in Cairns. Thanks also to Mr Paul Kerry for workstation support.

Thanks to Dr William Barford and Professor David Edwards for agreeing to be the examiners of this thesis.

To all the people who've shared an office with me during my PhD: Glenn, Steve, Daz, Janet, Fatma, Magnus, Hossein. An extra big thanks to 'Little' Leon Petit, Rik 'Trickster' Tyer and Cully for the patience and help during the writing of this thesis when I may just possibly have been a little difficult to 'live' with.

To Luke and John, my housemates, for good humour in the face of adversity (don't mention Banner Cross) and for the inspiration to finish my thesis because if they can do it anyone can!

To Dan, Amanda, Claire and Simon for making me welcome in my new home.

To George and all the staff at the Mad Greek Restaurant for keeping me sane (and well fed).

Everyone at Sheffield University Karate Club, especially again Ricky T for inspiring we when I have no spirit. As the man from Manc says, 'Let's Go!'.

To Alun, Mike and Claire in Liverpool, for always being there and not minding that I don't phone for months on end.

A massive thank you to Melanie, whose love and patience during the writing of this thesis has meant more to me than I can ever say. See you in Las Vegas! Thanks also to the 'inlaws': Margaret, Andy, Dennis and Jane.

My love, as always, to Mum, Jane and Helen whose love and support throughout twenty years of education has been a constant inspiration and comfort.

Finally, to my Dad who sadly died shortly before the completion of this thesis, who was always so encouraging of everything we did and proud of what we achieved. This is for you.

Publications

"Calculation of the Susceptibility of the S = 1 Antiferromagnetic Heisenberg Chain with Single-ion Anisotropy Using the Transfer Matrix Renormalization Group Method" D Coombes, T Xiang and G A Gehring. J. Phys.: Condensed Matter **10** (1998) L159-L165.

"Towards Control of the Switching Field: Manganite Permalloy Heterostructures" M R J Gibbs, M Ziese, G A Gehring, H J Blythe, D J Coombes, S P Sena and C Shearwood. Phil. Trans. R. Soc. Lond. A (1998) **356**, 1681-1692.

"The Theory of Small Polarons in Manganite" G A Gehring and D J Coombes. Journal of Magnetism and Magnetic Materials. **177-181** (1998) 873-874.

"Perturbation Produced on Manganites by a Metallic Interface" D J Coombes and G A Gehring. Journal of Magnetism and Magnetic Materials. **177-181** (1998) 862-863.

"Thermodynamics of the Dimerised S = 1/2 Heisenberg Chain" D Coombes, T Xiang and G A Gehring. *To be submitted to J. Phys.: Condensed Matter.*

Table of Contents

1. THE HEISENBERG INTERACTION 1

1.1 Origin of the Heisenberg Model. 1

1.2 Spin waves in a ferromagnet. 6

1.3 Spin waves in an antiferromagnet 9

1.4 Calculations using spin wave theory. 11

1.5 One Dimensional Magnetic Systems 13

1.6 The Bethe Ansatz 14

1.7 The Lieb-Shultz-Mattis Theorem 15

1.8 Exact Diagonalisation and Quantum Monte Carlo Methods 16

1.9 Modified Spin Wave Theory and Green's Function Techniques 17

1.10 References 18

2. DENSITY MATRIX RENORMALISATION GROUP METHODS. 19

2.1 Real Space Renormalisation Group. 19

2.2 Density Matrix Renormalisation Group . 22

2.3 The Transfer Matrix 29
2.3.1 Transfer matrix in 1D. 30
2.3.2 Transfer matrix in 2D. 32

2.4 Applying the DMRG to Classical Transfer Matrices. 34

2.5 Trotter-Suzuki-decomposition 36

2.6 Transfer Matrix Renormalisation Group (TMRG). 39

2.7 References 43

Figures 44

3. S=1/2 HEISENBERG HAMILTONIANS. 48

3.1 Introduction. 48

3.2 Dimerised X-Y model 49

3.3 Alternating Chain Heisenberg Model. 56
3.3.1 AF/AF Heisenberg Chain. 57
3.3.2 Comparison with experiment. 60
3.3.3 F/AF Heisenberg Chain 61

3.4 References 63

Figures 64

4. S=1 HEISENBERG HAMILTONIANS 81

4.1 Introduction 81

4.2 Valence Bond Solid 82

4.3 Isotropic Chain. 84

4.4 Single Ion Anisotropy 86

4.5 Biquadratic Exchange 93

4.6 References 95

Figures 96

5. ELECTRONIC AND MAGNETIC PROPERTIES OF MIXED VALENCE MANGANITES. 112

5.1 Double Exchange Ferromagnetism 113

5.2 Correlated Regions and Polaron Formation. 114

5.3 Perturbation produced on manganites by a metallic interface 118
5.3.1 Haydock Recursion Scheme 119

5.4 References 121

Figures 122

APPENDIX 1 - MATRIX METHODS 126

The Lanczos Algorithm 127

Modified Lanczos Algorithm 127

Conjugate Gradient Method 128

Asymmetric Matrices 129

Arnoldi Algorithm 130

References 130

APPENDIX 2: FITTING PROCEDURES 131

References 133

APPENDIX 3: IMPLEMENTATION OF SPIN SYMMETRIES 134

1. The Heisenberg Interaction

1.1 Origin of the Heisenberg Model.

Much of the work in this thesis is devoted to studying properties of one dimensional Heisenberg models. This model, introduced in 1928 [1], is widely used to model the interaction of magnetic moments in magnetic insulators and has been extensively studied over the last 60 years. As such it is interesting to see how the Heisenberg interaction arises naturally from the treatment of the Schrodinger equation for an electron in a solid [2,3,4].

Consider the Hamiltonian

$$H = \sum_i \left[\frac{p_i^2}{2m} + V(\underline{\mathbf{r}}_i) \right] + \sum_{i \neq j} \frac{e^2}{|\underline{\mathbf{r}}_i - \underline{\mathbf{r}}_j|} = \sum_i h(\mathbf{r}_i) + \sum_{i \neq j} v(\mathbf{r}_i - \mathbf{r}_j) \tag{1.1}$$

where $V(\underline{\mathbf{r}}_i)$ represents the electron ion interaction and the third term is the electron-electron Coulomb interaction.

It is convenient to work with the second quantised form of the Hamiltonian and we choose a basis consisting of Bloch functions which are eigenstates of h the one electron part of H. We also make the approximation of only considering a single band (i.e. an s-band model). Although most magnetic phenomena are due to interactions between d-band electrons, the five fold degeneracy makes an analytic treatment prohibitive. It will be seen that the one band model contains many of the features for a many body treatment of magnetism that would be produced by a more exact treatment. It should also be noted that this approximation is the same starting point used by Hubbard in deriving what is now known as the Hubbard Hamiltonian [5].

We can now write the Hamiltonian as

$$H = \sum_{\underline{k}\sigma} \varepsilon_{\underline{k}} a^{+}_{\underline{k}\sigma} a_{\underline{k}\sigma} + \sum_{\mathbf{k}_1\mathbf{k}_2\mathbf{k}_1'\mathbf{k}_2'} \sum_{\sigma\sigma'} \langle \mathbf{k}_1 \mathbf{k}_2 | \frac{1}{r} | \mathbf{k}_1' \mathbf{k}_2' \rangle a^{+}_{\mathbf{k}_1\sigma} a^{+}_{\mathbf{k}_2\sigma'} a_{\mathbf{k}_2'\sigma'} a_{\mathbf{k}_1'\sigma_1} \tag{1.2}$$

where $\varepsilon_{\mathbf{k}}$ are the one electron eigenvalues of the one electron part of the Hamiltonian given by $\langle \psi_{\mathbf{k}} | h | \psi_{\mathbf{k}} \rangle$.

We can cast the Hamiltonian into a site representation by introducing Wannier functions, defined as the inverse Fourier transform of the Bloch functions

$$W(\mathbf{r} - \mathbf{R}_i) = \frac{1}{\sqrt{N}} \sum_{\mathbf{k}} \psi_{\mathbf{k}}(\mathbf{r}) e^{-i\mathbf{k}\cdot\mathbf{R}_i} \tag{1.3}$$

and the creation and annihilation operators for the Wannier functions are defined by

$$a^{+}_{i\sigma} = \frac{1}{\sqrt{N}} \sum_{\mathbf{k}} a^{+}_{\mathbf{k}\sigma} e^{-i\mathbf{k}\cdot\mathbf{R}_i} \tag{1.4}$$

and

$$a_{i\sigma} = \frac{1}{\sqrt{N}} \sum_{\mathbf{k}} a_{\mathbf{k}\sigma} e^{i\mathbf{k}\cdot\mathbf{R}_i} \tag{1.5}$$

In systems for which the band width is small, the Wannier functions are localized on the ionic sites which will emphasize the site nature of the Heisenberg model.

In terms of these functions, H is given by

$$H = \sum_{ij} \sum_{\sigma} \varepsilon_{ij} a^{+}_{i\sigma} a_{j\sigma} + \frac{1}{2} \sum_{ijkl} \sum_{\sigma\sigma'} \langle ij | \frac{1}{r} | kl \rangle a^{+}_{i\sigma} a^{+}_{j\sigma'} a_{l\sigma'} a_{k\sigma} \tag{1.6}$$

where

$$\varepsilon_{ij} = \int w^{*}(\mathbf{r} - \mathbf{R}_i) h(\mathbf{r}) w(\mathbf{r} - \mathbf{R}_j) d\mathbf{r} \tag{1.7}$$

and

$$\langle ij | \frac{1}{r} | kl \rangle = e^2 \int \frac{w^{*}(\mathbf{r} - \mathbf{R}_i) w^{*}(\mathbf{r}' - \mathbf{R}_j) w(\mathbf{r} - \mathbf{R}_k) w(\mathbf{r}' - \mathbf{R}_l)}{|\mathbf{r}' - \mathbf{r}|} d\mathbf{r} d\mathbf{r}' \tag{1.8}$$

Expanding the last term of the Hamiltonian into the various one and two centre terms gives

$$H = \sum_{ij}\sum_{\sigma} \varepsilon_{ij} a_{i\sigma}^{+} a_{j\sigma} + U \sum_{i}\sum_{\sigma} n_{i\sigma} n_{i-\sigma} + \frac{1}{2}\sum_{i\neq j}\sum_{\sigma\sigma'} \langle ij|\frac{1}{r}|ij\rangle n_{i\sigma} n_{j\sigma'} \qquad (1.9)$$
$$-\frac{1}{2}\sum_{i\neq j}\sum_{\sigma\sigma'} J_{ij} a_{i\sigma}^{+} a_{i\sigma'} a_{j\sigma'}^{+} a_{j\sigma} + \sum_{i\neq j}\sum_{\sigma\sigma'} \langle ii|\frac{1}{r}|jj\rangle a_{i\sigma}^{+} a_{i\sigma'}^{+} a_{j\sigma'} a_{j\sigma}$$

where $n_{i\sigma}$ is the number operator for electrons on the ith site with spin σ,

$$U = \frac{1}{2} e^2 \int \frac{|w(\mathbf{r})|^2 |w(\mathbf{r}')|^2}{|\mathbf{r}-\mathbf{r}'|} d\mathbf{r} d\mathbf{r}' \qquad (1.10)$$

$$J_{ij} = e^2 \int \frac{w^*(\mathbf{r}-\mathbf{R}_i) w(\mathbf{r}'-\mathbf{R}_j) w^*(\mathbf{r}-\mathbf{R}_j) w(\mathbf{r}'-\mathbf{R}_i)}{|\mathbf{r}'-\mathbf{r}|} d\mathbf{r} d\mathbf{r}' \qquad (1.11)$$

the first two terms of the Hamiltonian constitute the Hubbard model, which assumes that the one centre integral , U ,corresponding to the Coulomb repulsion between two electrons of opposite spin on the same site, dominates the electron-electron interaction. If the summations are performed in the third term it turns out to be spin independent and hence doesn't contribute to magnetic effects. J_{ij} is the direct electron exchange term and the last term is a pair hopping term which we won't consider.

We will now consider the case of a magnetic insulator at half filling. In the limit $U \to \infty$, the Coulomb repulsion prohibits double occupancy on the same site and hence the system has one electron localized on each site. We can therefore completely describe states of the system by specifying the spin configuration of each electron $|\sigma_1 \cdots \sigma_N\rangle$.

Now consider matrix elements of the Hamiltonian between these states. The first three terms only contribute to diagonal elements and so it is the exchange term which

governs the magnetic states of the system in the $U \to \infty$ limit. We represent the spin state of each site by a two component vector

$$\uparrow \equiv \begin{pmatrix} 1 \\ 0 \end{pmatrix} \qquad \downarrow \equiv \begin{pmatrix} 0 \\ 1 \end{pmatrix} \tag{1.12}$$

and in this basis we can represent the fermion operators as 2×2 matrices.

$$a_{\uparrow}^{+}a_{\uparrow} = \begin{pmatrix} 1 & 0 \\ 0 & 0 \end{pmatrix} \qquad a_{\downarrow}^{+}a_{\downarrow} = \begin{pmatrix} 0 & 0 \\ 0 & 1 \end{pmatrix} \tag{1.13}$$

$$a_{\uparrow}^{+}a_{\downarrow} = \begin{pmatrix} 0 & 1 \\ 0 & 0 \end{pmatrix} \qquad a_{\downarrow}^{+}a_{\uparrow} = \begin{pmatrix} 0 & 0 \\ 1 & 0 \end{pmatrix}$$

We can represent these in terms of Pauli matrices defined by

$$\sigma_x = \begin{pmatrix} 0 & 1 \\ 1 & 0 \end{pmatrix} \quad \sigma_y = \begin{pmatrix} 0 & -i \\ i & 0 \end{pmatrix} \quad \sigma_z = \begin{pmatrix} 1 & 0 \\ 0 & 1 \end{pmatrix} \tag{1.14}$$

By expanding out the exchange term we see that

$$\sum_{\sigma\sigma'} a_{i\sigma}^{+}a_{i\sigma'}a_{j\sigma'}^{+}a_{j\sigma} = \frac{1}{2}\left(\mathbf{s}_i \cdot \mathbf{s}_j + 1\right) \tag{1.15}$$

where we have defined the spin operator which has components $\sigma_x . \sigma_y$ and σ_z. Therefore we can write the Hamiltonian for the spin configuration of the system in the limit of single occupancy as

$$H = -\frac{1}{4}\sum_{i \neq j} J_{ij}\mathbf{s}_i \cdot \mathbf{s}_j \tag{1.16}$$

which is the Heisenberg Hamiltonian.

It is interesting to note that the exchange integral of equation (1.11) is positive and hence favours ferromagnetism. This can be understood as a consequence of the antisymmetrisation of the wave function. The exclusion principle will on average keep electrons of the same spin further apart and hence their Coulomb interaction energy is lower. However, as many magnetic insulators actually exhibit antiferromagnetic

ordering it is interesting to see how by perturbing away from the $U \to \infty$ we can show that an antiferromagnetic Heisenberg interaction can be induced. First we will make the approximation that there is only significant overlap of Wannier orbitals when they are centred on nearest neighbour sites. We now consider the first term in the Hamiltonian of equation (1.9) and separate it into diagonal and off diagonal terms.

$$\sum_{ij}\sum_{\sigma}\varepsilon_{ij}a_{i\sigma}^{+}a_{j\sigma} = \sum_{i}\sum_{\sigma}\varepsilon_{0}n_{i\sigma} + \sum_{\langle ij\rangle}\sum_{\sigma}ta_{i\sigma}^{+}a_{j\sigma} \tag{1.17}$$

where the first term just sets the zero of energy for the system and t is the one electron Hamiltonian matrix element between Wannier orbitals centred on nearest neighbour sites. This term can be thought of as *hopping* an electron from one site to another while conserving its spin. If we are in the $U \to \infty$ limit then at half filling the system will be in the state with one electron per site, hopping processes can only occur between adjacent sites if the electrons have opposite spin and the large Coulomb repulsion prohibits this. However, if we perturb away from this limit we can calculate the second order change in energy due to hopping conductivity as

$$\Delta E = \sum_{i}\frac{\langle\phi_0|H|\phi_i\rangle\langle\phi_i|H|\phi_0\rangle}{E_0 - E_i} \tag{1.18}$$

The states connected to the ground state by a non-zero matrix element have one site vacant and one site doubly occupied by an antiparallel spin pair. The energy of this state is dominated by the Coulomb interaction of this spin pair and hence $E_0 - E_i \sim -U$. Therefore

$$\Delta E = \sum_{i}\frac{\langle\phi_0|H|\phi_i\rangle\langle\phi_i|H|\phi_0\rangle}{-U} = -\frac{\langle\phi_0|H^2|\phi_0\rangle}{U} \tag{1.19}$$

Expanding the operator H^2 out gives

$$H^2 = \sum_{\langle ij \rangle} t^2 \sum_{\sigma\sigma'} a^+_{i\sigma} a_{i\sigma'} a_{j\sigma} a^+_{j\sigma'} \tag{1.20}$$

which can again be expressed in terms of Pauli matrices as $\frac{1}{2}\sum_{\langle ij \rangle} \frac{t^2}{U}(\mathbf{s}_i \cdot \mathbf{s}_j - 1)$.

Therefore the hopping of electrons from site to site induces an antiferromagnetic Heisenberg interaction of order $\frac{t^2}{2U}$. This is the basis of the *t-J* model [6] which consists of a one band model with doubly occupied sites projected out and parameterized by hopping integral *t* and Heisenberg interaction energy *J*.

As mentioned earlier, most magnetic interactions are due to d-band electrons. The spins of these electrons can be coupled on each site and the Heisenberg Hamiltonian can be generalised to higher spins by considering the relevant Pauli matrices.

Now that it has been shown that the magnetic interaction in insulating materials can be modeled by the Heisenberg Hamiltonian we will discuss some of the properties of its ground state and low lying excitations to give some background to the calculations described in the next two chapters.

1.2 Spin waves in a ferromagnet.

In this section will develop the theory of spin waves in a ferromagnet and show that at low temperatures they can be thought of as non-interacting collective effect which determine the excitation spectrum of the system.

Taking a general ferromagnetic Heisenberg Hamiltonian of spin *S* with nearest neighbour interaction

$$H = -J\sum_{\langle ij \rangle} \mathbf{S}_i \cdot \mathbf{S}_j \tag{1.21}$$

we can describe states of the system by giving the z-component of spin at each site, $\left|s_1^z \cdots s_N^z\right\rangle$. The quantum ground state has all spins aligned in the state with $s^z = S$. Alternatively we can label the states by giving the deviation n of each spin from saturation i.e. $n_i = S - s_i^z$. States labeled in terms of their deviation we will denote by $\left|\overline{n_1} \cdots \overline{n_N}\right\rangle$. It will be useful to express the spin operators in terms of the usual spin raising and lowering operators defined by

$$S^+ = S^x + iS^y \qquad S^- = S^x - iS^y \tag{1.22}$$

Using these operators we can write the Hamiltonian as

$$H = -J\sum_{\langle ij\rangle} S_i^z S_j^z + \frac{1}{2}\left(S_i^+ S_j^- + S_i^- S_j^+\right) \tag{1.23}$$

We want to determine the effect of the spin operators on states represented by their deviation from saturation n. Considering first the z-terms acting on a pair of spins

$$\begin{aligned} S_i^z S_j^z \left|\overline{n_i}, \overline{n_j}\right\rangle &\equiv S_i^z S_j^z \left|S - n_i, S - n_i\right\rangle \\ &= S^2 - S\left(n_i + n_j\right) + n_i n_j \end{aligned} \tag{1.24}$$

For the off diagonal terms we need to use the results for the spin raising and lowering operators acting on a state of spin S and z component m:

$$S^+|m\rangle = \left[S(S+1) - m(m+1)\right]^{\frac{1}{2}} |m+1\rangle \tag{1.25}$$

$$S^-|m\rangle = \left[S(S+1) - m(m-1)\right]^{\frac{1}{2}} |m-1\rangle \tag{1.26}$$

We can therefore write

$$S^+\left|\overline{n}\right\rangle \equiv S^+\left|S-n\right\rangle \tag{1.27}$$

$$= \left[S(S+1)-(S-n)(S-n+1)\right]^{\frac{1}{2}}\left|S-n+1\right\rangle$$

$$= \left[2S\left(1-\frac{n-1}{2S}\right)\right]^{\frac{1}{2}}\sqrt{n}\left|\overline{n-1}\right\rangle$$

and similarly

$$S^-\left|\overline{n}\right\rangle \equiv S^-\left|S-n\right\rangle \tag{1.28}$$

$$= \left[S(S+1)-(S-n)(S-n-1)\right]^{\frac{1}{2}}\left|-S-n-1\right\rangle$$

$$= \left[2S\left(1-\frac{n}{2S}\right)\right]^{\frac{1}{2}}\sqrt{n+1}\left|\overline{n+1}\right\rangle$$

These expressions suggest a transformation to bosonic operators and this was first introduced by Holstein and Primakoff [7] who defined

$$a\left|\overline{n}\right\rangle = \sqrt{n}\left|\overline{n-1}\right\rangle \qquad a^+\left|\overline{n}\right\rangle = \sqrt{n+1}\left|\overline{n+1}\right\rangle \tag{1.29}$$

using which we can write

$$n = a^+a \tag{1.30}$$

$$S^+ = (2S)^{\frac{1}{2}}\left(1-\frac{a^+a}{2S}\right)^{\frac{1}{2}}a \tag{1.31}$$

$$S^- = (2S)^{\frac{1}{2}}a^+\left(1-\frac{a^+a}{2S}\right)^{\frac{1}{2}} \tag{1.32}$$

We can now express the Hamiltonian as

$$H = -JS^2NZ + JSZ\sum_i a_i^+a_i - J\sum_{\langle ij\rangle} a_i^+a_ia_j^+a_j \tag{1.33}$$

$$-JS\sum_{\langle ij\rangle}\left(1-\frac{a_i^+a_i}{2S}\right)^{\frac{1}{2}}a_ia_j^+\left(1-\frac{a_j^+a_j}{2S}\right)^{\frac{1}{2}}$$

$$-JS\sum_{\langle ij\rangle}a_i^+\left(1-\frac{a_i^+a_i}{2S}\right)^{\frac{1}{2}}\left(1-\frac{a_j^+a_j}{2S}\right)^{\frac{1}{2}}a_j$$

This is a complex Hamiltonian which can't be solved exactly. However, we can expand the series and only keep quadratic terms. This gives the Hamiltonian as

$$H = JSZ\sum_i a_i^+ a_i - JS\sum_{\langle ij\rangle} a_i a_j^+ + a_i^+ a_j \tag{1.34}$$

which can be diagonalised by introducing the Fourier transformed variables

$$b_{\mathbf{k}} = \frac{1}{\sqrt{N}}\sum_j e^{-i\mathbf{k}\cdot\mathbf{j}} a_j \qquad b_{\mathbf{k}}^+ = \frac{1}{\sqrt{N}}\sum_j e^{i\mathbf{k}\cdot\mathbf{j}} a_j^+ \tag{1.35}$$

in terms of which

$$H = JSZ\sum_{\mathbf{k}} b_{\mathbf{k}}^+ b_{\mathbf{k}} - JS\frac{Z}{2}\sum \gamma_{\mathbf{k}} b_{\mathbf{k}}^+ b_{\mathbf{k}} + \gamma_{-\mathbf{k}} b_{\mathbf{k}} b_{\mathbf{k}}^+ \tag{1.36}$$

where

$$\gamma_{\mathbf{k}} = \frac{1}{Z}\sum_{\delta} e^{i\mathbf{k}\cdot\delta} \tag{1.37}$$

with the sum over δ being over the nearest neighbours. For lattices with a symmetry centre $\gamma_{\mathbf{k}} = \gamma_{-\mathbf{k}}$ and $\sum_{\mathbf{k}} e^{i\mathbf{k}\cdot\delta} = 0$. Using these relations and the commutation relations for b and b^+ allows the Hamiltonian to be written

$$H = JSZ\sum_{\mathbf{k}} (1-\gamma_{\mathbf{k}}) b_{\mathbf{k}}^+ b_{\mathbf{k}} \tag{1.38}$$

This equation gives the dispersion relation for spin waves, or magnons as they are often referred to as, for a ferromagnet as

$$\omega(\mathbf{k}) = JSZ(1-\gamma_{\mathbf{k}}) \tag{1.39}$$

1.3 Spin waves in an antiferromagnet

The Holstein-Primakoff transformation to bosonic variables can also be carried out for an antiferromagnetic Heisenberg Hamiltonian. In this case we define creation and

annihilation operators for each of the two sublattices and consider deviations away from the Néel state which has all the spins on one sublattice saturated with z-component $+S$ and the other with all the spins in the $-S$ state. We define a_i^+ and a_i which create and destroy deviations from the saturated state on the ith site on one sub-lattice and similarly b_i^+ and b_i are defined for the other sub-lattice. Forming the Fourier transformed operators

$$c_{\mathbf{k}} = \frac{1}{\sqrt{N}}\sum_j e^{i\mathbf{k}\cdot\mathbf{j}} a_j \qquad c^+{}_{\mathbf{k}} = \frac{1}{\sqrt{N}}\sum_j e^{-i\mathbf{k}\cdot\mathbf{j}} a_j^+ \tag{1.40}$$

$$d_{\mathbf{k}} = \frac{1}{\sqrt{N}}\sum_j e^{i\mathbf{k}\cdot\mathbf{j}} b_j \qquad d^+{}_{\mathbf{k}} = \frac{1}{\sqrt{N}}\sum_j e^{-i\mathbf{k}\cdot\mathbf{j}} b_j^+$$

allows the Hamiltonian to be written as

$$H = 2NZJS^2 - 2JZS\sum_{\mathbf{k}} \gamma_{\mathbf{k}}\left(c_{\mathbf{k}}^+ d_{\mathbf{k}}^+ + c_{\mathbf{k}} d_{\mathbf{k}}\right) + c_{\mathbf{k}}^+ c_{\mathbf{k}} + d_{\mathbf{k}}^+ d_{\mathbf{k}} \tag{1.41}$$

This Hamiltonian can be diagonalised exactly by making use of the Bogoliubov transformation [8] from which the dispersion relation can be shown to be

$$\omega(\mathbf{k}) = JZS^{\frac{1}{2}}\left[1-\gamma_{\mathbf{k}}^2\right]^{\frac{1}{2}} \tag{1.42}$$

Once the dispersion relations for the magnons in both the ferromagnetic and antiferromagnetic models are determined they can be used to calculate the thermodynamic properties of the system. We have so far neglected any interaction between the spin waves which arise from including the higher order terms in the Hamiltonian (1.33). It would therefore be expected that spin wave analysis of these systems would be most accurate at low temperatures when the number of magnons excited above the ground state would be small. As we shall demonstrate now, this is

correct in three dimensions, however in lower dimensions simple spin wave theory is insufficient and magnon - magnon interactions cannot be neglected.

1.4 Calculations using spin wave theory.

For the case of a ferromagnet, the quantum ground state has all spins aligned parallel with z-component of spin equal to S. We can investigate the change in magnetization as a function of temperature by calculating the expectation value for the number of magnons excited which is obtained from applying Bose statistics to the spin waves. The mean number of magnons excited with wave vector $\boldsymbol{k}$ is given by

$$\langle n_{\mathbf{k}} \rangle = \frac{1}{e^{\beta E(\mathbf{k})} - 1} \tag{1.43}$$

and so the number of flipped spins is given by

$$\sum_{\mathbf{k}} \langle n_{\mathbf{k}} \rangle \tag{1.44}$$

with the summation over all allowed $\boldsymbol{k}$ values in the first Brillouin zone. This sum can be evaluated by converting the sum to an integral which is valid if the number of sites N is large. We can also use the fact that the Bose factor becomes very small for increasing $\boldsymbol{k}$ allowing the integral to be taken over all of $\boldsymbol{k}$-space and $E(\mathbf{k})$ can be expanded in terms of $\boldsymbol{k}$. For a simple cubic crystal with lattice constant a.

$$\gamma_{\mathbf{k}} = \frac{1}{3}\left[\cos(k_x a) + \cos(k_y a) + \cos(k_z a)\right] \approx 1 - \frac{a^2}{6}|\mathbf{k}|^2 \tag{1.45}$$

which allows us to write

$$\sum_{\mathbf{k}} \langle n_{\mathbf{k}} \rangle = \frac{V}{(2\pi)^3} \int_0^{\infty} \frac{d^3}{e^{\beta E(\mathbf{k})} - 1} \approx \frac{V}{(2\pi)^3} \int_0^{\infty} \frac{4\pi k^2 dk}{e^{\beta J S a^2 k^2} - 1} \tag{1.46}$$

The integral can be performed analytically and expressed in terms of the Riemann zeta function and gives the temperature dependence of the reduction in magnetization as

$\Delta M \sim T^{\frac{3}{2}}$. This result was first derived by Bloch [9] and accurately reproduces the magnetization curves of many ferromagnetic materials. By similar calculation the internal energy and heat capacity can be shown to vary like $T^{\frac{5}{2}}$ and $T^{\frac{3}{2}}$ respectively.

In the case of an antiferromagnet the classical, or Néel, ground state which has all the spins on one sublattice in the $s^z = +S$ state and all those on the other sublattice in the $s^z = -S$ state, is not the quantum ground state. This is due to the off diagonal terms in the Heisenberg Hamiltonian which flip pairs of opposite spins. In order to give an indication of what the system looks like at $T = 0$, it is instructive to calculate the average magnetization on each sublattice which is given by

$$\frac{1}{2}\sum_{\mathbf{k}}\left[\left(1-\gamma_{\mathbf{k}}^2\right)^{-\frac{1}{2}}-1\right] \tag{1.47}$$

which for a simple cubic lattice gives a sublattice magnetization of $\sim 0.87S$ [10], the reduction being due to quantum fluctuations. This shows that the Néel state, although not the exact quantum ground state, is a good approximation for many purposes.

For small $\boldsymbol{k}$, the magnon dispersion relation is approximately linear. In an analogous way to the Debye model for phonon dispersion, the decrease of sublattice magnetization, the internal energy and the specific heat can be shown to behave like T^2, T^4 and T^3 respectively in three dimensions [2].

Spin wave theory has proved accurate in describing experimentally derived results for a wide range of magnetic systems. However, when treating systems with reduced dimensionality, the situation is less encouraging. To illustrate the problem, consider again the calculation of reduction of magnetization with temperature for a ferromagnet

but now considering a one dimensional chain. The mean number of magnons excited is given by

$$\sum_k \langle n_k \rangle = \frac{V}{2\pi} \int_0^\infty \frac{dk}{e^{\beta JSa^2k^2} - 1} \tag{1.48}$$

This integral is divergent, meaning that although the classical fully aligned state is the quantum ground state in 1D, at any finite temperature this state is destroyed and the system becomes disordered. This lack of long range order is a typical property of one dimensional systems. In two dimensions, the situation is the same as is true in all 2D systems in which a continuous symmetry is broken. This is known as the Mermin-Wagner theorem.[11]

The case of an antiferromagnet is also changed in one dimension. Not only does the magnon occupation diverge at finite temperature, but so also does the T=0 sublattice magnetization. This indicates that in 1D, the Néel state is no longer a good approximation to the true quantum ground state. Hence, to study the properties of one dimensional magnetic systems a different approach is required.

1.5 One Dimensional Magnetic Systems

The Heisenberg model for a one dimensional chain has been the subject of a great deal of theoretical study for over sixty years for a number of reasons. Foremost amongst these is the fact that often problems can be solved in one dimension that are intractable in three dimensions in addition to the fact that the physics of 1D systems is often strikingly different to that found in higher dimensionality [12]. Furthermore recent experimental studies have shown that a number of magnetic materials can be very accurately approximated by quasi 1D models [13]. Much recent attention has been

concentrated on understanding the consequences of the Haldane conjecture [14]. This is the proposal put forward in 1983 that there is a fundamental difference in the nature of the excitation spectra of integer and half integer spin chains, namely that in the thermodynamic limit, integer spin chains have a finite energy gap between their ground and first excited states while half integer chains have a gapless spectrum. The existence of this gap has been confirmed by experiment on quasi 1D magnets and has been calculated numerically to high accuracy. The next two chapters describe numerical calculations on a number of $S = \frac{1}{2}$ and $S = 1$ models and their comparison with experiment, but first a brief description of what can be solved exactly will be presented and then a discussion of the Lieb-Shultz-Mattis theorem is made which gives a possible explanation for the non-existence of a gap in half integer spins chains.

1.6 The Bethe Ansatz

In 1930 Bethe [15] investigated the interaction between spin waves for an $S = 1/2$ Heisenberg chain. His method allows two sets of equations to be formed for describing the spin states for the chain with a particular number of up and down spins. The equations determine the velocities and momenta of the excitations. The exact ground state of the antiferromagnetic chain was shown to have an energy of $1/4 - \ln 2$ per site, which is significantly lower than the energy of the Néel state, and to exhibit no long range order. The Bethe Ansatz also allows the thermodynamics of the system to be represented as an infinite set of non-linearly coupled integral equations. These can be solved numerically to obtain the free energy of the system. Higher spin models cannot be solved by the Bethe ansatz except in certain circumstances [16] and generally such

systems can only be tackled numerically by techniques such as exact diagonalisation, Monte-Carlo methods and series expansion.

1.7 The Lieb-Shultz-Mattis Theorem

In 1961, Lieb, Shultz and Mattis (LSM) gave a rigorous proof that for $S = 1/2$, the Heisenberg chain has no energy gap between its ground state and first excitation [17]. This argument was extended by Affleck and Lieb to arbitrary half integer S. The LSM theorem proceeds as follows.

Starting with the Hamiltonian $H = J\sum_{i=1}^{L} \mathbf{S}_i \cdot \mathbf{S}_{i+1}$ we observe that H conserves parity as all the interactions along the chain are equal. The ground state of this model is denoted by $|\psi_0\rangle$ and the ground state energy as E_0. Now consider another state $|\psi_1\rangle$ which is created from the ground state by taking a section of the chain containing an odd number of spins and rotating them about the z-axis, with the twist varying from 0 to 2π over the section. This can be expressed as $|\psi_1\rangle = U|\psi_0\rangle$ with

$$U = e^{\left(\frac{i\pi}{l}\right)\sum_{j=-l}^{l}(j+l)S_j^z} \tag{1.49}$$

where the number of twisted spins is $2l+1$.

The difference between the energy of this state and the ground state is given by

$$\Delta E = \langle\psi_1|H - E_0|\psi_1\rangle = \frac{2}{3}\frac{E_0}{N}\left(\cos\left(\frac{\pi}{l}\right) - 1\right)(2l+2) \tag{1.50}$$

which is of order $1/l$.

This shows that in the limit $L \to \infty$, we can construct a state with vanishingly small energy gap between it and the ground state. In order to show that $|\psi_0\rangle$ and $|\psi_1\rangle$ are distinct states, we consider the relative parity of them. If we apply the transformation

$S_i^z \rightarrow -S_{-i}^z$ this is equivalent to a product of parity and reflection about the y-axis by π and can be expressed as $\exp(-2i\pi\sum_{j=-l}^{l} S_i^z)$. As the summation contains an odd number of spins, the above expression takes the values +1 and -1 for integer and half integer spin respectively. Hence, in the half integer case $|\psi_0\rangle$ and $|\psi_1\rangle$ are distinct states and the excitation spectrum is gapless.

1.8 Exact Diagonalisation and Quantum Monte Carlo Methods

Much information about quantum many-body systems is derived from exact diagonalisation studies of finite chains. That is, numerically calculating all or some fraction of the eigenvalue spectrum of a particular Hamiltonian and then using these results to obtain ground state and/or thermodynamic properties of the finite size system. Finite size scaling can then be employed to infer information about the system in the thermodynamic limit. The limiting factor in exact diagonalisation calculations is computational resources. In general for a lattice system of l sites with n degrees of freedom per site, the size of the Hilbert space scales like n^l. With regard to spin chains, this limits the size of lattice currently feasible to about 30 sites for $S = 1/2$, 22 sites for $S = 1$ and 14 for $S = 2$. Calculations on lattices of these sizes are very memory and CPU intensive, requiring supercomputing resources. Another point to consider is the validity of extrapolating finite size results to the thermodynamic limit. This may be of relevance when the system is near criticality and the correlation length diverges hence becoming larger than the size of the lattice being treated.

Quantum Monte Carlo methods involve sampling random configurations of the Hilbert space of the Hamiltonian and calculating the properties of the system statistically. Such methods can generally deal with larger size lattices than exact diagonalisation but larger errors occur due to the random nature of the process.

1.9 Modified Spin Wave Theory and Green's Function Techniques

An extension of spin wave theory was developed by Takahashi for low dimensional ferromagnets [18]. This involved adding the constraint that the magnetization is zero for all finite temperature. This was achieved by including an effective chemical potential which acts as a Lagrange multiplier when the Hamiltonian is diagonalised. The results for the $S = 1/2$ Heisenberg chain agreed well with the numerical solution of the Bethe ansatz integral equations.

The theory was extended to antiferromagnets by Hirsch and Tang [19] and also by Rezende [20]. The latter showed that this theory predicted a gap in 1D for integer spin, which was qualitatively in accordance with the Haldane conjecture. However, it could not prove the non-existence of a gap for half integer spin.

Kondo and Yamaji [21] developed a Green's function method for investigating the thermodynamic properties of low dimensional ferromagnets for $S = 1/2$ and this was extended to arbitrary spin by Suzuki, Shibata and Ishii [22]. This involves forming the equations of motion for the double time Green's function $\langle\langle S_0^z(t); S_n^z(t')\rangle\rangle$ and then decoupling them when the terms reach fourth order. The results compared favourably with exact diagonalization values.

1.10 References

[1] Heisenberg W, Z. Phys., **49,** 619 (1928)
[2] Yosida K, "Theory of Magnetism", Springer, Berlin (1991)
[3] Jones W and March N H, "Theoretical Solid State Physics" Vol 1, Dover Publications, Inc., New York (1973)
[4] Martin D H, "Magnetism of Solids", Iliffe Books Ltd., London (1967)
[5] Hubbard J, Proc. Roy. Soc., **A276**, 238, (1963)
[6] Anderson P W, Science, **235**, 1196, (1987)
[7] Holstein T and Primakoff H, Phys. Rev., **58**, 177 (1940)
[8] Kittel C, "Quantum Theory of Solids", John Wiley and Sons, Inc., New York, (1963)
[9] Bloch F, Z. Phys., **61**, 206 (1930)
[10] Davis H L, Phys. Rev.,**120**, 789 (1960)
[11] Mermin N D and Wagner H, Phys. Rev. Lett., **17**, 1133 (1966)
[12] Mattis D C, "The Many Body Problem", World Scientific, Singapore, (1993)
[13] Ito M, Mito M, Deguchi H and Takeda K, J. Phys. Soc. Japan, **63**, 1123 (1994)
[14] Haldane F D M, Phys. Rev. Lett., **50**, 1153 (1983)
[15] Bethe H, Z. Phys, **71**, 205 (1931)
[16] Affleck I, J. Phys. C., **1**, 3047 (1989)
[17] Lieb E H, Schultz T and Mattis D J, Ann. Phys. **16**, 407 (1961)
[18] Takahashi M, Phys. Rev. Lett., **58**, 168 (1987)
[19] Hirsch J E and Tang S, Phys. Rev. B, **40**, 4769 (1989)
[20] Rezende S M, Phys. Rev. B, **42**, 2589 (1990)
[21] Kondo J and Yamaji K, Prog. Theor. Phys. **47**, 807 (1972).
[22] Suzuki F, Shibata N and Ishii C, J. Phys. Soc. Japan, **63**, 1539 (1994)

2. Density Matrix Renormalisation Group Methods.

This chapter describes the density matrix renormalisation group methods which will be used in the following two chapters. The failure of the real space methods is discussed and the DMRG is introduced. Its application to the study of quantum lattice models at both $T = 0$ and at finite temperature is described.

2.1 Real Space Renormalisation Group.

The concept of renormalisation is a common one in physics. The rescaling of a problem in order to make it a tractable one or to extrapolate results to the thermodynamic limit are techniques common to many fields. The renormalisation methods discussed in this chapter stem from the work of Kenneth Wilson and relate to the application of renormalisation group transformations applied to interacting quantum systems on a lattice [1]. The introduction of the Real Space Renormalisation Group (RSRG) and it's success in treating the Kondo problem was a milestone in the understanding of critical phenomena and earned Wilson a Nobel prize. The RSRG appeared to offer a systematic but non-perturbative way of reducing the number of degrees of freedom associated with a particular quantum lattice model and hence allow calculations of quantities in the thermodynamic limit (Number of sites, $N \rightarrow \infty$). Applications of the RSRG, however, where discouraging. The results obtained from applying the method to systems such as the Hubbard [2] models in 1D and to investigating Anderson

localisation on a 2D lattice [3] gave results that were inaccurate and misleading. In order to appreciate the shortcomings in the RSRG method it is necessary to understand the algorithmic steps involved in a typical RSRG calculation.

Consider a 1D lattice with n degrees of freedom per lattice site (i.e. n=2 for a S=1/2 chain; n=4 for the 1D Hubbard model). The first step of the calculation involves isolating a small block (usually a single site) of the lattice B. The Hamiltonian H_B describes all the interactions between sites contained within B. Now consider two identical blocks B and B joined together. We can denote the state of one block B by $|i\rangle$, the state of the other by $|j\rangle$ and hence the combined block BB by $|i\rangle|j\rangle$. Matrix elements of the Hamiltonian for the block BB will be of the form:

$$\langle i'|\langle j'|H_{BB}|i\rangle|j\rangle = \langle i'|H_B|i\rangle\delta_{jj'} + \langle j'|H_B|j\rangle\delta_{ii'} + \langle i'|\langle j'|H_{\text{int}}|i\rangle|j\rangle \qquad (2.1)$$

where H_{int} describes the interaction between the blocks, which for a system with only nearest neighbour interactions involves only the end sites of each block. H_{BB} is diagonalised to obtain the eigenstates of BB. We can now use BB as the basic block in our procedure (i.e. $BB \rightarrow B$) and consider a system consisting of it joined to a copy of itself and repeat the process above iteratively. In this way the Hamiltonian H_{BB} obtained at each stage of the iteration describes longer and longer chains and calculations of expectation values of observables should tend towards their thermodynamic limits. However, as the chain length increases, so does the size of the Hilbert space required to describe it. If the chain is ℓ sites long then the number of states needed to fully describe it is n^{ℓ}. A system of truncation is obviously required if the calculation is to be feasible. If ground state properties and low lying excitations are of interest then an obvious way of restricting the basis states is to retain only the lowest energy eigenstates of

H_{BB} at each stage and use these to describe the combined block at the next iteration. Using this method of truncation the RSRG steps can be summarised in the following steps.

1. Construct the Hamiltonian H_B for an isolated block B.

2. Form a combined block BB and form its Hamiltonian H_{BB}.

3. Diagonalise H_{BB} and retain the m lowest energy eigenstates ψ_i.

4. Rotate H_{BB} into the basis described by the states ψ_i using $H_{B'} = OH_{BB}O^{+}$ where B' denotes the block BB represented in the ψ_i basis and O is the matrix whose rows comprise of the m lowest energy eigenstates ψ_i.

5. Replace B by B'

6. Go to step 2.

The reason for the failure of the RSRG in giving accurate results when applied to a variety of systems was not obvious until White and Noack published the first of a series of seminal papers describing quantum renormalisation groups [4]. They considered applying the RSRG to a 1D tight-binding model and it became apparent that the problem lay in the boundary conditions used when building up the chain from the individual blocks.

Consider a point in the calculation where we have a block B described by some basis states $|i\rangle$. Without loss of generality we can consider a point in the calculation where B is large and hence the $|i\rangle$'s are quantum mechanical particle-in-a-box states. If we consider the block in isolation then its eigenstates have a node at either end. For instance, the three lowest energy eigenstates would look like:

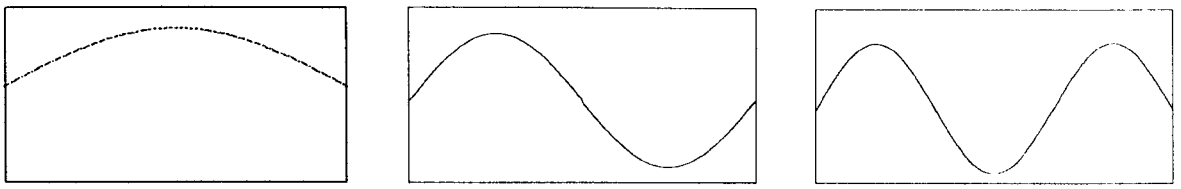

The next step of the calculation would be to use these eigenstates to describe a block of twice the size. It is easy to see that the lowest energy state that can be constructed has the form:

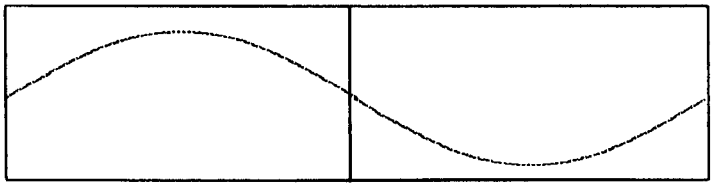

which is NOT the lowest energy eigenstate for a particle in a box of this size. It is seen that the boundary conditions imposed when diagonalising H_{BB} determine the form of its eigenstates. White and Noack showed that other choices of boundary conditions (eg. periodic, anti-periodic) fared no better and argued that an accurate truncated basis set must combine eigenstates obtained from diagonalising H_{BB} a number of times imposing different boundary conditions each time. In this way it is possible to simulate the effect of interactions between the isolated block and the rest of the lattice. It is this concept which lies at the heart of the Density Matrix Renormalisation Group.

2.2 Density Matrix Renormalisation Group .

Once it was realised that it was the incorrect treatment of boundary conditions that had lead to the inaccuracies in RSRG calculations, White devised a general systematic method of dealing with this problem (DMRG) [5]. Rather than diagonalise a section of the lattice several times,

each time with different boundary conditions, an alternative approach is to consider the block connected to two or more copies of itself at either end and diagonalise this 'superblock'. Having obtained the superblock eigenstates, the projection of these onto a section of the superblock comprising two of the initilal blocks is calculated. These projected states now form a basis for a two block system which becomes the basic unit of a larger superblock and the process continues iteratively. If one is interested in ground state properties of the lattice then the projection need only be made onto the lowest energy eigenstate of the superblock. In order to clarify this process, consider the first steps of a calculation.

The initial block B_1 consists of a single site and the superblock is made up of four such blocks.

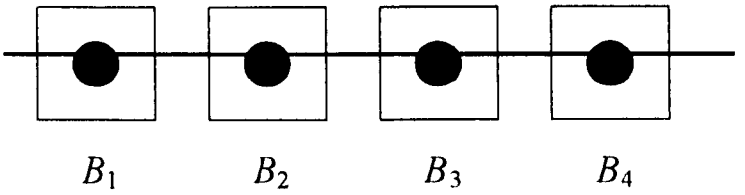

The state of the superblock can be described by

$$\Psi_{SB} = |i_1\rangle|i_2\rangle|i_3\rangle|i_4\rangle \tag{2.2}$$

and there will be n^4 possible states for the superblock where n is the number of degrees of freedom per site.

The Hamiltonian for the superblock is constructed and its lowest energy eigenstate Ψ_G obtained. Now consider blocking the sites together to make two blocks each containing two sites.

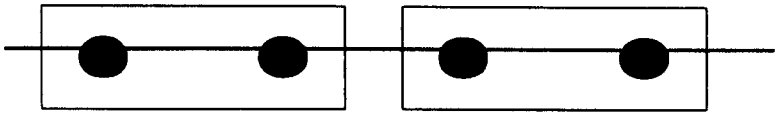

B_1' B_2'

The states of each block can be expressed as

$$|i\rangle = |i_1\rangle|i_2\rangle \tag{2.3}$$

$$|j\rangle = |i_3\rangle|i_4\rangle \tag{2.4}$$

We want to keep the states $|i\rangle$ which project onto Ψ_G in order to construct a basis set for the new two site block. The two site block then becomes the basic unit of a new superblock containing four of these new blocks and the process continues iteratively with the size of the lattice doubling at each iteration. However, in general all the states will project onto the ground state of the superblock and so we again have the problem of an increasing Hilbert space as in the RSRG method. Therefore we need a truncation scheme for deciding which states to keep and which to discard. The method of choosing the retained states is the main difference between the DMRG and the RSRG.

White formulated the problem as follows: The superblock, $B_1'B_2'$ is in its ground state Ψ_G which we can write as

$$\Psi_G = \sum_{i,j} \psi_{ij} |i\rangle|j\rangle \tag{2.5}$$

where $|i\rangle$, $i = 1...I$ is a complete set of states describing B_1' and $|j\rangle$, $j = 1...J$ is a complete set of states describing B_2'. We want to produce a truncated set of states $|u^\alpha\rangle$, $\alpha = 1...m$, $m < I$ which optimally describes B_1'. That is we want to construct a wave function

$$\overline{\psi} = \sum_{\alpha,j} a_{\alpha,j} |u^\alpha\rangle |j\rangle \tag{2.6}$$

which minimises $S = \||\psi\rangle - |\overline{\psi}\rangle\|^2$, varying all $a_{\alpha,j}$ and u^α. Without loss of generality we can perform a truncation on the $|j\rangle$'s as well i.e.

$$|\overline{\psi}\rangle = \sum_{\alpha} a_\alpha |u^\alpha\rangle |v^\alpha\rangle \tag{2.7}$$

where $v_j^\alpha = \langle j | v^\alpha \rangle$.

In terms of matrices

$$S = \sum_{i,j} \left(\psi_{ij} - \sum_{\alpha=1}^{m} a_\alpha u_i^\alpha v_j^\alpha \right)^2 \tag{2.8}$$

and S is to be minimised over all u^α, v^α and a_α for a given value of m. The solution to this equation is achieved by forming the singular value decomposition of the matrix ψ. This is a common technique in linear algebra and allows ψ to be expressed as the product of three matrices

$$\psi = UDV^T \tag{2.9}$$

where U and D are I x I matrices, V^T is an I x J matrix, U and V are orthogonal and D is a diagonal matrix whose diagonal elements are the singular values of ψ. For a given m, S is

minimised by choosing the a_α as the m largest modulus diagonal elements of D and the u^α and v^α as the corresponding columns of U and V respectively.

The matrix U is also seen to diagonalize the reduced density matrix ρ for B_1' which is defined by

$$\rho(i',i) = \sum_j \langle i'j|\Psi_G\rangle\langle ij|\Psi_G\rangle = \sum_j \psi_{ij}\psi_{i'j} \tag{2.10}$$

giving

$$\rho = UD^2U^T \tag{2.11}$$

The eigenvalues of ρ, w_α, are hence related to the singular values of ψ by $w_\alpha = a_\alpha^2$. We can therefore obtain the optimal set u^α by extracting the m eigenstates of ρ with largest corresponding eigenvalues.

The physical significance of choosing this basis set is that each reduced density matrix eigenvalue, w_α, gives the probability of B_1' being in state u^α given that the superblock is the state ψ_G. Forming a truncated basis from the states with largest eigenvalue therefore retains the most significant states required to reproduce the chosen superblock target wave function accurately for a given m. As $Tr\rho = 1$, an estimate of the truncation is given by $1 - \sum_{\alpha=1}^{m} w_\alpha$.

Computationally it is more efficient to construct the superblock at each stage from a block, a reflection of the block and two sites in between. For example the superblock at the first iteration would have the form

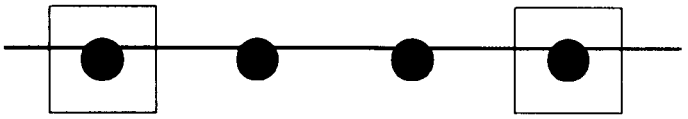

and at the second it would look like

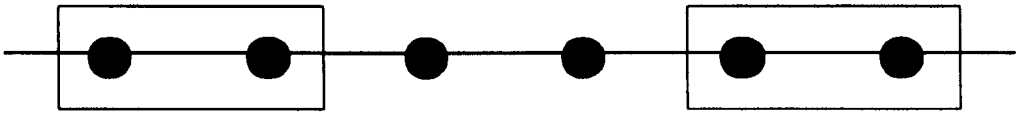

B_1 is usually referred to as the system block and B_2 as the environment block. At each stage an augmented block consisting of B_1 and its adjacent site is projected onto the ground state and becomes the basic block for the next iteration. This method of increasing the superblock size means that the lattice grows more slowly but the sizes of matrices to be diagonalised are reduced making their computation easier.

The steps in a typical DMRG calculation can be summarised as follows

1. Construct an initial block B consisting of one site and form its Hamiltonian.

2. Construct a superblock consisting of two blocks with two sites between them. Form the Hamiltonian for the superblock.

3. Calculate the lowest energy eigenstate of the superblock Hamiltonian.

4. Form the reduced density matrix ρ for an augmented block B' consisting of B and its neighbouring site.

5. Diagonalise ρ to find its eigenvalues w_i and corresponding eigenvectors u_i Retain the m most probable eigenstates as the new basis for B'.

6. Construct the Hamiltonian for B' and then rotate into the u_i truncated basis.

7. Replace B by B' and go back to step 2.

We now consider the effect of truncating the Hilbert space on calculations of ground state properties of the system under consideration. Suppose for some Hamiltonian, we know that the true eigenstates are $|\phi_1\rangle\cdots|\phi_N\rangle$ with corresponding eigenvalues $\lambda_1\cdots\lambda_N$ such that $\lambda_1 < \lambda_2\cdots < \lambda_N$. We represent a summation over some subset of this basis by Σ'. We now consider some approximation to the ground state of the system in the truncated basis which is given by

$$|\psi\rangle = \Sigma' a_i|\phi_i\rangle \tag{2.12}$$

We can calculate the energy of this state $\langle\psi|H|\psi\rangle$ giving

$$\langle\psi|H|\psi\rangle = \Sigma' a_i^2\lambda_i \tag{2.13}$$

if we denote the eigenvalue of the lowest energy eigenstate in the summation as λ_j then we can write

$$\begin{aligned}\langle\psi|H|\psi\rangle &= \Sigma' a_i^2\left[\lambda_j + (\lambda_i - \lambda_j)\right] \\ &= \Sigma' a_i^2\lambda_j + \Sigma' a_i^2(\lambda_i - \lambda_j) \\ &= \lambda_j + \Sigma' a_i^2(\lambda_i - \lambda_j)\end{aligned} \tag{2.14}$$

where we have assumed that $|\psi\rangle$ is normalised. As the second term in the above expression is positive we have shown that λ_j is a variational upper bound on energy of the state $|\psi\rangle$. If the truncated basis includes the true ground state then the upper bound is the ground state energy λ_1, else the upper bound is one of the excited states.

The first applications of the DMRG method were in the study of quantum spin chains. The method gave unprecedented accuracy in the calculation of the ground state of S=1/2 Heisenberg model reproducing the Bethe ansatz value correct to seven significant figures [5] and the ground state for S=1 was calculated to an accuracy of two orders of magnitude greater than Monte Carlo techniques [6].

The DMRG method can also be used to calculate low lying excitations. In order to do this, rather than to project onto the ground state of the superblock, the superblock state with energy closest to the region of interest at each iteration is used as the target state. Using this method, the DMRG method was the first to give strong evidence to support Haldane's conjecture that all integer spin chains have gapped excitation spectra [6].

The DMRG can also be applied to electron models. In this case the target state is taken as a linear combination of superblock states which bracket the required filling. Using this method systems such as the t-J model [7] and Kondo lattice [8] have been studied.

In the next two chapters we will use the DMRG to calculate zero temperature properties of a number of quantum spin systems.

2.3 The Transfer Matrix

In order to extend the DMRG to calculate properties at finite temperatures it will be prove to be necessary to understand the application of transfer matrix techniques to classical lattice models. This section describes the use of transfer matrices in the calculation of thermodynamic properties of classical spin systems in 1D and 2D.

2.3.1 Transfer matrix in 1D.

As an example of the use of transfer matrices in 1D, consider the one dimensional spin-1/2 Ising model. The Hamiltonian for the system, in the absence of an applied field is:

$$H = -J\sum_{i=0}^{N-1}\sigma_i\sigma_{i+1} \tag{2.15}$$

where the spin variable σ can take the values +1 or -1. We assume periodic boundary conditions i.e. $\sigma_{N+1} = \sigma_1$

The partition function for the system is:

$$Z = \sum_{\{\sigma\}} e^{\beta J(\sigma_1\sigma_2+\sigma_2\sigma_3\ldots+\sigma_{N-1}\sigma_N+\sigma_N\sigma_1)} \tag{2.16}$$

where $\{\sigma\}$ represents the sum over all states of all spins. Factorizing this expression gives

$$Z = \sum_{\{\sigma\}} e^{\beta J\sigma_1\sigma_2}e^{\beta J\sigma_2\sigma_3}\ldots e^{\beta J\sigma_N\sigma_1} \tag{2.17}$$

We introduce the transfer matrix defined by

$$\mathbf{T} = \begin{pmatrix} T_{++} & T_{+-} \\ T_{-+} & T_{--} \end{pmatrix} = \begin{pmatrix} e^{\beta J} & e^{-\beta J} \\ e^{-\beta J} & e^{\beta J} \end{pmatrix} \tag{2.18}$$

where $T_{\sigma_1\sigma_2} = e^{\beta J\sigma_1\sigma_2}$ We can now express the partition function as

$$Z = \sum_{\{\sigma\}} \mathbf{T}_{\sigma_1\sigma_2}\mathbf{T}_{\sigma_2\sigma_3}\ldots\mathbf{T}_{\sigma_N\sigma_1} \tag{2.19}$$

Performing the summation over all spin states gives

$$Z = \sum_{\sigma_1} \mathbf{T}^N{}_{\sigma_1\sigma_1} = Tr(\mathbf{T}^N) \tag{2.20}$$

which can be expressed in terms of the eigenvalues of $\mathbf{T}$ as

$$Z = \sum_i \lambda_i^N \tag{2.21}$$

which is a general result independent of the model being studied.

The usefulness 2.21 of can be illustrated by evaluating the free energy of the system. We consider a general $n \times n$ transfer matrix with eigenvalues λ_i such that $\lambda_0 > \lambda_1 > \ldots > \lambda_{n-1}$. The free energy per spin is given by

$$F = -kT\frac{1}{N}\ln Z = -kT\frac{1}{N}\ln\left\{\lambda_0^N\left(1 + \sum_i \frac{\lambda_i^N}{\lambda_0^N}\right)\right\} \tag{2.22}$$

Taking the thermodynamic limit $(N \to \infty)$ gives

$$F = -kT\ln\lambda_0 \tag{2.23}$$

reducing the problem of finding the free energy to that of calculating the maximal eigenvalue of a matrix. It can be shown by the Perron-Frobenius theorem that $\mathbf{T}$ always has a real, positive definite maximal eigenvalue [9].

For the case of the Ising model described above, the transfer matrix given by (2.15) has maximal eigenvalue $2\cosh\beta J$. Applying equation (2.23) in the limit $\beta \to \infty$ gives the free energy per spin as $-J$.

2.3.2 Transfer matrix in 2D.

The transfer matrix formalism can also be applied to classical spin models on a two dimensional lattice. The spin half Ising model in 2D is described by the Hamiltonian

$$H = -J\sum_{n=1}^{N}\sum_{m=1}^{M}\sigma_{n,m}\sigma_{n+1,m} + \sigma_{n,m}\sigma_{n,m+1} \tag{2.24}$$

where the n labels the rows of the lattice from 1 to N and m labels the columns from 1 to M as shown in figure 2.1. The partition function is given by

$$Z = \sum_{\sigma_{1,1}=\pm 1}\sum_{\sigma_{1,2}=\pm}\cdots\sum_{\sigma_{N,M}=\pm 1} e^{-\beta H} \tag{2.25}$$

giving

$$Z = \sum_{\sigma_{1,1}=\pm 1}\sum_{\sigma_{1,2}=\pm 1}\cdots\sum_{\sigma_{N,M}=\pm 1}\exp\left\{\beta J\sum_{n=1}^{N}\sum_{m=1}^{M}\sigma_{n,m}\sigma_{n+1,m} + \sigma_{n,m}\sigma_{n,m+1}\right\} \tag{2.26}$$

Writing the n summation explicitly and applying periodic boundary conditions

$$Z = \sum_{\sigma_{1,1}=\pm 1}\cdots\sum_{\sigma_{N,M}=\pm 1}\exp\left\{\begin{array}{l}\beta J\left(\sum_{m=1}^{M}\sigma_{1,m}\sigma_{2,m} + \sigma_{1,m}\sigma_{1,m+1}\right) + \\ \beta J\left(\sum_{m=1}^{M}\sigma_{2,m}\sigma_{3,m} + \sigma_{2,m}\sigma_{2,m+1}\right) + \cdots \\ \beta J\left(\sum_{m=1}^{M}\sigma_{N,m}\sigma_{1,m} + \sigma_{N,m}\sigma_{N,m+1}\right)\end{array}\right\} \tag{2.27}$$

It can be seen that each of the terms in the exponential only depends on the spin variables of two adjacent rows. We define $\bar{\sigma}_i$ as representing a spin configuration of the ith row and define a matrix $\mathbf{T}$ such that its elements are referenced by the spin configurations of adjacent rows:

$$\mathbf{T}_{\bar{\sigma}_{i+1}}^{\bar{\sigma}_i} = \exp\left\{\beta J \sum_{m=1}^{M} \sigma_{i,m}\sigma_{i+1,m} + \sigma_{i,m}\sigma_{i,m+1}\right\} \tag{2.28}$$

The partition function can now be written in terms of $\mathbf{T}$ and the summation is performed over the rows

$$Z = \sum_{\{\bar{\sigma}_1\}}\sum_{\{\bar{\sigma}_2\}}\cdots\sum_{\{\bar{\sigma}_1\}} \mathbf{T}_{\bar{\sigma}_2}^{\bar{\sigma}_1}\mathbf{T}_{\bar{\sigma}_3}^{\bar{\sigma}_2}\ldots\mathbf{T}_{\bar{\sigma}_1}^{\bar{\sigma}_N} \tag{2.29}$$

which can be expressed as

$$Z = Tr(\mathbf{T}^N) \tag{2.30}$$

As in the one dimensional case this is a general result.

For a finite lattice the matrix described by equation (2.28) is of dimensions $2^M \times 2^M$. If we denote the maximal eigenvalue by λ_0 then we can write the following inequality

$$\lambda_0{}^N \le Z \le 2^M \lambda_0{}^N \tag{2.31}$$

Taking the logarithms of all three terms and dividing by the number of sites, NM, gives

$$\frac{1}{M}\ln\lambda_0 \le \frac{1}{NM}\ln Z \le \frac{1}{M}\ln\lambda_0 + \frac{1}{2M}\ln 2 \tag{2.32}$$

In the thermodynamic limit then, the free energy per site is given by

$$F = \frac{-kT \ln Z}{NM} = \lim_{M \to \infty} \frac{1}{M} \ln \lambda_0 \tag{2.33}$$

The obvious difficulty involved in proceeding to the thermodynamic limit is that the size of the transfer matrix increases without limit. This is contrast with the 1-d case where the dimension of **T** was determined only by the number of degrees of freedom per site. We therefore require an approximation method for truncating the size of the transfer matrix as the lattice size is increased. The next section describes the application of DMRG methods to this problem.

2.4 Applying the DMRG to Classical Transfer Matrices.

In order to understand the application of the DMRG algorithm to a two dimensional classical lattice system we again consider the 2D spin half Ising model whose Hamiltonian is given by 2.21. If we consider the case of a 4×4 lattice, then the transfer matrix **T** has dimensions $2^4 \times 2^4$. The matrix element between two row spin configurations can be written in terms of Boltzmann weights W (figure 2.2) as

$$T^{(4)}(\sigma'_1\sigma'_2\sigma'_3\sigma'_4|\sigma_1\sigma_2\sigma_3\sigma_4) = W(\sigma'_1\sigma'_2|\sigma_1\sigma_2)W(\sigma'_2\sigma'_3|\sigma_2\sigma_3)W(\sigma'_3\sigma'_4|\sigma_3\sigma_4) \tag{2.34}$$

where

$$W(\sigma'_i\sigma'_{i+1}|\sigma_i\sigma_{i+1}) = \exp\left\{\frac{\beta J}{2}(\sigma'_i\sigma'_{i+1} + \sigma'_i\sigma_i + \sigma'_{i+1}\sigma_{i+1} + \sigma_i\sigma_{i+1})\right\} \tag{2.35}$$

Properties of this system can then be obtained from the eigenvalue spectrum of **T**. Now consider increasing the lattice dimensions to 6×6. We group the two leftmost spins of a row into the single spin variable ξ_L and the two rightmost into the variable ξ_R each of which can

take one of four values. The spin configuration of a row is now expressed as $(\xi_L\sigma_L\sigma_R\xi_R)$. The transfer matrix elements for this system are given by (see figure 2.3)

$$T^{(6)}(\xi'_L\sigma'_L\sigma'_R\xi'_R|\xi_L\sigma_L\sigma_R\xi_R) = T_L^{(3)}(\xi'_L\sigma'_L|\xi_L\sigma_L)W(\sigma'_L\sigma'_R|\sigma_L\sigma_R)T_R^{(3)}(\sigma_R\xi_R|\sigma_R\xi_R) \qquad (2.36)$$

where T_L and T_R are transfer matrices for the left and right halves of the lattice respectively.

We can repeat the blocking procedure, each time making the transformations $(\xi_L\sigma_L) \to \xi_L^{new}$ and $(\xi_R\sigma_R) \to \xi_R^{new}$ .while at each stage T_L and T_R describe transfer matrices for the two halves of the lattice augmented by one site. As the lattice size increases and we approach the thermodynamic limit the properties of the system are dominated by the maximal eigenvalue of the transfer matrix which is obtained from the eigenvalue equation

$$\sum_{\xi_L\sigma_L\sigma_R\xi_R} T^{(2M)}(\xi'_L\sigma'_L\sigma'_R\xi'_R|\xi_L\sigma_L\sigma_R\xi_R)\Psi_R(\xi_L\sigma_L\sigma_R\xi_R) = \lambda^{(2M)}\Psi_R(\xi'_L\sigma'_L\sigma'_R\xi'_R) \qquad (2.37)$$

where Ψ_R is the right eigenvector of T. In general T is not symmetric and its left eigenvector corresponding to the maximal eigenvalue λ is obtained from the equation $\Psi_L T = \Psi_L \lambda$.

Of course as the lattice size increases so does the size of the transfer matrix which must be diagonalized and we again require a systematic truncation scheme to make calculations feasible. Nishino applied the DMRG algorithm to this problem [10]: The reduced density matrix for the left hand side of the lattice is defined by

$$\rho_L(\xi'_L\sigma'_L|\xi_L\sigma_L) = \sum_{\sigma''_R\xi''_R} \Psi_L(\xi'_L\sigma'_L\sigma''_R\xi''_R)\Psi_R(\xi_L\sigma_L\sigma''_R\xi''_R) \qquad (2.38)$$

(where n is the number of degrees of freedom per site) matrix $O\left(\xi_L^{new}|\xi_L\sigma_L\right)$ whose rows are the m retained left eigenvectors of ρ_L expressed in the product basis $\xi_L\sigma_L$ and similarly the $mn \times m$ matrix $Q\left(\xi_L\sigma_L|\xi_L^{new}\right)$ whose columns are the m retained right eigenvectors of ρ_L we can express the transformation $T_L^{(M)} \rightarrow T_L^{(M+1)}$ by

$$T_L^{(M+1)}\left(\xi_L'^{new}\sigma'|\xi_L^{new}\sigma\right) = \sum_{\xi_L\sigma'\xi_L'\sigma} O\left(\xi_L'^{new}|\xi_L'\sigma'\right)T_L^{(M)}\left(\xi_L'\sigma'|\xi_L\sigma\right)W\left(\sigma'\sigma_L'|\sigma\sigma_L\right)Q\left(\xi_L\sigma|\xi_L^{new}\right) \qquad (2.39)$$

The corresponding mapping for T_R is obtained in a similar manner. Using this application of the DMRG algorithm the thermodynamic properties of classical 2D systems in the thermodynamic limit can be calculated. As with the 1D case the deviation from unity of the sum of the m retained eigenvalues of the density matrix gives a measure of the truncation error introduced into the calculation.

2.5 Trotter-Suzuki-decomposition

The transfer matrix technique can be extended to the study of the thermodynamics of one dimensional quantum spin systems by the application of a decomposition of the Hamiltonian developed by Trotter and Suzuki [11]. Consider the spin half Heisenberg model for an even chain of length N. The Hamiltonian is given by

$$H = \sum_{i=1}^{N} \mathbf{S}_i \cdot \mathbf{S}_{i+1} \qquad (2.40)$$

where we impose periodic boundary conditions.

where we impose periodic boundary conditions.

The Trotter-Suzuki decomposition is invoked by writing the Hamiltonian as

$$H = H_1 + H_2 \tag{2.41}$$

where

$$H_1 = \sum_{i=1}^{N/2} h_{2i-1} \qquad H_2 = \sum_{i=1}^{N/2} h_{2i} \tag{2.42}$$

and $h_i = \mathbf{S}_i \cdot \mathbf{S}_{i+1}$.

In order to study the thermodynamics of the system we require the partition function

$$Z_N = Tr\left[e^{-\beta H}\right] = Tr\left[e^{-\beta(H_1+H_2)}\right] \tag{2.43}$$

We define

$$Z_{MN} = Tr\left[e^{-\beta H_1/M} e^{-\beta H_2/M}\right]^M \text{ for integer } M. \tag{2.44}$$

Then $Z_N = \lim_{M\to\infty} Z_{MN}$

If we let σ_i be the z-component of spin on the ith site we can denote a configuration of the spin chain by $\left|\sigma_1{}^j \ldots \sigma_N{}^j\right\rangle$. Then by inserting 2M complete sets of such states and summing over them, we can write

$$\begin{aligned} Z_{MN} = \sum_s \prod_{j=1}^{M} & \left\langle \sigma_1{}^{2j-1} \cdots \sigma_N{}^{2j-1} \left| e^{-\beta H_1/M} \right| \sigma_1{}^{2j} \cdots \sigma_N{}^{2j} \right\rangle \\ & \times \left\langle \sigma_1{}^{2j} \cdots \sigma_N{}^{2j} \left| e^{-\beta H_2/M} \right| \sigma_1{}^{2j+1} \cdots \sigma_N{}^{2j+1} \right\rangle \end{aligned} \tag{2.45}$$

where $\left|\sigma_1^1 \cdots \sigma_N^1\right\rangle = \left|\sigma_1^{2M+1} \cdots \sigma_N^{2M+1}\right\rangle$ being a necessary condition for the evaluation of the trace.

Each of H_1 and H_2 contain terms which commute and act on different pairs of sites. Hence, Z_{MN} can be written in terms of two site matrix elements:

$$Z_{MN} = \sum_s \prod_{i=1}^{N/2} \prod_{j=1}^{M} \left\langle \sigma_{2i-1}^{2j-1} \sigma_{2i}^{2j-1} \left| e^{-\beta h_{2i-1}/M} \right| \sigma_{2i-1}^{2j} \sigma_{2i}^{2j} \right\rangle \left\langle \sigma_{2i}^{2j} \sigma_{2i+1}^{2j} \left| e^{-\beta h_{2i}/M} \right| \sigma_{2i}^{2j+1} \sigma_{2i+1}^{2j+1} \right\rangle \tag{2.46}$$

This leads to the standard 'checkerboard' depiction of the Suzuki-Trotter decomposition (figure 2.4) as a 2d lattice of dimensions $N \times 2M$ with periodic boundary conditions where the shaded regions indicate the sites connected by the two site matrix elements of equation (2.46). M is referred to as the Trotter number. Rewriting 2.43 in terms of local transfer matrices τ given by

$$\tau\left(\sigma_i^j \sigma_i^{j+1} \middle| \sigma_{i+1}^j \sigma_{i+1}^{j+1}\right) = \left\langle \sigma_i^j \sigma_{i+1}^j \left| e^{-\beta h_i/M} \right| \sigma_i^{j+1} \sigma_{i+1}^{j+1} \right\rangle \tag{2.47}$$

gives

$$Z_{MN} = \sum_{\sigma} \prod_{i=1}^{N/2} \prod_{j=1}^{M} \tau\left(\sigma_{2i-1}^{2j-1} \sigma_{2i-1}^{2j} \middle| \sigma_{2i}^{2j-1} \sigma_{2i}^{2j}\right) \tau\left(\sigma_{2i}^{2j} \sigma_{2i}^{2j+1} \middle| \sigma_{2i+1}^{2j} \sigma_{2i+1}^{2j+1}\right) \tag{2.48}$$

Representing a configuration of the spins in the Trotter direction as $\left|\sigma_i^1 \cdots \sigma_i^{2M}\right\rangle$, we can write

$$Z_{MN} = \sum_{\sigma} \prod_{i=1}^{N/2} T\left(\sigma_{2i-1}^1 \cdots \sigma_{2i-1}^{2M} \middle| \sigma_{2i+1}^1 \cdots \sigma_{2i+1}^{2M}\right) \tag{2.49}$$

where

$$T\left(\sigma^{1}_{2i-1}\cdots\sigma^{2M}_{2i-1}\middle|\sigma^{1}_{2i+1}\cdots\sigma^{2M}_{2i+1}\right)=\prod_{j=1}^{M}\tau\left(\sigma^{2j-1}_{2i-1}\sigma^{2j}_{2i-1}\middle|\sigma^{2j-1}_{2i}\sigma^{2j}_{2i}\right)\tau\left(\sigma^{2j}_{2i}\sigma^{2j+1}_{2i}\middle|\sigma^{2j}_{2i+1}\sigma^{2j+1}_{2i+1}\right) \tag{2.50}$$

We identify T as the quantum transfer matrix between states of the chain in the Trotter direction (figure 2.5). The periodic boundary conditions allow this to be written as

$$Z_{MN} = Tr\left(T^{N/2}\right) \tag{2.51}$$

In the thermodynamic limit ($N \rightarrow \infty$), the free energy is given by

$$F = -\frac{1}{2\beta}\ln\lambda_{\max} \tag{2.52}$$

where $\lambda_{\max}$ is the maximal eigenvalue of the transfer matrix T. In order to calculate F at different temperatures, we fix $\varepsilon = \beta/M$ in the above expressions and systematically increase M. At each stage we identify the temperature as $1/M\varepsilon$. As M increases, so does the size of T. Most previous studies of spin systems using the quantum transfer matrix have involved applying Monte Carlo methods to T to determine its eigenvalue spectrum. In order to limit the size of matrices involved, we use Nishino's implementation of the DMRG for 2d transfer matrices.

2.6 Transfer Matrix Renormalisation Group (TMRG).

Following the method of Bursill, Xiang and Gehring [12], we define a system block as one site and calculate the transfer matrix between it and its neighbouring sites (figure 2.6)

$$T_s(\sigma' n' \mu' | \sigma n \mu; \sigma'' \mu'') = \sum_{n''} \tau(\sigma' n' | \sigma'' n'') \tau(n'' \mu'' | n \mu) \tag{2.53}$$

A single site is also used to create the environment block, whose transfer matrix T_e has the same elements as that for the system. For the spin half model being considered, the system and environment blocks have two possible states. A superblock is constructed, consisting of the system and environment blocks plus two sites with periodic boundary conditions. This gives a lattice with Trotter number M = 2. The superblock transfer matrix elements are given by (figure 2.7)

$$T(\sigma_1' n_1' \sigma_2' n_2' | \sigma_1 n_1 \sigma_2 n_2) = \sum_{\sigma_1'' \sigma_2''} T_s(\sigma_1' n_1' \sigma_2' | \sigma_1 n_1 \sigma_2; \sigma_1'' \sigma_2'') T_e(\sigma_2' n_2' \sigma_1' | \sigma_2 n_2 \sigma_1; \sigma_2'' \sigma_1'') \tag{2.54}$$

T is in general asymmetric. By calculating $\lambda_{\max}$ we can determine the free energy for M=2, i.e. at a temperature of $1/2\varepsilon$.

We increase the size of the Trotter dimension by augmenting both system and environment blocks with an extra site. Taking an augmented system block n, consisting of a system state p and a spin state ν, the transfer matrix T_s' for the augmented system block is determined from (figure 2.8)

$$T_s'(\sigma' n' \mu' | \sigma n \mu; \sigma'' \mu'') = \sum_{\nu''} T_s(\sigma' p' \nu' | \sigma p \nu; \sigma'' \mu'') \tau(\nu' \mu' | \nu'' \mu'') \tag{2.55}$$

Similarly for the augmented environment (figure 2.9)

$$T_e'(\sigma' n' \mu' | \sigma n \mu; \sigma'' \mu'') = \sum_{\nu''} T_e(\nu' p' \mu' | \nu p \mu; \nu'' \mu'') \tau(\sigma'' \nu'' | \sigma \nu) \tag{2.56}$$

A superblock is again constructed, corresponding to a lattice of Trotter number M=3, its transfer matrix formed and its maximal eigenvalue found. For larger M we need to have a way of truncating the basis states used to describe the system and environment blocks and this is done using a DMRG method. We use the left and right eigenvectors $\langle \psi^{L}_{\max} |$ and $| \psi^{R}_{\max} \rangle$ of the superblock transfer matrix corresponding to the eigenvalue $\lambda_{\max}$ to construct density matrices for the augmented system and environment blocks. The matrix elements between augmented system states n' (consisting of system state n_1' and spin state σ_2') and n (consisting of system state n_1 and spin state σ_2) are given by

$$\rho_s(n'|n) = \sum_{\sigma_1 n_2} \langle \sigma_1 n_1' \sigma_2' n_2 | {}^{R}_{\psi \max} \rangle \langle \psi^{L}_{\max} | \sigma_1 n_1 \sigma_2 n_2 \rangle \tag{2.57}$$

The matrix elements between augmented environment states n' (consisting of system state n_2' and spin state σ_2') and n (consisting of system state n_2 and spin state σ_2) are given by

$$\rho_e(n'|n) = \sum_{\sigma_1 n_1} \langle \sigma_1 n_1 \sigma_2' n_2' | \psi^{R}_{\max} \rangle \langle \psi^{L}_{\max} | \sigma_1 n_1 \sigma_2 n_2 \rangle \tag{2.58}$$

We retain the m most probable eigenstates of the augmented system and environment blocks and use these as the new basis to describe the transfer matrices. The rotation into this basis is given by

$$T_s(\sigma' n' \mu' | \sigma n \mu; \sigma'' \mu'') = \sum_{n'', n'''=1}^{2m} \langle n' | n'' \rangle T_s'(\sigma' n'' \mu' | \sigma n''' \mu; \sigma'' \mu'') \langle n''' | n \rangle \tag{2.59}$$

where n' and n are augmented block states in the new basis and n'' and n''' are in the old basis. The augmented environment block transfer matrices are similarly rotated and truncated. The process continues iteratively, using the new system and environment blocks to construct

the superblock. Each iteration produces the free energy at a temperature corresponding to $1/M\varepsilon$ and this can then be used to calculate other thermodynamic quantities.

Considering the effect of truncation on the free energy, the partition function of the system is given by

$$Z = Tr\exp(-\beta H) \tag{2.60}$$

where the trace is taken over all the states in the Hilbert space. If we now consider a truncated space and evaluate the partition function by taking the trace over only these states

$$Z' = Tr'\exp(-\beta H) \tag{2.61}$$

As all the terms in the trace are positive we can write $Z \geq Z'$. Evaluating the free energy in the complete and truncated bases

$$F = -kT\ln Z \qquad F' = -kT\ln Z' \tag{2.62}$$

hence

$$F - F' = -kT\ln\left(\frac{Z}{Z'}\right) \tag{2.63}$$

as $Z \geq Z'$, $\ln\left(\frac{Z}{Z'}\right) \geq 0$ and hence $F \leq F'$. Therefore we have shown that the effect of truncating the basis in the TMRG method is to give a variational upper bound on the free energy.

2.7 References

[1] Wilson K G, Rev. Mod. Phys., **47**, 773 (1975)

[2] Bray J W and Chui S T, Phys. Rev. B, **19**, 4876 (1979)

[3] Lee P A, Phys. Rev. Lett. **42**, 1492 (1979)

[4] White S R and Noack R M, Phys. Rev. Lett., **68**, 3487 (1992)

[5] White S R, Phys. Rev. Lett., **69**, 2863 (1992); White S R, Phys. Rev. B, **48**, 10345 (1993)

[6] White S R and Huse D A, Phys. Rev. B, **48**, 3844 (1993)

[7] Chen L and Moukouri S, Phys. Rev. B, **53**, 1866 (1996)

[8] Yu C C and White S R, Phys. Rev. Lett., **71**, 3866 (1993)

[9] Binney J J, Dowrick N J, Fisher A J and Newman M E J, "The Theory of Critical Phenomena", Oxford University Press, Oxford (1992)

[10] Nishino T, J. Phys. Soc. Japan, **64**, 3598 (1995)

[11] Suzuki M and Inoue M, Prog. Theor. Phys., **78**, 645 (1987)

[12] Bursill R J, Xiang T and Gehring G A, J. Phys. C, **8**, L583 (1996)

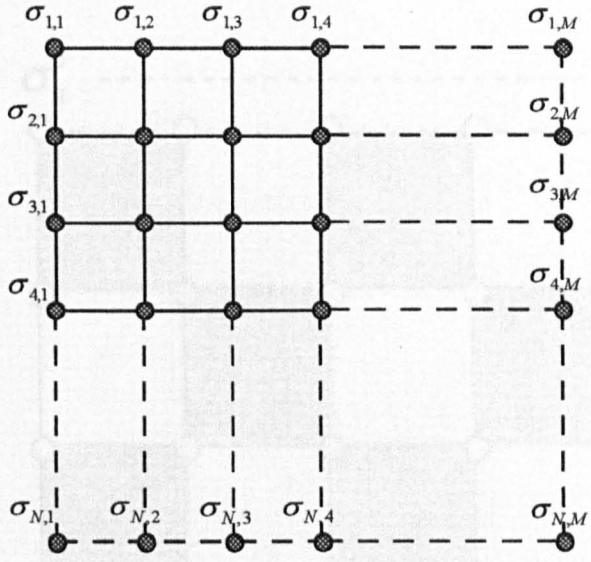

Fig 2.1

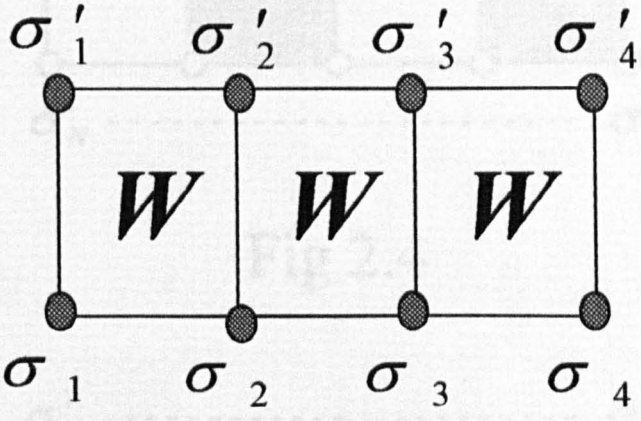

Fig 2.2

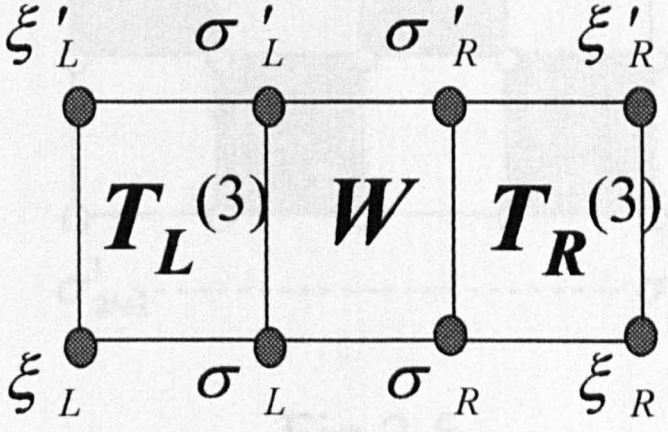

Fig 2.3

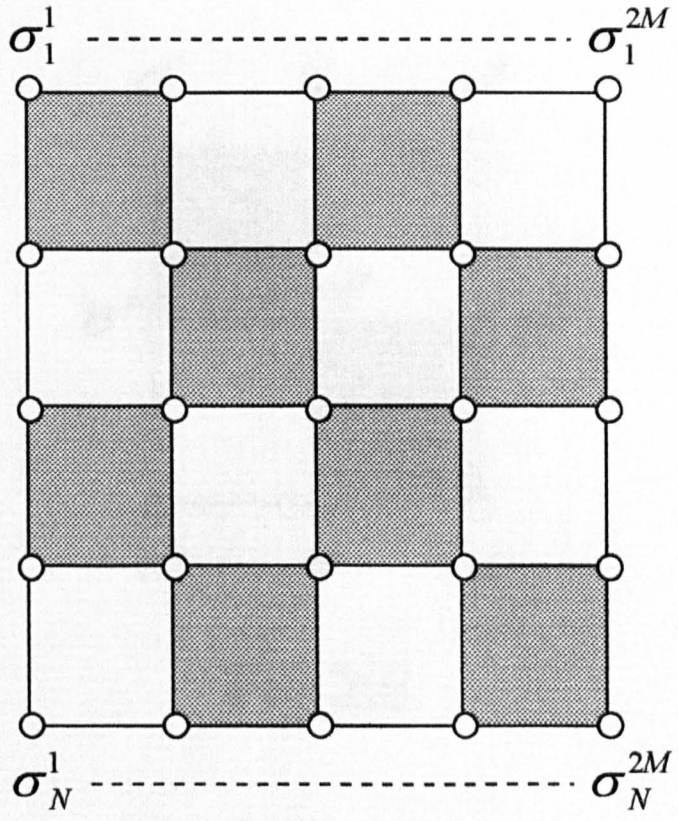
σ_1^1
σ_1^{2M}
σ_N^1
σ_N^{2M}

Fig 2.4

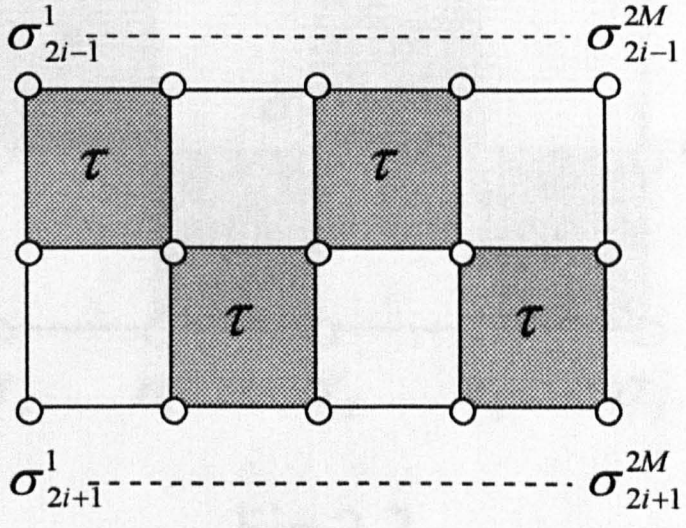
σ_{2i-1}^1
σ_{2i-1}^{2M}
τ
τ
τ
τ
σ_{2i+1}^1
σ_{2i+1}^{2M}

Fig 2.5

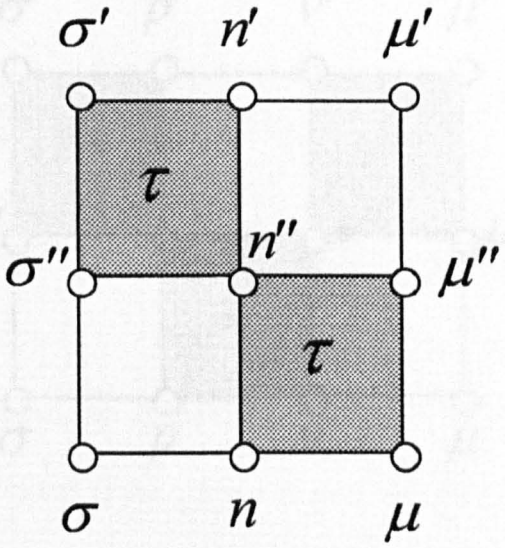

Fig 2.6

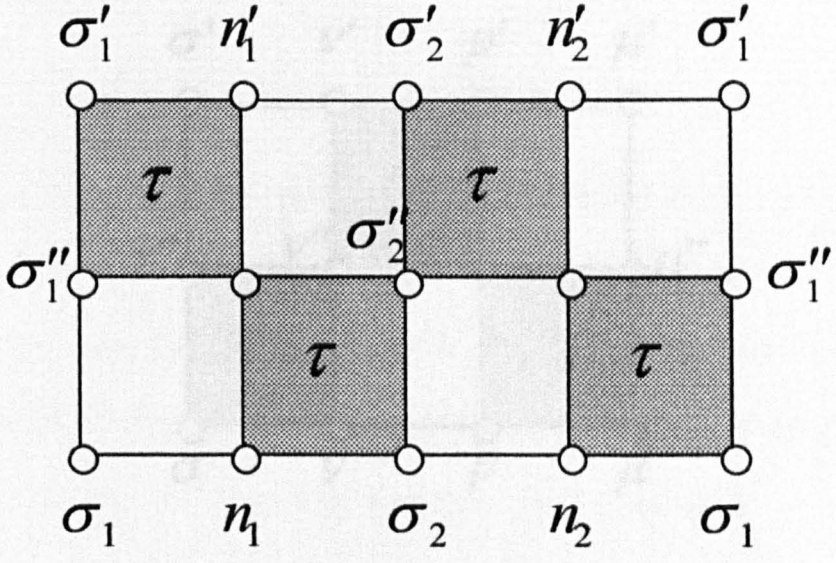

Fig 2.7

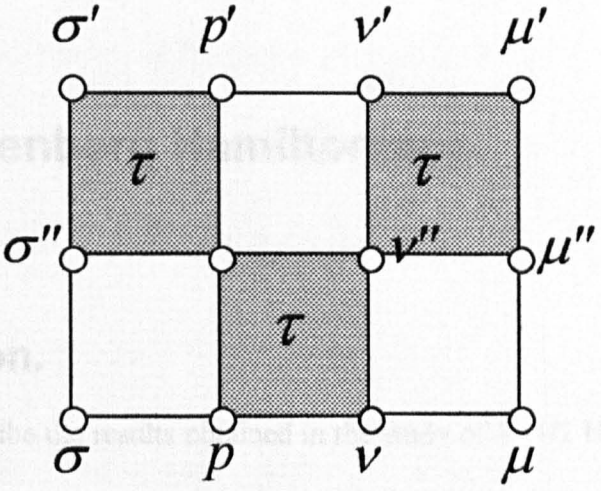

Fig 2.8

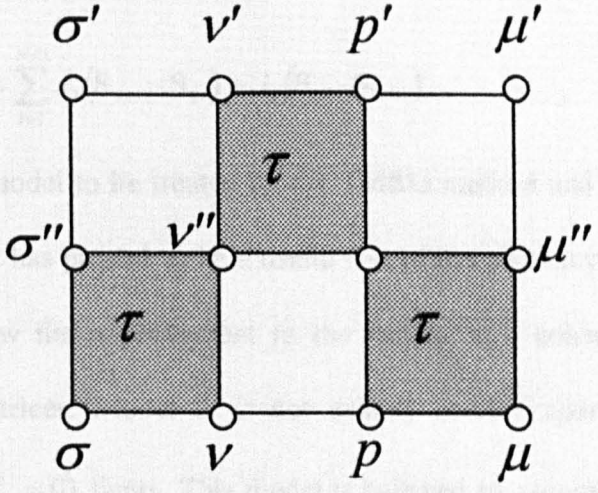

Fig 2.9

3. S=1/2 Heisenberg Hamiltonians.

3.1 Introduction.

In this chapter we describe the results obtained in the study of S=1/2 Heisenberg models using the DMRG at T=0 and the TMRG at finite temperatures. The Hamiltonians considered are

1. Dimerised X-Y model

$$H = \sum_{i=1}^{N/2} J_1\left(S_{2i-1}^x S_{2i}^x + S_{2i-1}^y S_{2i}^y\right) + J_2\left(S_{2i}^x S_{2i+1}^x + S_{2i}^y S_{2i+1}^y\right) \tag{3.1}$$

2. Alternating Heisenberg model

$$H = \sum_{i=1}^{N/2} J_1\left(\mathbf{S}_{2i-1} \cdot \mathbf{S}_{2i}\right) + J_2\left(\mathbf{S}_{2i} \cdot \mathbf{S}_{2i+1}\right) \tag{3.2}$$

Model 1. was the first model to be treated by the TMRG method and is exactly soluble at all temperatures. As such it has proved to be a useful test of the accuracy of the TMRG method. In this chapter we show the improvement to the results as a consequence of introducing *asymmetric* density matrices. Model 2. is not exactly soluble apart from in the uniform $\left(J_1 = J_2\right)$ and dimer $\left(J_2 = 0\right)$ limits. This model is believed to accurately model a number of quasi one dimensional systems and as such the results can be directly compared with experiment.

3.2 Dimerised *X-Y* model

The dimerised *X-Y* model is described by equation (3.1) or in terms of α, the alternation parameter

$$H = J\sum_{i=1}^{N/2}\left(S_{2i-1}^{x}S_{2i}^{x} + S_{2i-1}^{y}S_{2i}^{y}\right) + \alpha\left(S_{2i}^{x}S_{2i+1}^{x} + S_{2i}^{y}S_{2i+1}^{y}\right) \tag{3.3}$$

where $J = J_1$ and $\alpha = J_2/J_1$.

As already mentioned this model is exactly soluble [1] and its thermodynamics can be obtained from the free energy given by

$$F = -\frac{1}{2\pi\beta}\int_{0}^{2\pi}\ln\left(2\cosh\frac{\beta\phi(\theta)}{4}\right)d\theta \tag{3.4}$$

where $\beta = 1/kT$, $\phi(\theta) = \cos\xi(\theta) + \alpha\cos\left(\theta + \xi(\theta)\right)$ and $\xi(\theta) = -\tan^{-1}\dfrac{\alpha\sin\theta}{1+\alpha\cos(\theta)}$.

As a test of the T=0 DMRG algorithms discussed, we have calculated the ground state energy and energy gap to the first excited state. Although the Hamiltonian contains no z-component of spin, we can still work within a basis in which S^z is diagonal. As H conserves S^z, the superblock can be block diagonalised in this basis. This symmetry of the superblock is utilised when finding the ground state target wave function of the superblock which is calculated using the Lanczos or conjugate gradient methods (see Appendix 1). If a single superblock state is targeted, as is the case in our calculations, then the density matrix ρ is also block diagonal and this symmetry was also exploited in our code.

The table below shows the ground state energy per bond of the ground state as a function of α for different values of *m* the number of retained states in the system and environment

blocks and also the lattice size required to converge to the given accuracy for the $m = 32$ case.

α	m=8	m=16	m=32	L	Exact
0.1	-0.25062539160	-0.25062539160	-0.25062539160(5)	10	-0.25062539228
0.2	-0.252506313(4)	-0.25250631349	-0.25250631349(6)	14	-0.25250631482
0.3	-0.25565737(5)	-0.2556573787(3)	-0.25565737873(0)	18	-0.25565738066
0.4	-0.2601042(4)	-0.2601042715(5)	-0.26010427155(9)	22	-0.26010427406
0.5	-0.265885(8)	-0.2658861023(2)	-0.26588610249(3)	30	-0.26588610553
0.6	-0.27305(8)	-0.273059643(6)	-0.27305964588(7)	34	-0.27305964942
0.7	-0.2817(0)	-0.28170714(5)	-0.2817071668(6)	42	-0.2817071708
0.8	-0.2919(4)	-0.2919521(4)	-0.291952376(3)	62	-0.291952381
0.9	-0.303(9)	-0.30399(8)	-0.304000(2)	84	-0.304000233
1.0	-0.31(8)	-0.3182(6)	-0.31830(1)	164	-0.31830989

The convergence of the ground state energy for the uniform case $(\alpha = 1)$ is plotted in figure 3.1 as a function of the lattice size L and as functions of $1/L$ and $1/L^2$. This shows the small size dependence which appears to be of the form $E_0(L) \approx E_0(\infty) + \frac{a}{L^2}$ with $E_0(\infty) = -0.318308$ and $a = 0.1322878$

Similarly for the first excited state the energy per bond is shown in the table below.

α	m=8	m=16	m=32
0.1	-0.250625(7)	-0.250625(6)	-0.250625(6)
0.2	-0.25250(6)	-0.252507(0)	-0.252506(9)
0.3	-0.2556(5)	-0.255658(5)	-0.255658(4)
0.4	-0.260(0)	-0.26010(5)	-0.260105(8)
0.5	-0.265(8)	-0.26588(8)	-0.265888(4)
0.6	-0.272(9)	-0.27306(1)	-0.273063(0)
0.7	-0.28(1)	-0.28170(4)	-0.281712(2)
0.8	-0.29(1)	-0.2919(3)	-0.291960(3)
0.9	-0.30(3)	-0.3039(4)	-0.30401(3)
1.0	-0.31(8)	-0.3182(5)	-0.31832(9)

Again, in figure 3.2 we plot the size dependence of the energy and it is well fitted by $E_0(L) \approx E_0(\infty) - \frac{a}{L^2}$ with $E_0(\infty) = -0.318306$ and $a = 1.423991$. The convergence to the thermodynamic limit is seen to be much slower than in the ground state. We have also calculated the energy gap between the ground and first excited states shown in the table below. For this model, the ground state is a singlet and the first excited state a triplet. The

energy gap is therefore given by the difference between the lowest lying eigenvalues of the Hamiltonian in the $S^z = 0$ and $S^z = 1$ subspaces for $L = 100$.

α	$m = 16$	$m = 32$	Exact
0.1	0.45005	0.45003	0.45
0.2	0.40009	0.40008	0.40
0.3	0.35015	0.35013	0.35
0.4	0.30023	0.30019	0.30
0.5	0.25037	0.25028	0.25
0.6	0.20071	0.20040	0.20
0.7	0.15173	0.15059	0.15
0.8	0.10498	0.10098	0.10
0.9	0.06484	0.05222	0.05
1.0	0.01795	0.00936	0.00

To estimate the size dependence of the gap we show in figure 3.3 the gap as a function of L, $1/L$ and $1/L^2$. The scaling behaviour is seen to change from $\sim 1/L$ form in the uniform case to a $1/L^2$ form in the highly dimerised case. The extrapolated gaps are shown below for the slowest converging cases.

α	ΔE ($L \to \infty$)	ΔE (exact)

0.9	0.05(0)	0.05
1.0	0.001(4)	0.0

From these results we can draw some conclusions about the convergence properties of the DMRG method. It is seen that the results for both the ground state energy and the energy gap are much more accurate and converge to the thermodynamic limit when the energy gap is large. The reason for this is twofold. Firstly, when there is a large gap, the target wave function is well separated from the next highest energy eigenstate of the superblock and so can be calculated more accurately by the sparse matrix algorithms used in the calculations. Secondly, when the system is gapless, it is in some sense at a critical point, and hence large lattices are required to accurately describe its thermodynamic properties. This necessitates many DMRG iterations and hence introduces larger truncation and accumulated round-off errors in the calculation. Also, as is the case when calculating energy gaps by other methods such as exact diagonalization, the gap is generally not obtained to the same accuracy as the energies themselves as the absolute errors add giving a larger relative error in ΔE. We have also seen that if the finite size scaling behaviour can be determined for a particular quantity, then its thermodynamic limit value can be more accurately determined by extrapolation. The functional form of the size-scaling of the energy gap can also be understood qualitatively by considering the nature of the excitations in the gapped and gapless cases. For gapless system, the long wavelength excitations have a dispersion relation of the form $E(k) \sim k$, and will have a wavelength of the order of the lattice size, L. The energy gap from the ground state will therefore scale like $1/L$. Gapped systems, however, have a dispersion relation of the form

$E \sim \Delta + k^2$. The energy gap to the first excited state will therefore scale like $\Delta + 1/L^2$. This is the scaling behaviour we have observed.

Bursill, Xiang and Gehring (BXG) [2] calculated the thermodynamics of this system using the TMRG method. We will now consider a number of subsequent improvements to this technique. BXG only calculated the right eigenvector of the superblock and used the projection operator $|\psi^R\rangle\langle\psi^R|$ to calculate the density matrix elements. As described in the previous chapter we have calculated both the left and right superblock eigenvectors by means of a power method and the Arnoldi algorithm and used the projection operator $|\psi^R\rangle\langle\psi^L|$ to produce an asymmetric density matrix. The added difficulty involved when dealing with asymmetric matrices is discussed in Appendix 1. We have also considered the symmetry properties of the transfer matrix. Consider the local transfer matrix which is related to the local Hamiltonian by

$$\tau\left(\sigma_1^1\sigma_1^2|\sigma_2^1\sigma_2^2\right) = \left\langle\sigma_1^1\sigma_2^1\left|e^{-\beta h/M}\right|\sigma_1^2\sigma_2^2\right\rangle \tag{3.5}$$

As h conserves the z-component of spin, the following conservation law holds

$$\sigma_1^1 + \sigma_2^1 = \sigma_1^2 + \sigma_2^2 \tag{3.6}$$

If we make a change of basis $\tilde{\sigma}_j^i = (-1)^{i+j}\sigma_j^i$ then from equation (3.6) we have

$$\tilde{\sigma}_1^1 - \tilde{\sigma}_2^1 = -\tilde{\sigma}_1^2 + \tilde{\sigma}_2^2 \tag{3.7}$$

or

$$\tilde{\sigma}_1^1 + \tilde{\sigma}_1^2 = \tilde{\sigma}_2^1 + \tilde{\sigma}_2^2 \tag{3.8}$$

Transforming τ into this basis means that it is diagonal in $\tilde{\sigma}^z$. This conservation law is true for the superblock transfer matrix as a whole and so it may be block diagonalised greatly reducing the size of the matrices needing to be treated.

Another development of the method is that BXG calculated the free energy of the system and then calculated the internal energy as a numerical first derivative and the specific heat as a second derivative. As numerical differentiation has associated errors it is better to calculate the internal energy directly. This done by evaluating the quantity $\langle H \rangle / N$, where $\langle \cdots \rangle$ denotes a thermal average. This is achieved by constructing a superblock matrix U_H, replacing one of the local transfer matrices by the operator

$$\tau_h\left(\tilde{\sigma}_i^j \tilde{\sigma}_i^{j+1} \middle| \tilde{\sigma}_{i+1}^j \tilde{\sigma}_{i+1}^{j+1}\right) = \left\langle \tilde{\sigma}_i^j \tilde{\sigma}_{i+1}^j \middle| he^{-\beta h/M} \middle| \tilde{\sigma}_i^{j+1} \tilde{\sigma}_{i+1}^{j+1} \right\rangle \tag{3.9}$$

and then evaluating $\langle \psi^L | U_H | \psi^R \rangle / \lambda$ to give the internal energy. This can then be numerically differentiated to give the specific heat.

Similarly, the magnetisation of the system can be obtained by constructing the superblock transfer matrix M_z constructed by replacing one of the τ by the operator

$$\tau_z\left(\tilde{\sigma}_i^j \tilde{\sigma}_i^{j+1} \middle| \tilde{\sigma}_{i+1}^j \tilde{\sigma}_{i+1}^{j+1}\right) = \left\langle \tilde{\sigma}_i^j \tilde{\sigma}_{i+1}^j \middle| \frac{1}{2}\left(\tilde{\sigma}_i^{j+1} - \tilde{\sigma}_{i+1}^{j+1}\right) e^{-\beta h/M} \middle| \tilde{\sigma}_i^{j+1} \tilde{\sigma}_{i+1}^{j+1} \right\rangle \tag{3.10}$$

(where the minus sign in the operator is a result of the basis change in equation(3.7)) and then evaluating the magnetisation $\langle \sigma^z \rangle$ from $\langle \psi^L | M_z | \psi^R \rangle / \lambda$. By adding a small field term $B \sum_i \sigma_i^z$ to the Hamiltonian, the susceptibility can be determined from $\chi = \langle \sigma^z \rangle / B$.

Figure 3.4 show the free energy, internal energy and specific heat for the three cases $\alpha = 1.0$, 0.5 and 0.1 representing the uniform system and intermediate and strong dimerisation. The free energy is obtained to an accuracy of ~ 1 part in 10^6 for $\alpha = 0.1$ and ~ 1 part in 10^4 for $\alpha = 1.0$ for $m = 32$, $\beta_0 = 0.05$. The specific heat is also accurately reproduced and shows characteristic exponential low temperature behaviour in the gapped cases and algebraic behaviour in the uniform, gapless system. The introduction of asymmetric transfer and density matrices produces a marked improvement in the results compared with those of BXG, especially at lower temperatures. As with the zero temperature DMRG calculations, the results are most accurate in the gapped case. Only the low temperature region of the specific heat in the $\alpha = 1$ case suffers from any appreciable error which is due to errors in numerically differentiating the internal energy as well as inaccuracies in the TMRG. method Now that the accuracy and convergence properties of the DMRG and TMRG methods have been discussed, we move onto tackling a model which is not exactly soluble.

3.3 Alternating Chain Heisenberg Model.

The alternating chain Heisenberg model is described by the Hamiltonian (3.2) or, in terms of the alternation parameter α,

$$H = J\sum_{i=1}^{N/2} \left(\mathbf{S}_{2i-1} \cdot \mathbf{S}_{2i}\right) + \alpha\left(\mathbf{S}_{2i} \cdot \mathbf{S}_{2i+1}\right) \tag{3.11}$$

where $J = J_1$ and $\alpha = J_2/J_1$. This model is exactly soluble only in the limits $\alpha = 0$ and $\alpha = 1$. The Hamiltonian arises in two classes of quasi 1D compounds which will be discussed later. Previous work on this model has mainly been concerned with

a) Exact diagonalization of small chains and then extrapolating to the thermodynamic limit using some form of finite size scaling [3,4].

b) Perturbation theory using α as a perturbation away from dimer theory [5].

c) Bosonization in the continuous field limit [6].

We will compare our DMRG methods with previous studies and hopefully show it to be an accurate and competitive computational tool. We will consider first the case where both J and α are positive and hence both interactions favour antiferromagnetism and refer to this as the AF/AF chain.

3.3.1 AF/AF Heisenberg Chain.

For all α, the AF/AF has a singlet ground state and for all $\alpha \neq 1$ there is a finite energy gap to a triplet state. We have calculated the ground state energy per bond using the DMRG method on open chains of up to $L = 200$ keeping 64 states in the system and environment blocks at each iteration. The results show quick convergence for all α with only the uniform case showing any significant size dependence. Figure 3.5 shows the uniform case plotted as a function of $L, 1/L$ and $1/L^2$. The ground state energy is well fitted by $E(L) = -0.4431460 + \frac{0.1086}{L^2}$ which is correct to $\sim 3 \times 10^{-6}$ compared with the Bethe Ansatz result $1/4 - \ln 2 = -0.44314718$. The energy per bond of the first excited state is also shown in figure 3.6 and is seen to converge more slowly than the ground state. The size dependence for the uniform case is fitted by $E(L) = -0.4431244 - \frac{3.657711}{L^2}$. The energy gap has also been calculated (figure 3.7) . Again, an open chain of 200 sites appears to reach the thermodynamic

limit except in the uniform case, where the gap is fitted by $0.00276+\frac{3.575}{L}$. As a comparison we show our results below along with those of Barnes et al [5] who have carried out exact diagonalisation on chains of up to 28 sites and then extrapolated to the thermodynamic limit.

α	E_0 (DMRG)	E_0 (ED)	ΔE (L=200) (DMRG)	ΔE (ED)
0.1	-0.37548080549	-0.375480805	0.94631	0.946279339
0.2	-0.37697449359	-0.376974494	0.88529	0.885209996
0.3	-0.37956632136	-0.379566321	0.81697	0.816844275
0.4	-0.38335625029	-0.383356250	0.74124	0.74106141
0.5	-0.38846561408	-0.388465614	0.65773	0.6574777
0.6	-0.39504842294	-0.395048423	0.56565	0.565296
0.7	-0.4033124321	-0.40331243	0.46350	0.46298
0.8	-0.413564585	-0.4135644	0.34831	0.3474
0.9	-0.426337689	-0.426330	0.21314	0.2098
1.0	-0.443146(0)	-	0.002(8)	-

The results for both the ground state and the gap are in excellent agreement with the exact diagonalisation results, the highest accuracy being obtained when the gap is large the reasons being the same as discussed before in relation to the convergence of the X-Y model.

We also show in figure 3.8 the comparison between our DMRG data and a ninth order perturbation expansion in α by Barnes et al for the ground state energy density and the energy gap [5]. Again very good agreement is observed especially for small α as would be expected as the perturbation expansion becomes less accurate further from the dimer limit.

Considering now the thermodynamics of this model, figure 3.9 shows the temperature dependence of the zero field spin susceptibility for varying α. All curves show a rounded maximum at $T \approx 0.6J$. The position of the peak is seen to be independent of α. The height of the peak is reduced as the uniform limit $(\alpha = 1)$ is approached. The low temperature behaviour shows an exponential decrease as $T \to 0$ for all $\alpha < 1$, characteristic of an energy gap. It would be interesting to determine an analytic form for the low temperature behaviour. The susceptibility of gapped systems are often modelled by an expression of the form $\chi \sim T^{\delta} e^{-\frac{\Delta}{T}}$ where Δ is the energy gap and δ is some power to be determined. A possible method of determining the parameters is to plot $\ln\left(\chi T^{-\delta}\right)$ against $1/T$ for various values of δ. The correct choice of δ should give a straight line in the $T \to 0$ limit whose gradient is $-\Delta$. However, it was found that the fit is not very sensitive to δ. In order to clarify the situation we can compare the values of Δ obtained from the fit with those of the DMRG method. Figure 3.10 (a) shows the comparison of the values of Δ obtained for fits with $\delta = -1/2$ and $\delta = -1$ with those of the zero temperature DMRG. These functional forms

appear to bound the $T = 0$ data. This is also reasonable as in the dimer limit $(\alpha = 0)$, the susceptibility has the form $\chi \sim \frac{1}{T} e^{-\frac{1}{T}}$, the energy gap in this case being exactly 1.

We can compare our susceptibility results with those of Hall et al [7] who fitted the susceptibility of 10 site rings to a function of the form $\chi \sim \frac{AT^2 + BT + C}{T^3 + DT^2 + ET + F}$ truncating the fit at T/J=0.5 . Figure 3.10 (b) shows the comparison of the results. The curves coincide most accurately for small α suggesting that the 10 site system closely approximates the thermodynamic limit in this region.

Considering now the specific heat, figure 3.11 shows this for various α . In this case both the peak position and peak height are α dependent. Again, exponential behaviour is observed in the low temperature region revealing the presence of an energy gap. Carrying out a similar fitting procedure as for the susceptibility, figure 3.12 (a) shows the energy gap as a function of α obtained by fitting Cv to a function of the form $\frac{1}{T^2} e^{-\frac{\Delta}{T}}$. These forms seem to reproduce the gap relatively accurately.

3.3.2 Comparison with experiment.

Two classes of experimentally realisable systems have been described by the alternating chain Heisenberg Hamiltonian. The first class, spin-Peierls compounds, generally also require the consideration of next-nearest-neighbour interactions which introduce frustration. This is currently beyond the scope of our TMRG method and hence will not be considered here. The second class of compounds consists of chains of magnetic ions that have two structurally

inequivalent exchange mechanisms which are of comparable strength and negligible interchain interaction. We consider the compound $(VO)_2P_2O_7$.

Until recently, $(VO)_2P_2O_7$ was believed to be a two leg spin ladder system consisting of pairs of chains of spins coupled along and perpendicular to the chain direction [8]. However, recent neutron scattering measurements were inconsistent with this model and 'VOPO' is now recognised to be a quasi 1-D alternating chain system [9]. The interchain interaction energy is estimated to be $\leq 0.02J$. In figure 3.12 (b), we compare susceptibility measurements made by Johnston et al [10] with our TMRG data for J=65.7K/k_B, g=2.0, α = 0.8. The procedure used for fitting the data is described in appendix 2. The fit is seen to be very good over the whole temperature range. The value of alternation parameter is in very good agreement with that obtained by Barnes et al [5] by comparing exact diagonalisation results with the magnon dispersion.

3.3.3 F/AF Heisenberg Chain

We have also considered the properties of the alternating chain Heisenberg model for values of $\alpha < 0$, that is for systems with spins alternately coupled ferromagnetically and antiferromagnetically, which is referred to as the F/AF chain. We have calculated the ground state energy density as well as the energy gap. Figure 3.13 shows these quantities. If we consider the limit $\alpha \to -\infty$, then pairs of spins couple into triplets i.e. S=1 objects and hence in this limit, the model becomes the S=1 uniform Heisenberg chain. In this limit we can consider a quasi-Neel state $|\uparrow\uparrow\downarrow\downarrow\uparrow\uparrow\downarrow\downarrow\rangle$ as a variational approximation to the ground state. In this case each ferromagnetic bond contributes an energy $-J\alpha/4$ and each

antiferromagnetic bond makes a contribution $-J/4$. This leads to an estimate of the average energy per bond of $-J(\alpha+1)/8$. Figure 3.14 (a) shows the ground state energy per bond for large α and the variational energy estimate of the Neel-like state which is seen to be an asymptotic upper-bound of the true energy. Obviously in this limit the ferromagnetic contribution dominates the ground state energy and so in order to more clearly see the connection between the F/AF chain and the isotropic S=1 chain we measure the bond strength across the antiferromagnetic bond. This is plotted in figure 3.14 (b) as a function of $1/\alpha$. The dotted line shows the DMRG value for the ground state of the S=1 chain (see Chapter 4) scaled by a factor of 4 to account for the S=1/2 Pauli matrices. The antiferromagnetic bond strength is seen to tend to this value as $\alpha \to \infty$. Figure 3.14 (c) shows the energy gap as a function of $1/\alpha$, the point at $\alpha = 0$ being the value of the gap obtained by the DMRG (Chapter 4) for the spin 1 chain, again divided by a factor of 4.

Figures 3.15 and 3.16 show the susceptibility and specific heat for various α. Again, exponential low temperature behaviour indicates the presence of a gap.

The compound $(CH_3)_2CHHNH_3CuCl_3$ is believed to be described by this Hamiltonian. The Cu ions form dimers which are arranged stepwise leading to different exchange integrals. Due to the difference in bond angles, the exchange favours alternately ferromagnetic and antiferromagnetic interactions. We have compared our TMRG data with susceptibility measurements by Manaka, Yamada and Yamaguchi [11] (figure 3.17). We see good agreement for J=49K/k_B, g=2.13, $\alpha \approx 2.3$. The gap estimated from the zero temperature DMRG is ~0.384J which gives a gap for $IPACuCl_3$ of 18.8K/k_B which is in excellent agreement with Manaka et al's estimate.

3.4 References

[1] Bulaevskii L N, Sov. Phys. -JETP, **17**, 1008 (1963)

[2] Bursill R J, Xiang T and Gehring G A, J. Phys. C, **8**, L583 (1996)

[3] Bonner J C, Friedberg S A, Kobayashi H, Meier D L and Blote H, Phys. Rev. B, **27**, 248 (1983)

[4] Barnes T and Riera J, Phys. Rev. B, **50**, 6817 (1994)

[5] Barnes T, *preprint* cond-mat/9801224

[6] Hida K, Phys. Rev. B, **45**, 2207, (1992)

[7] Hall J W, Marsh W E, Weller R R and Hatfield W E, Inorg. Chem., **20**, 1033 (1981)

[8] Johnston D C, Johnson J W, Goshorn D P and Jacobson A J, Phys. Rev. B, **35**, 219 (1987)

[9] Garrett A W, Nagler S E, Tennant_D A, Sales D A and Barnes T, Phys. Rev. Lett., **79**, 745 (1997)

[10] Johnston et al, *preprint*

[11] Manaka H, Yamada I and Yamaguchi K, J. Phys. Soc. Japan, **60**, 564 (1997)

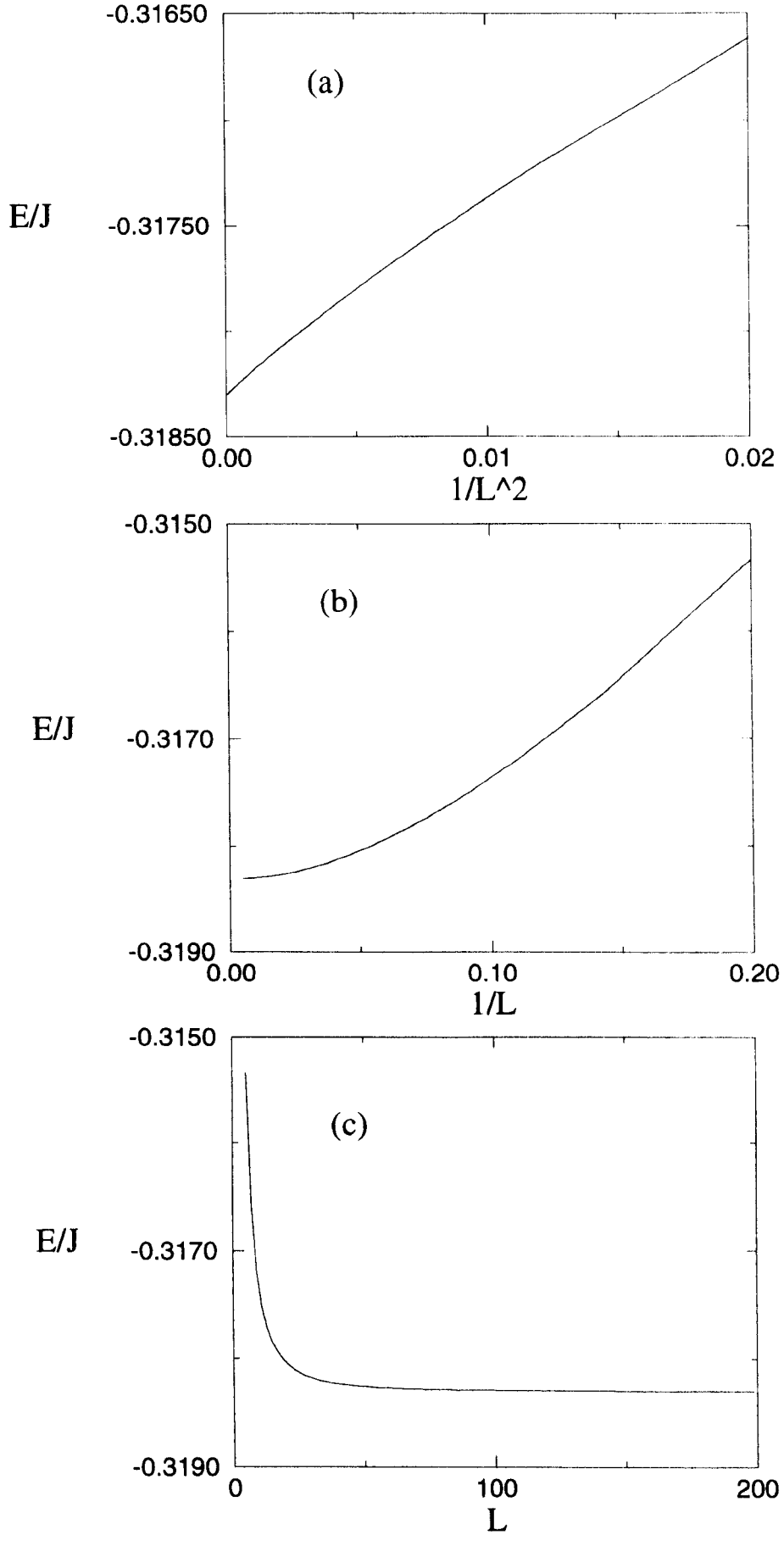

Fig 3.1 Ground state energy per bond of isotropic XY model as a function of (a) 1/L^2 (b) 1/L (c) L.

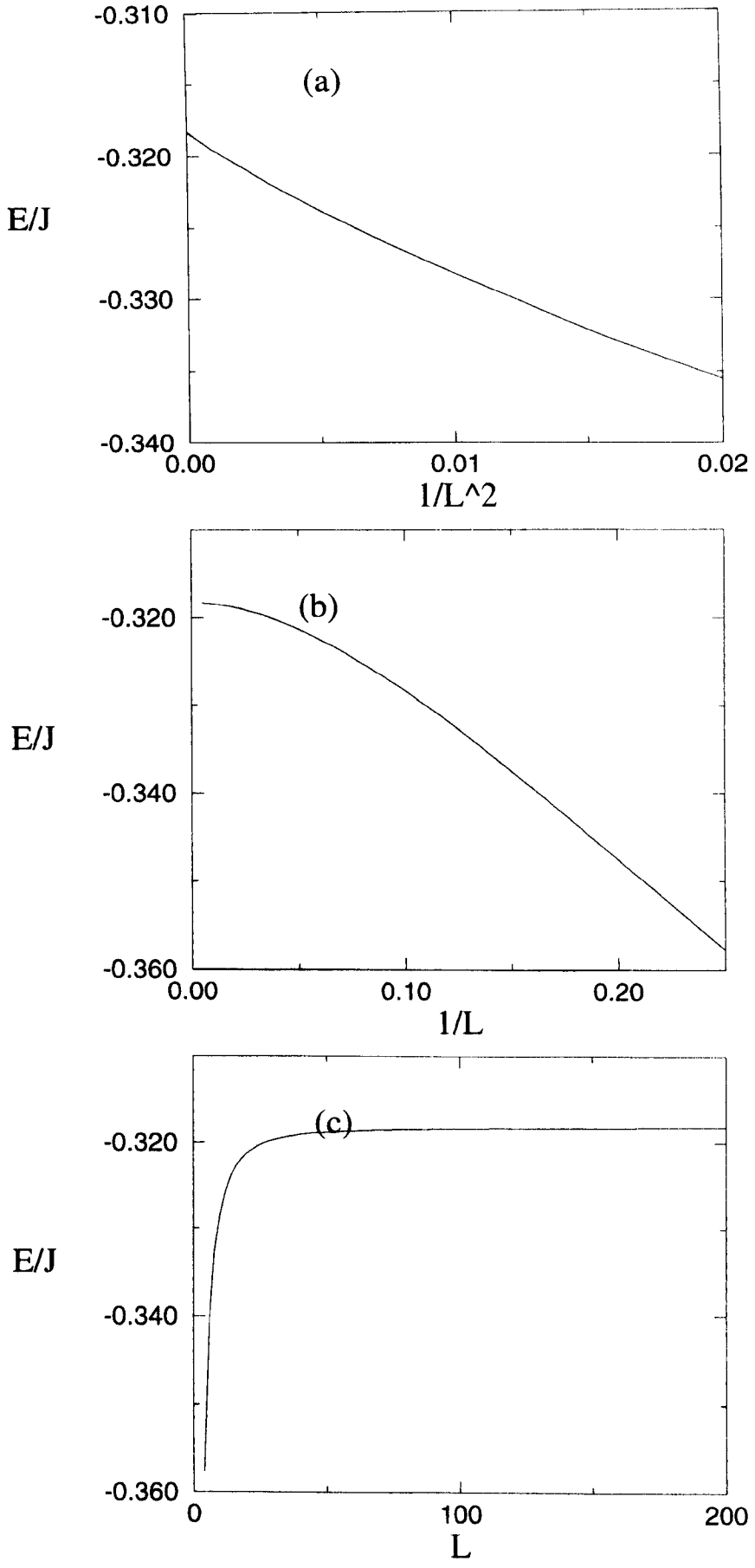

Fig 3.2 First excitation energy per bond of isotropic XY model as a function of (a) 1/L^2 (b) 1/L (c) L

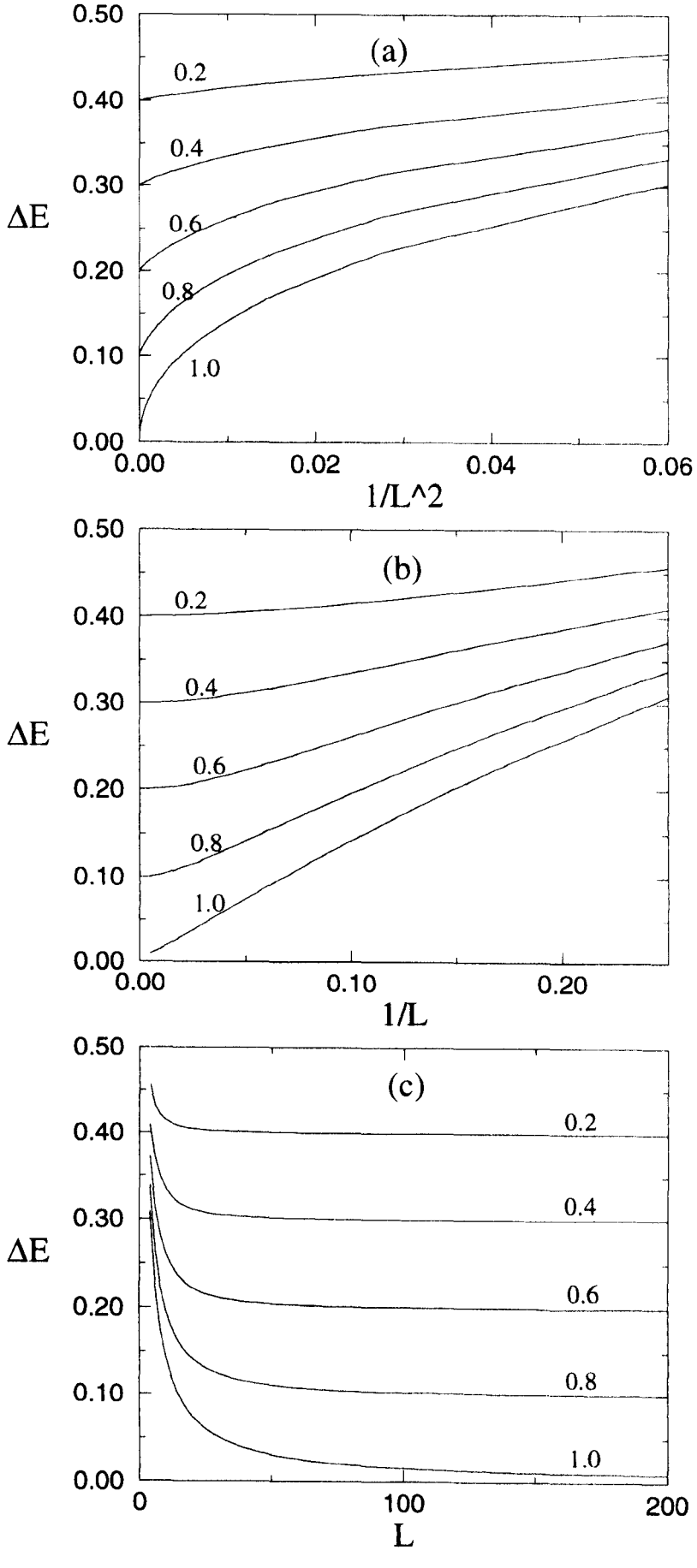

Fig 3.3 Energy gap for dimerised X-Y model for varying α as a function of (a) 1/L^2 (b) 1/L (c) L.

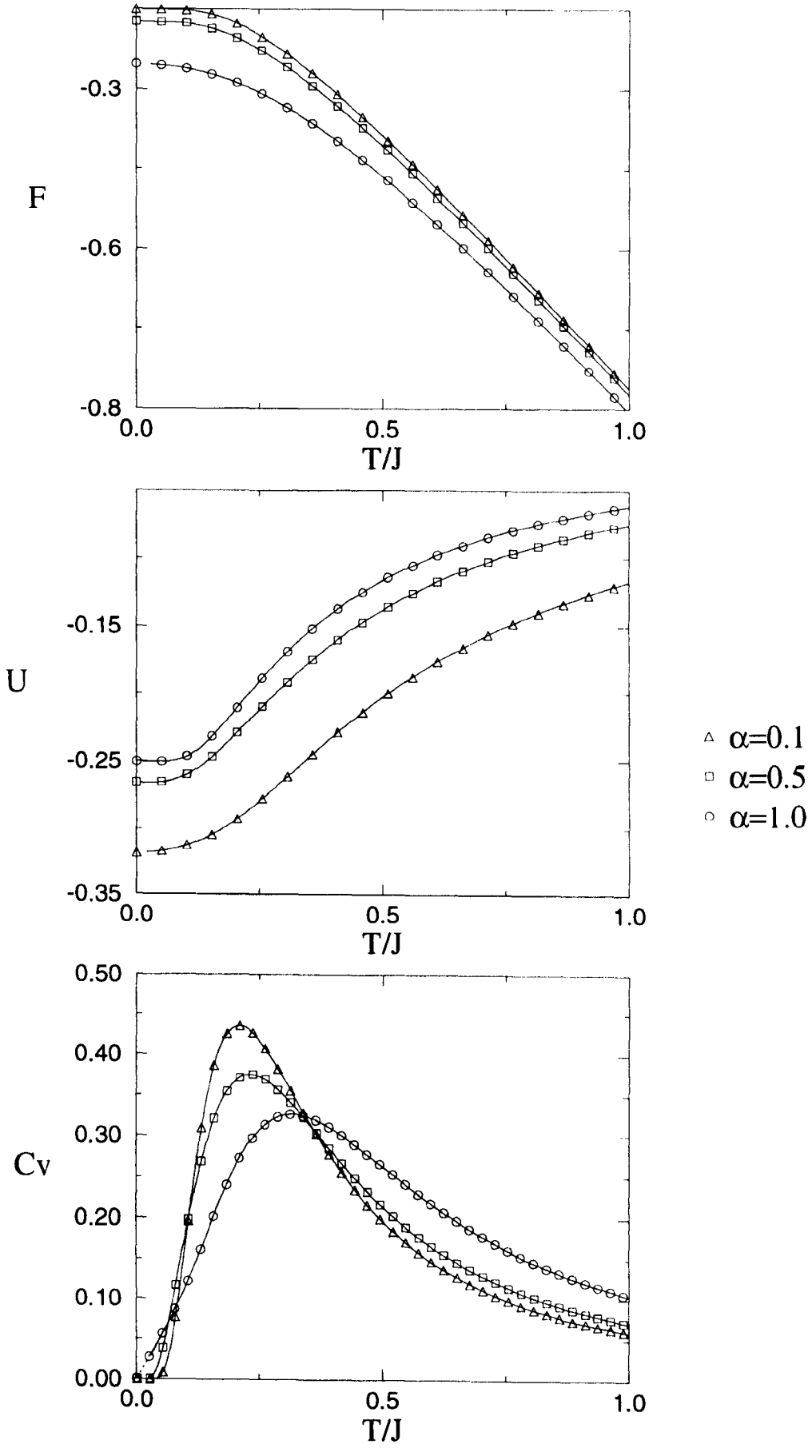

Fig 3.4 Temperature dependence of (a) free energy (b) internal energy and (c) specific heat. Symbols indicate exact result.

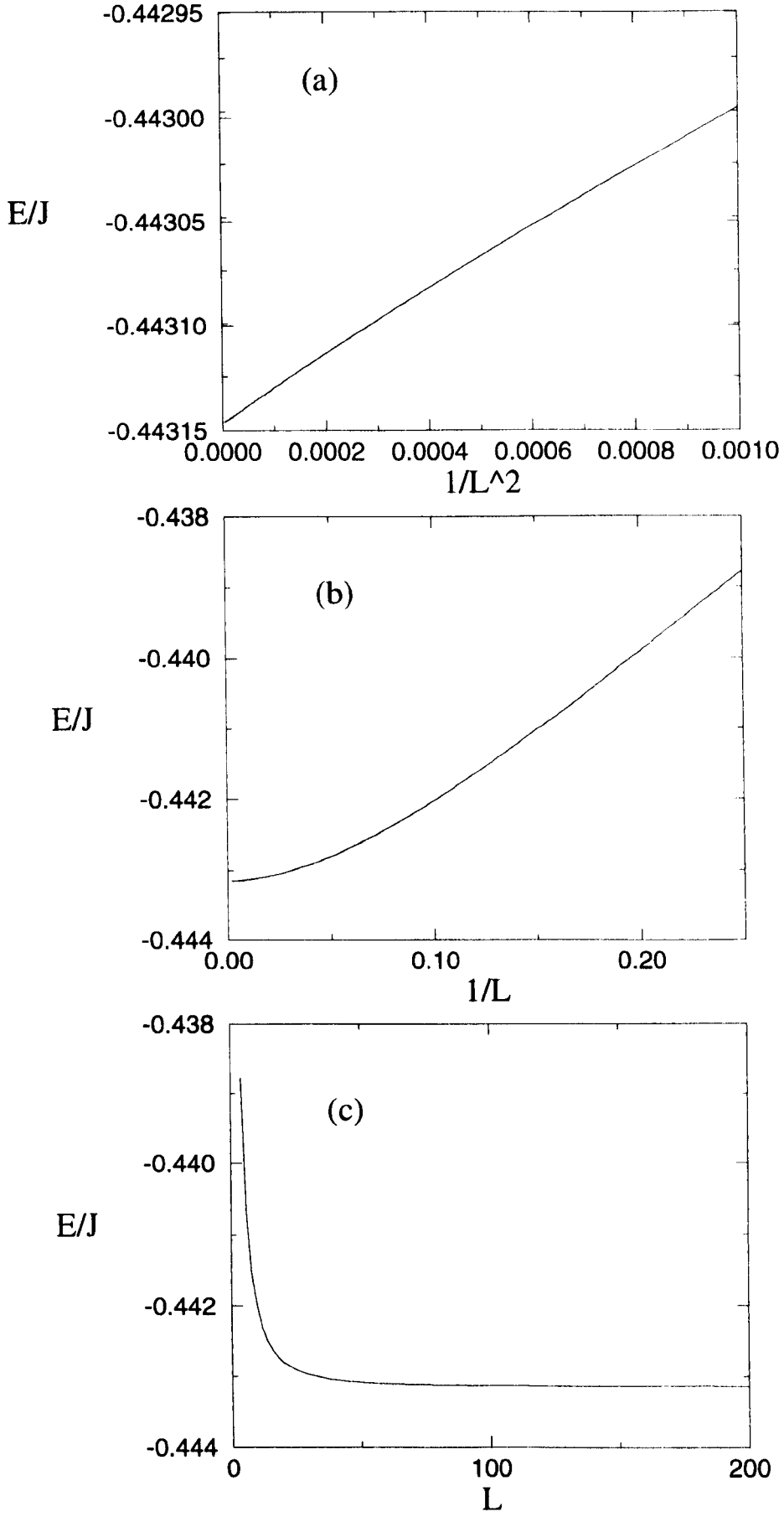

Fig 3.5 Ground state energy per bond of isotropic Heisenberg model as a function of (a) 1/L^2 (b) 1/L (c) L.

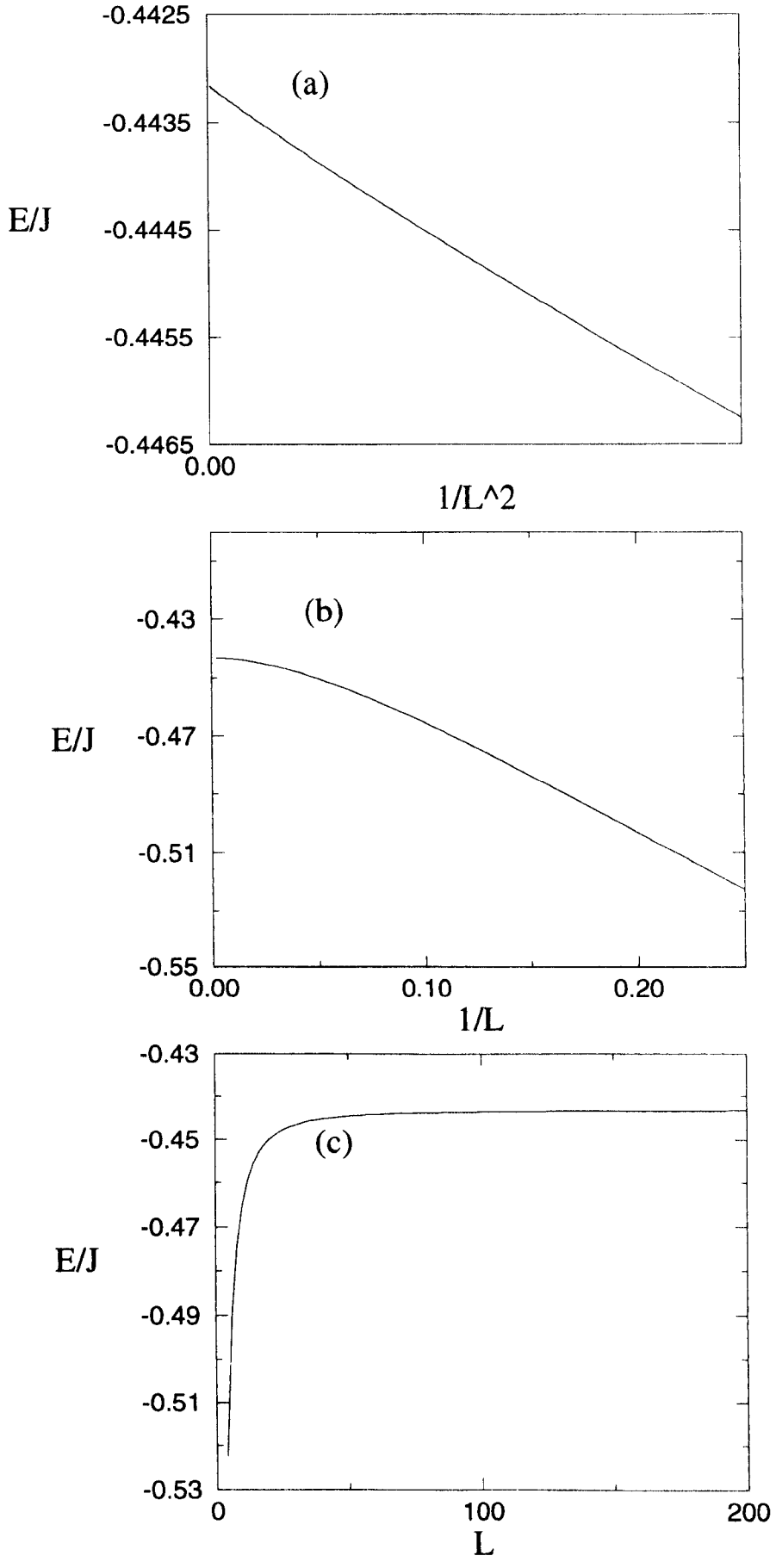

Fig 3.6 First excitation energy per bond of isotropic Heisenberg model as a function of (a) 1/L^2 (b) 1/L (c) L.

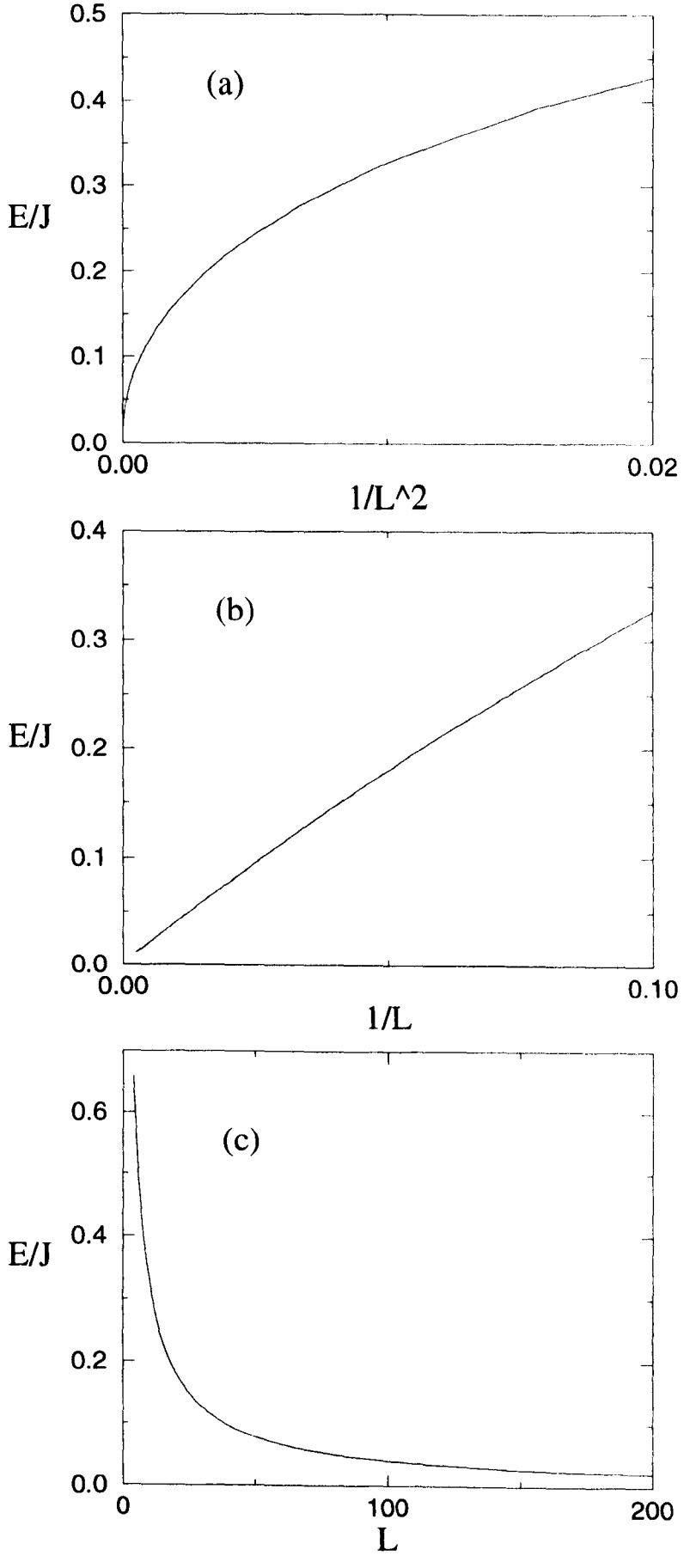

Fig 3.7 Energy gap for isotropic Heisenberg model as a function of (a) 1/L^2 (b) 1/L (c) L.

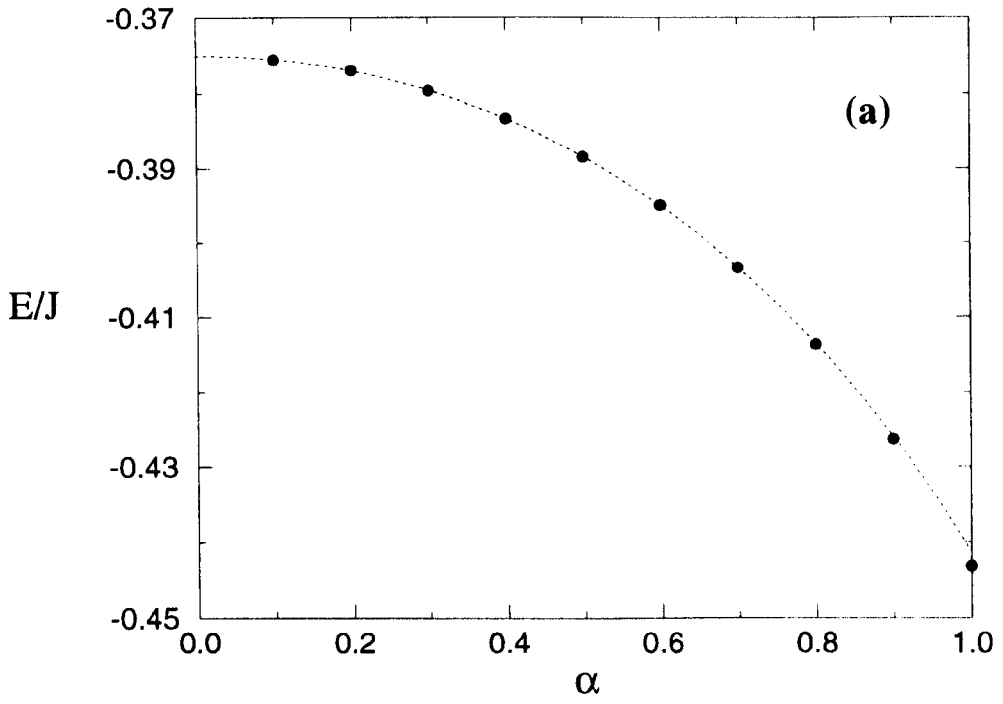

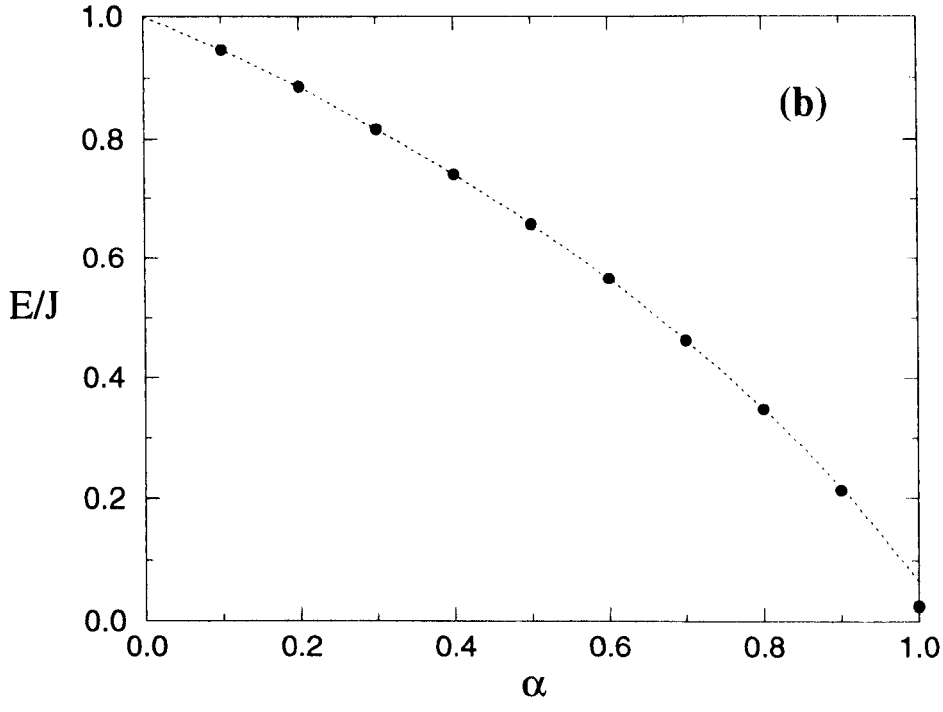

Fig 3.8 Comparison between DMRG (circles) and perturbation theory (dotted line) for (a) ground state energy and (b) energy gap.

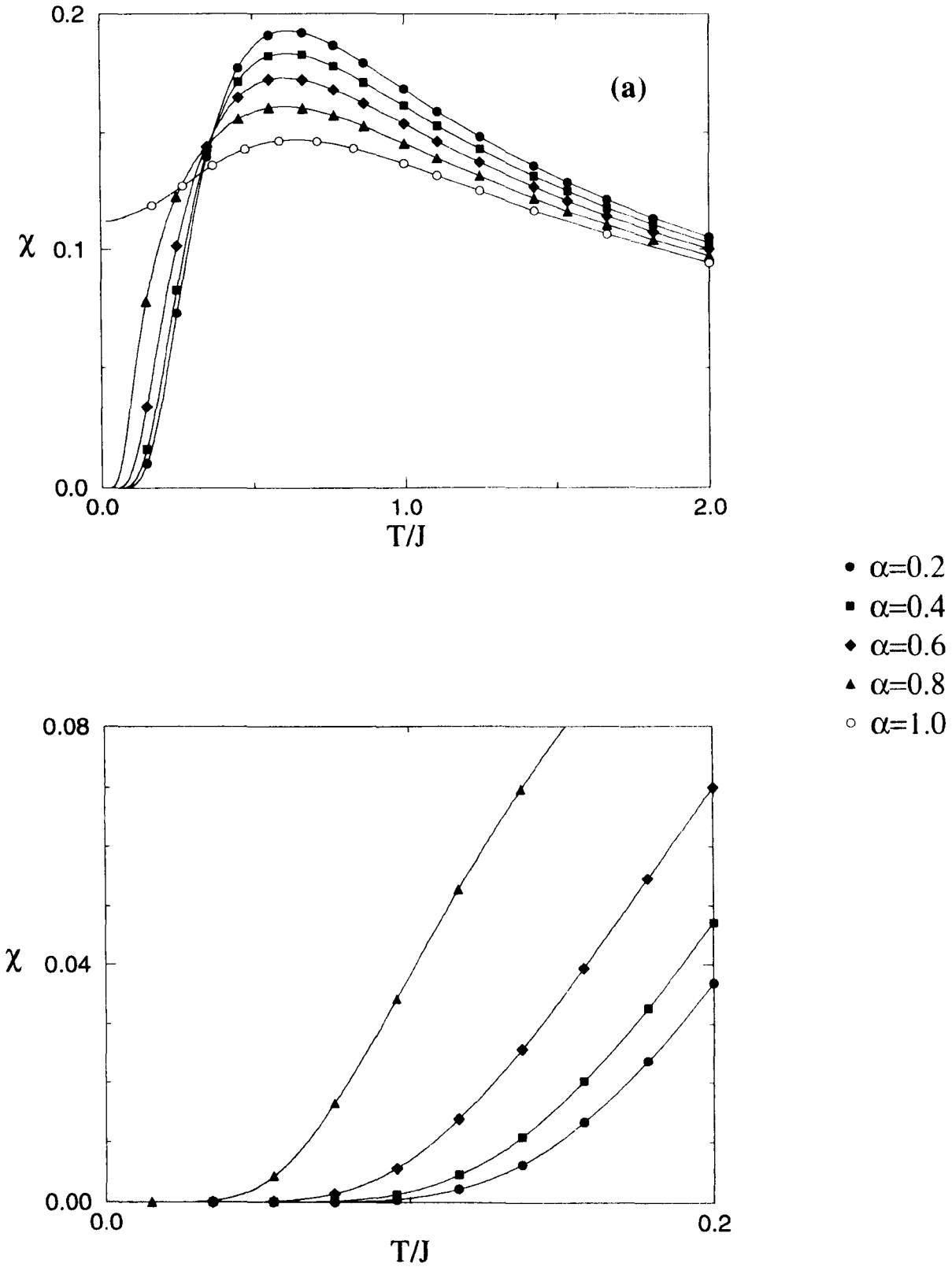

Fig 3.9 Temperature dependence of spin susceptibility for varying α

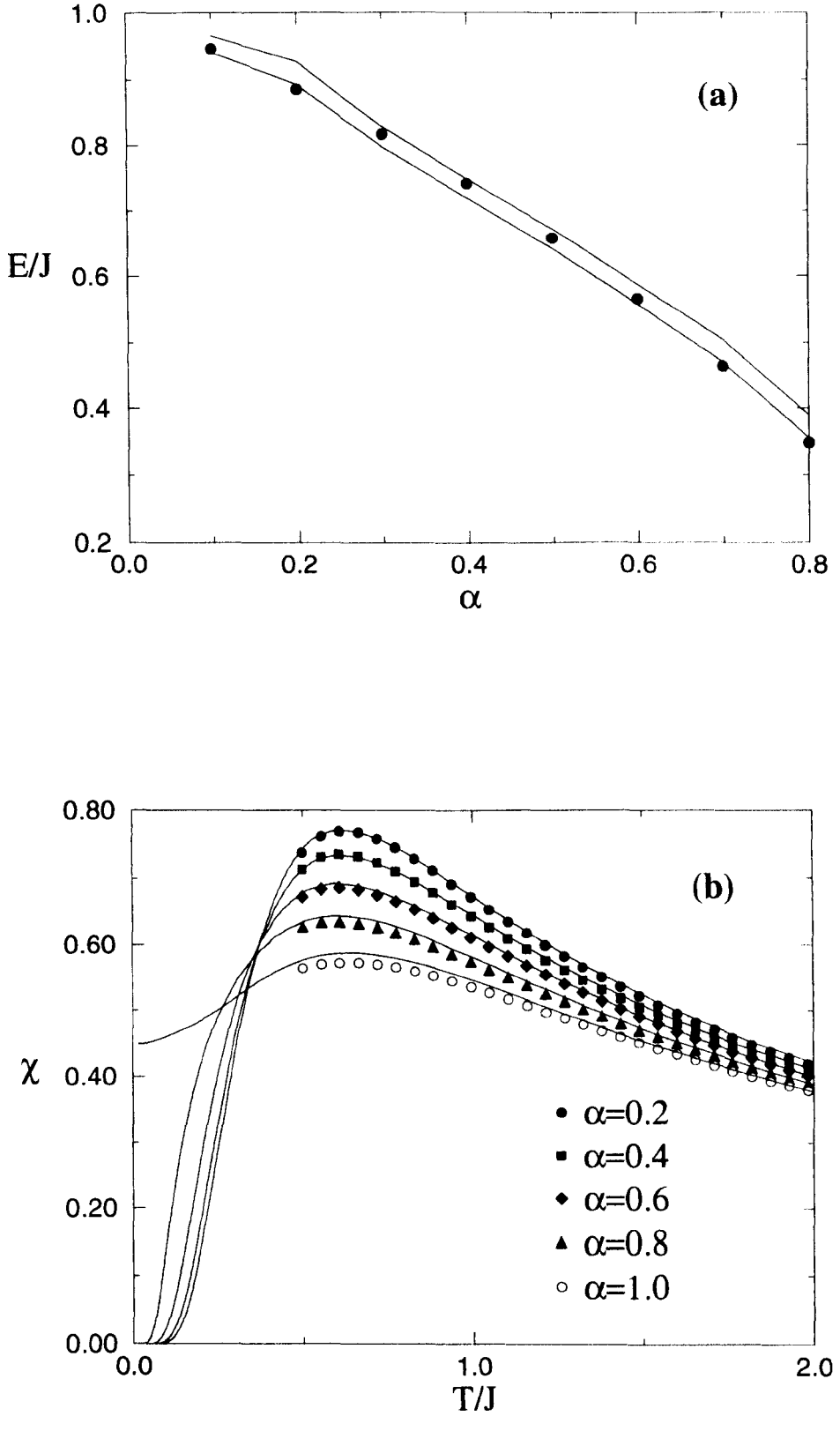

Fig 3.10 (a) Comparison of gap obtained from DMRG(circles) and TMRG (lines) (b) Comparison of TMRG with exact diagonalisation of 10 site ring.

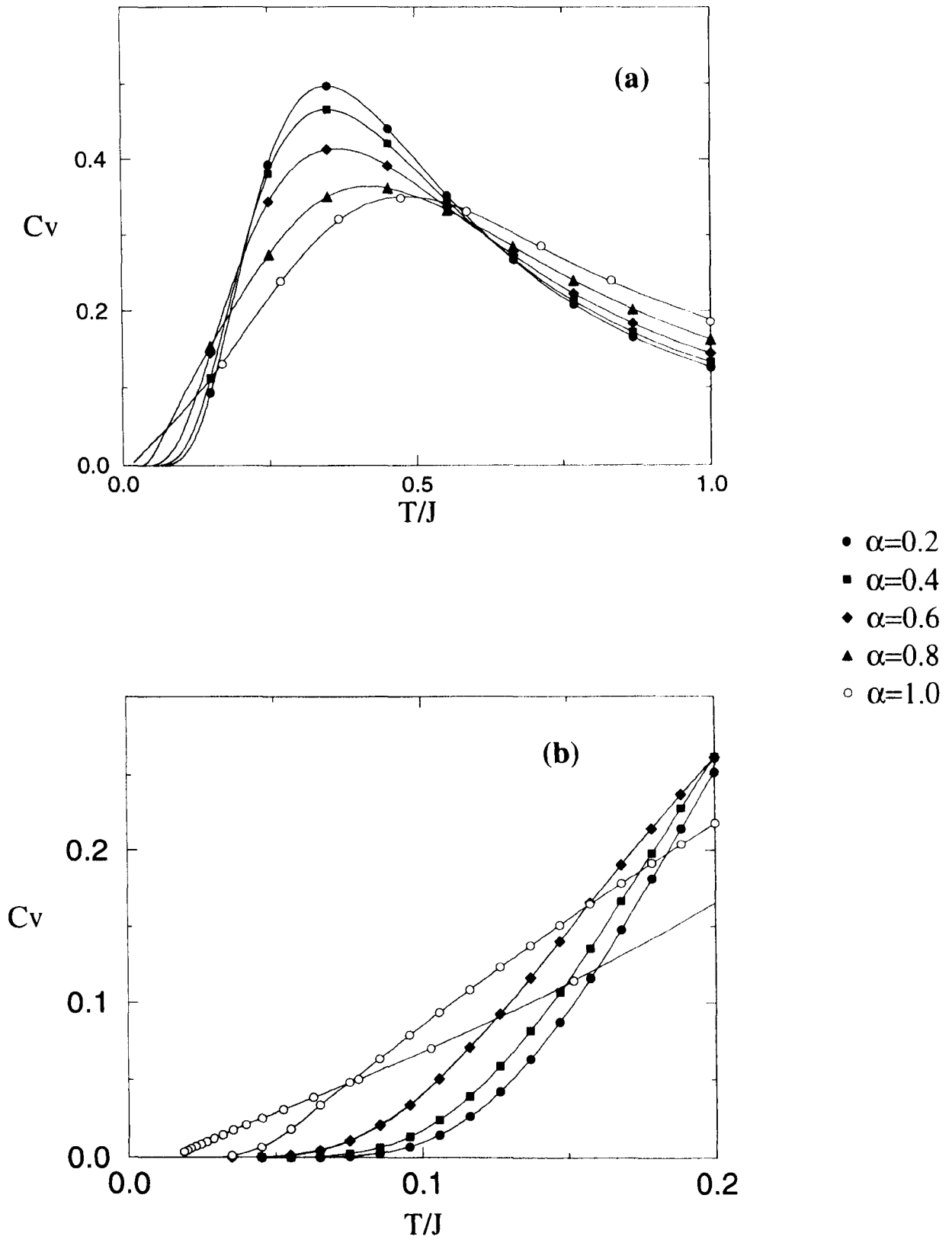

Fig 3.11 Temperature dependence of specific heat for varying α

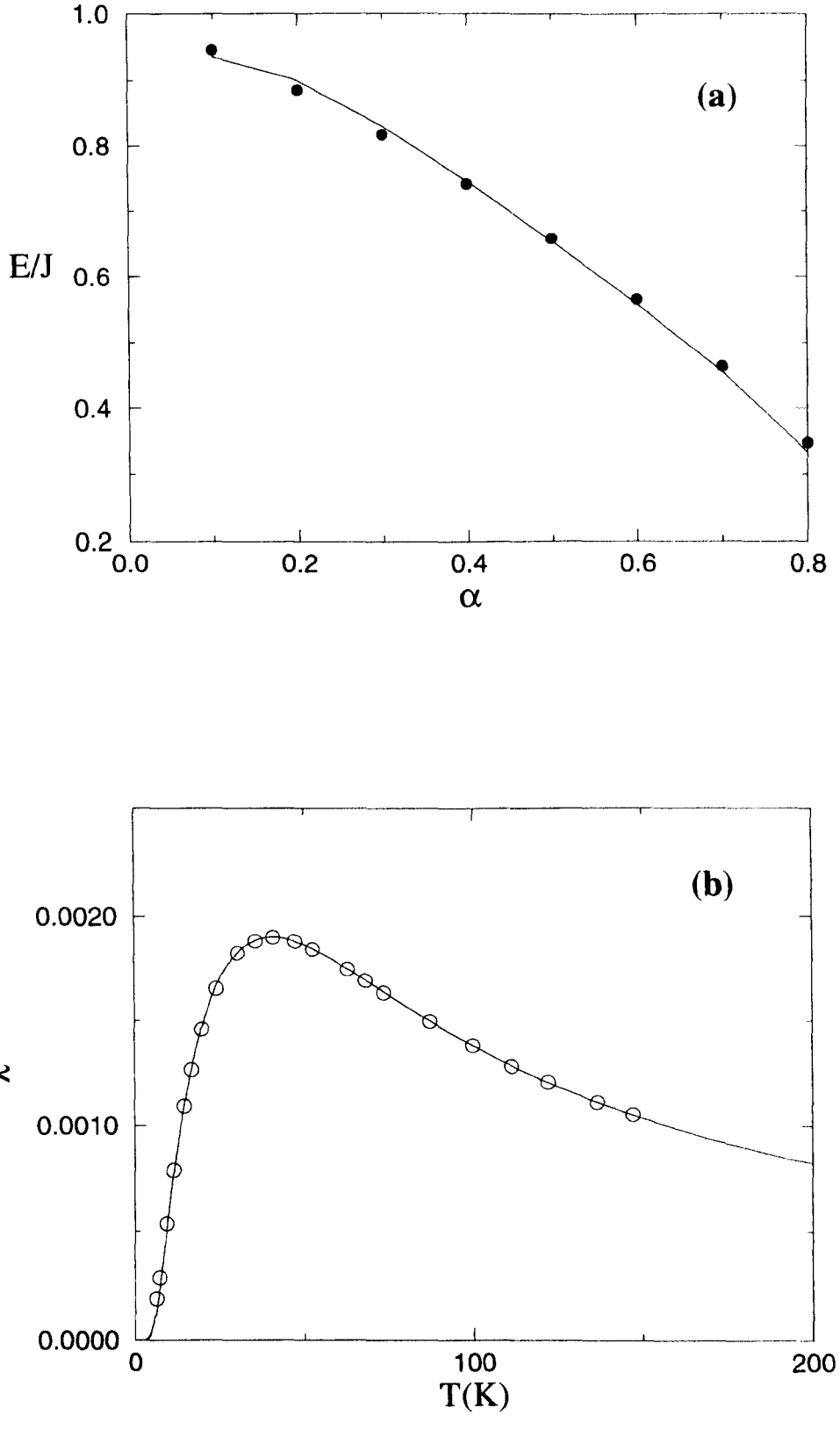

Fig 3.12(a)Comparison of gap calculated by DMRG (circles) and TMRG (lines) (b) Comparison of susceptibility calculted by TMRG and experimental data.

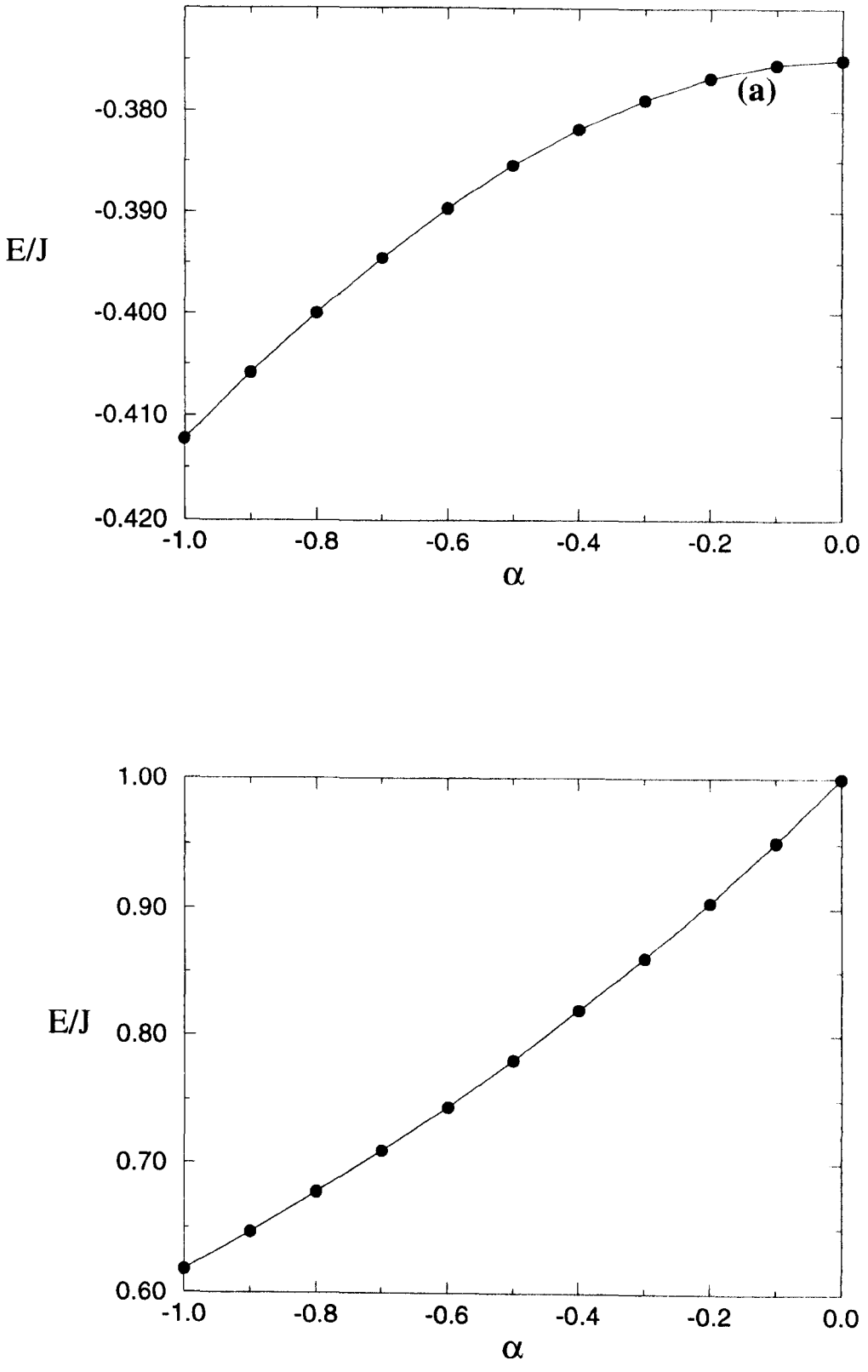

Fig 3.13 (a) Ground state energy and (b) energy gap as a function of α.

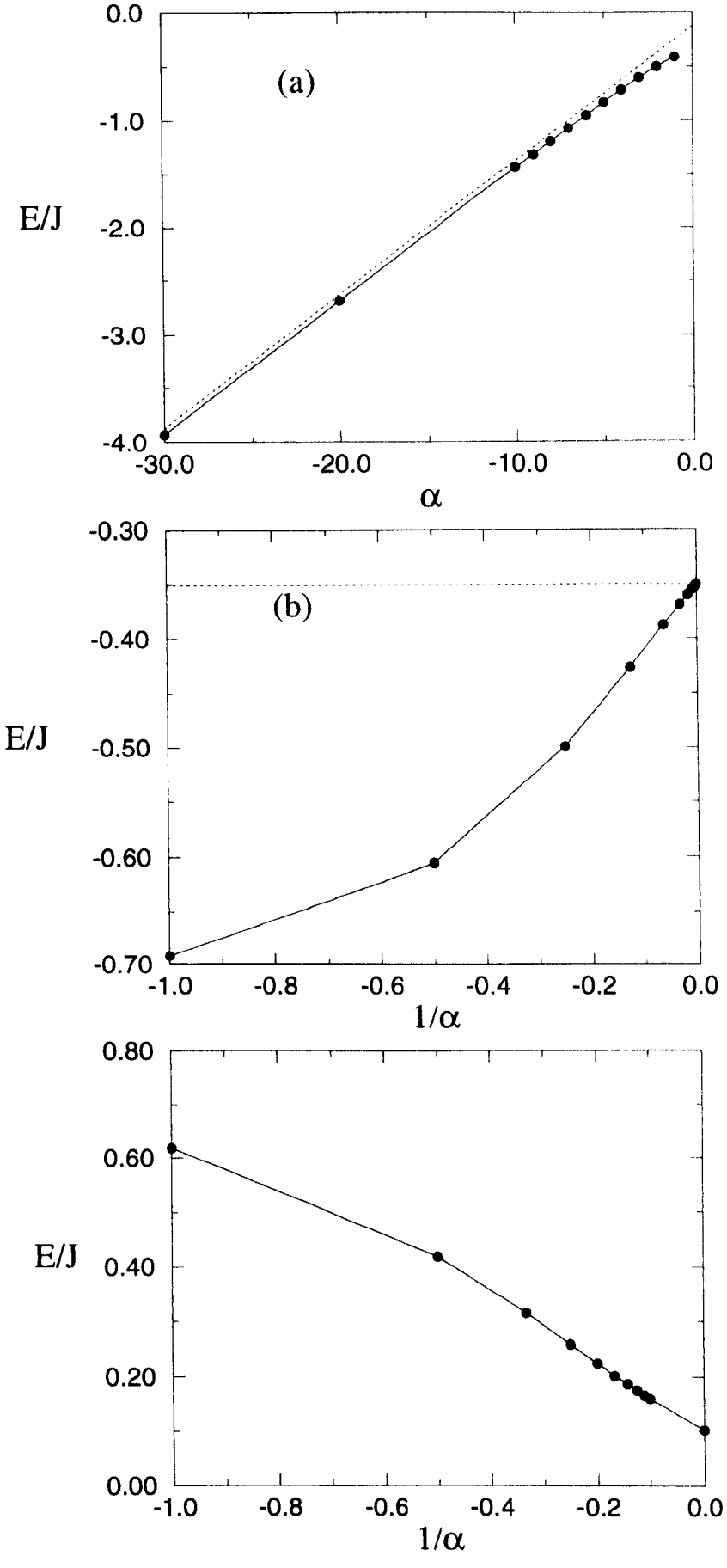

Fig 3.14 (a) Ground state (b) AF bond strength and (c) energy gap for F/AF chain as function of α.

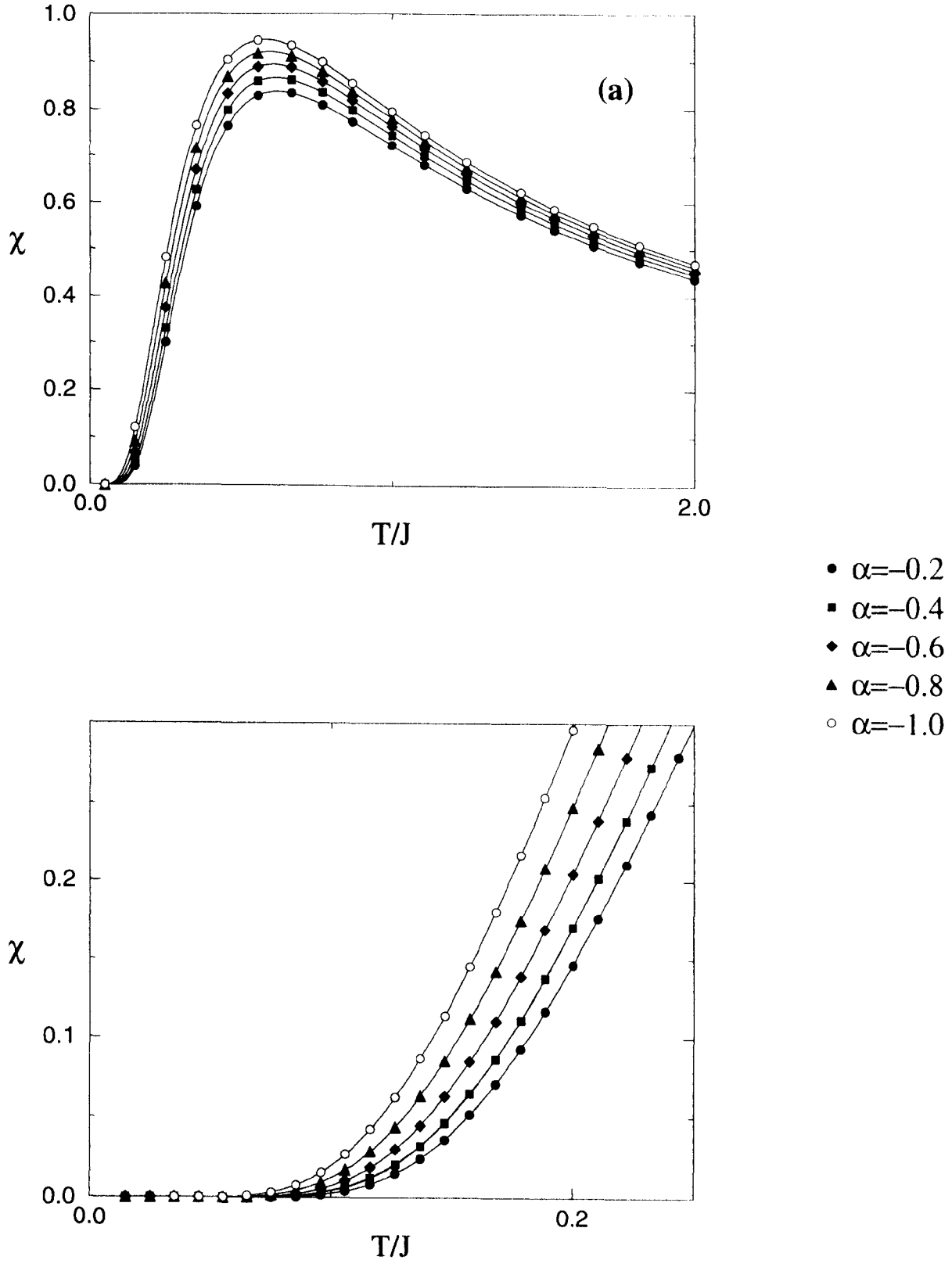

Fig 3.15 Temperature dependence of spin susceptibility for varying α

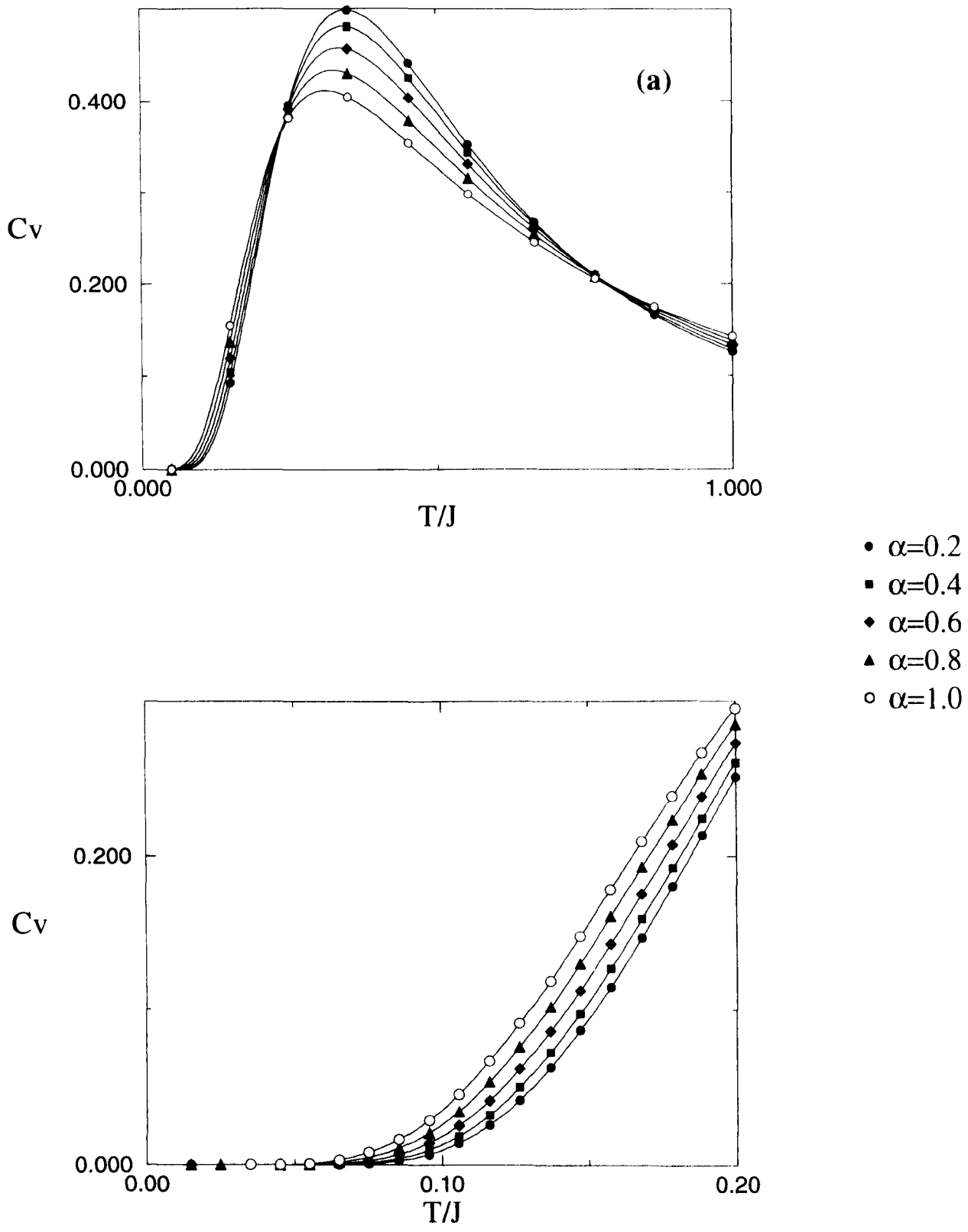

Fig 3.16 Temperature dependence of specific heat for varying α

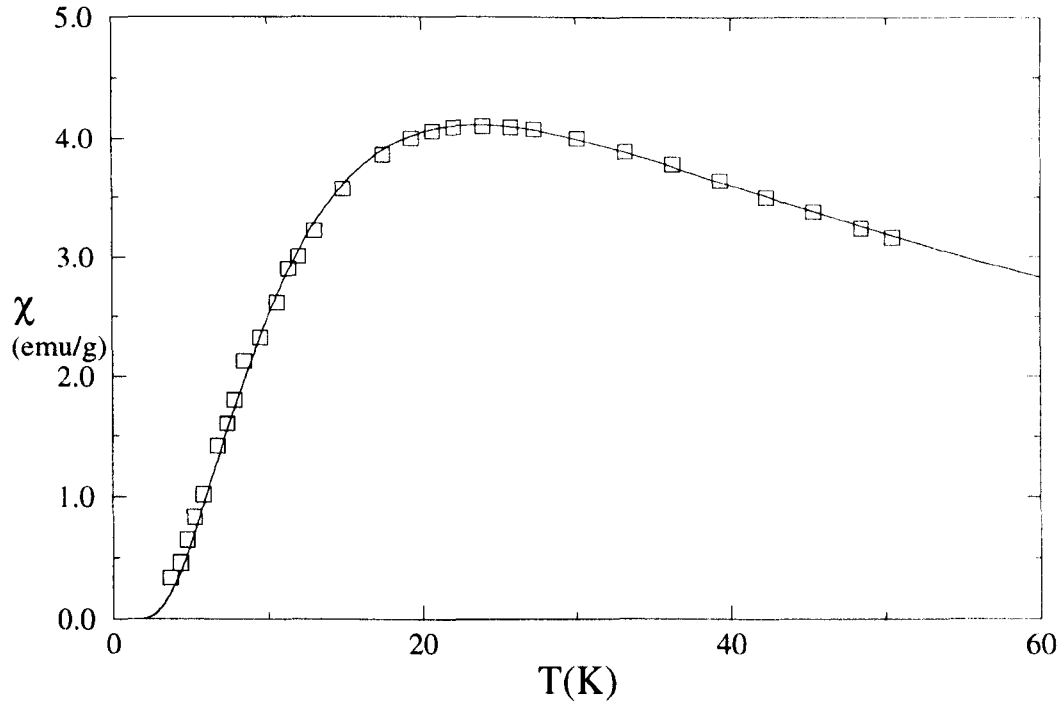

Fig 3.17 Comparison of TMRG susceptibility calculation with experimental data from IPACCl3.

4. S=1 Heisenberg Hamiltonians

4.1 Introduction

The S=1 Heisenberg chain has been the subject of vigorous study in recent years. Theoretically, it has been treated by a wide variety of techniques ranging from exact diagonalisation [1] to field theoretic methods [2]. Experimentally, a wide range of quasi one dimensional magnetic materials have been fabricated which exhibit characteristic 1D behaviour [3]. In this chapter, we describe the work carried out on S=1 Heisenberg chains using the DMRG and TMRG methods. We consider the effect of anisotropy and the introduction of a biquadratic term. We also show comparison with experiment for a number of compounds.

As was shown in Chapter 1 the LSM theorem showed that for S=1/2 the isotropic Heisenberg chain has a singlet ground state and a gapless excitation spectrum. Gaps in the spectrum could only be introduced by the inclusion of dimerisation or anisotropy effects. Until 1983, this was believed to also probably be the case for higher spin models. When Haldane [4] conjectured from field theoretic arguments that integer and half integer spin chains had fundamentally different excitation spectra, there was a great interest in confirming this. Although limited to short chain lengths, exact diagonalisation[1] gave some evidence supporting a gap in the S=1 case. QMC [5] results also confirmed these results. Concurrently, quasi 1D magnetic compounds, NENP[3] being the best example, exhibited gapped behaviour in inelastic neutron scattering experiments and susceptibility measurements. The introduction of the DMRG, with its ability to treat long chains with unprecedented accuracy, has allowed

Haldane's conjecture to be confirmed beyond doubt, this being the method's first major success [6]. Knowledge of the ground state and low-lying excitations has been obtained from the DMRG results as well as other theoretical models [7]. Before presenting our results we will discuss the Valence Bond Solid model which gives a simple, but accurate picture of the nature of the ground state of the S=1 chain.

4.2 Valence Bond Solid

Affleck, Kennedy, Lieb and Tasaki (AKLT) [8] introduced the concept of the Valence Bond Solid (VBS) in order to try and understand the nature of the ground state of integer spin chains. A valence bond (VB) is formed by the contraction of two S=1/2 spins to form a singlet state. That is a VB consists of a pair wave function of the form

$$\psi_{12} = \frac{1}{\sqrt{2}}\left[\uparrow_1 \downarrow_2 - \downarrow_1 \uparrow_2\right] \tag{4.1}$$

For a spin half chain the formation of valence bonds leads to dimerisation (see figure 4.1), where the bonds represent the contracted spins. The translational symmetry of the chain is seen to be modified by the formation of this state.

Figure 4.1

In order to extend this idea to higher spins, we consider a spin S object as being formed by a symmetric combination of 2S S=1/2 spins. These decomposed spins can then form valence bonds. We show in figure 2 an S=1 chain where the circles indicate the lattice sites and the points the S=1/2 spins.

Figure 4.2

We can form valence bonds between adjacent sites as shown in figure 3. This state retains the translational symmetry of the lattice and is referred to as the valence bond solid.

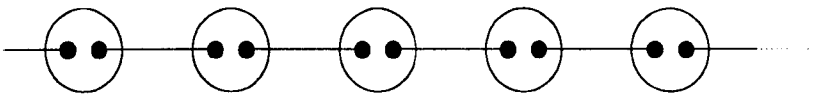

Figure 4.3

AKLT considered a Hamiltonian formed by making a projection on the S=2 subspace of the operator $\mathbf{S}_1 + \mathbf{S}_2$ giving

$$H = \sum_i P_2(\mathbf{S}_i + \mathbf{S}_{i+1}) \tag{4.2}$$

which they showed to have the form

$$H = \sum_i \left[\frac{1}{2}\mathbf{S}_i \cdot \mathbf{S}_{i+1} + \frac{1}{6}(\mathbf{S}_i \cdot \mathbf{S}_{i+1})^2 + \frac{1}{3} \right] \tag{4.3}$$

If we consider any pair of sites in the VBS, two of the S=1/2 spins form a singlet (due to the VB) and hence the total spin of the two sites can only be 0 or 1. Therefore the VBS has zero energy and is the ground state of the above Hamiltonian. The consequence of this is that by the addition of a biquadratic term to the isotropic Hamiltonian the ground state is seen to have a particularly simple form. AKLT also rigorously showed that this system was gapped [9]. Due to the similarity between this Hamiltonian and the isotropic case, it is believed that the isotropic ground state will have qualitatively similar properties. We will discuss later the justification for this claim, but before considering the results of our calculations we will make an observation on the effect of boundary conditions on the VBS. Figure 4 shows a VBS state for periodic and open boundary conditions. It is seen that in the open case, an unpaired S=1/2 spin is left at each end of the chain. This implies a four-fold degeneracy

in this state which is absent in the periodic case. As will be shown, this degeneracy is directly observed in numerical calculations and in experiment.

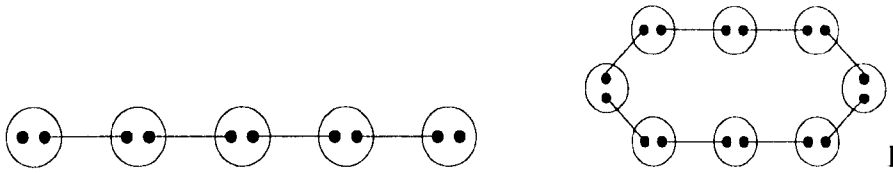

Figure 4.4

4.3 Isotropic Chain.

We consider first the isotropic S=1 chain, which was treated by White and Huse [6] and gave the first indication of the accuracy of the DMRG method, with open boundary conditions:

$$H = \sum_i J\mathbf{S}_i \cdot \mathbf{S}_{i+1} \tag{4.4}$$

We work in a basis in which S^z is diagonal and we use this symmetry to block diagonalise the superblock Hamiltonian and the density matrix. As all the interactions along the chain are equal, parity is also conserved by H. We therefore would like to use this symmetry to further reduce the size of matrices needing to be diagonalised and this is achieved as follows.

We consider the basis set of superblock wavefunctions of the form

$$\psi = |n_1 s_1 s_2 n_2\rangle \tag{4.5}$$

where n_1 and n_2 describe the system and environment blocks and s_1 and s_2 the two sites in between.

In general these are not states of definite parity. However, we can construct states of the form

$$\psi = |n_1 s_1 s_2 n_2\rangle \pm |n_2 s_2 s_1 n_1\rangle \tag{4.6}$$

i.e. a linear combination of two states which are related to each other by reflection through the middle of the chain, which are parity eigenstates. In this way we can construct a new basis in which the states have definite parity. If we are looking to target states of a particular parity, this symmetry approximately halves the size of the superblock Hamiltonian.

We have carried out T=0 DMRG calculations of chains up to 200 sites retaining 81 states in both the system and environment blocks. We have calculated the energies of the lowest lying states in each of the blocks S^z=0,1,2 with both positive and negative parity. We show below the ordering of the energy levels.

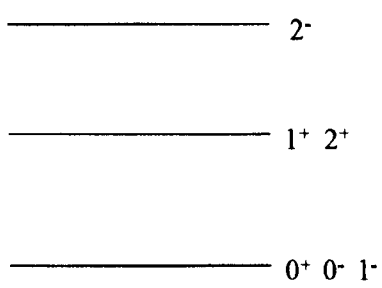

It is seen that as the thermodynamic limit is approached, the 0^+,0^- and 1^- states are degenerate. By symmetry, the -1^- state would also be degenerate with this state. This fourfold degeneracy is an indication that the VBS model is in some way similar to the ground state of the isotropic chain. The Haldane gap is given by the energy difference between these states and the 2^+ state.

In figures 4.5 and 4.6 we show the scaling behaviour of the ground state and the energy gap. The gap is seen to scale like $\sim \Delta + a/L^2$ as expected for a gapped system.. Extrapolating to the thermodynamic limit $L \to \infty$ gives a ground state energy density of $e_0 = -1.401484(0)J$ and the Haldane gap as $\Delta = 0.410(7)$.

We consider now the thermodynamics of this system using the TMRG. We have calculated both the specific heat and spin susceptibility as shown in figures 4.7 and 4.8.

Both show exponential low temperature behaviour indicating the presence of a gap. Sorensen and Affleck [10] examined this system by considering a dilute system of polarised magnons which could be treated as a system of non-interacting fermions. For k near π, they obtained a dispersion relation of the form

$$E(k) = \sqrt{v^2(k-\pi)^2 + \Delta^2} \tag{4.7}$$

where v is the spin wave velocity. This leads to a density of states given by

$$g(E) = \frac{1}{\pi v} \frac{E}{\sqrt{E^2 - \Delta^2}} \tag{4.8}$$

From this, the zero field susceptibility has the low temperature form

$$\chi(T) = \frac{1}{v}\sqrt{\frac{2\Delta}{\pi T}} \exp\left(-\frac{\Delta}{T}\right) \tag{4.9}$$

Sorensen and Affleck estimated the spin wave velocity as $v = 2.49$. Using this value for v and the DMRG result for Δ, we show in figure 4.8 (b) the comparison of this curve with the TMRG results.

We can also compare our results with experiment. The compound TMNIN consists of Ni chains with negligible interchain interaction. Figure 4.9 show the comparison with susceptibility and specific heat measurements by Ito et al for $J = 12K/k$, $g = 2.1$ [11].

4.4 Single Ion Anisotropy

The isotropic Heisenberg model has full spherical symmetry. In real compounds this is rarely the case. The crystal structure of real systems leads to a lowering of the symmetry of the system which we can incorporate into our Hamiltonian by introducing an anisotropy term. We have considered single-ion anisotropy which is represented by

the addition of the term $H_{SI} = D\sum_i \left(S_i^z\right)^2$. Using the DMRG and TMRG methods we have investigated the T=0 and finite temperature properties of the Hamiltonian

$$H = J\sum_i \mathbf{S}_i \cdot \mathbf{S}_{i+1} + D\sum_i \left(S_i^z\right)^2 \qquad (4.10)$$

over a wide range of the parameter D/J. Of particular interest to us is the effect of D on the Haldane gap. Previous studies on this system have included exact diagonalisation on small chains [12] and quantum Monte-Carlo calculations [12,13]. These studies have suggested, though by no means conclusively, that the Haldane gap vanishes at $D/J \approx 1$. We have investigated this region, as well as the large D region where the system is XY-like in character.

The diagram below shows schematically the ordering of the energy levels in the region $0 < D < 1$ alongside those with those of the isotropic chain for comparison.

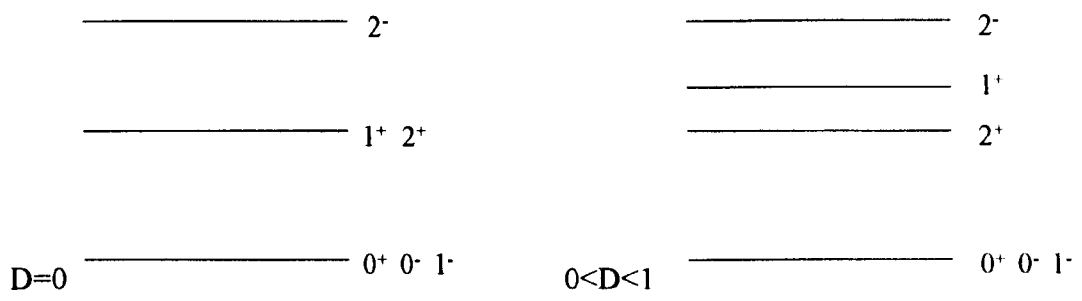

An interesting observation is that the ground state degeneracy of the open isotropic chain is still present with the introduction of anisotropy. The Haldane gap is characterised by the energy difference between the 0^+ and 2^+ states. We have calculated the gap using the DMRG on an open chain keeping 81 states in both the system and environment blocks. Figure 11 (a) shows the ground state energy density as a function of D. It is seen to increase approximately linearly with D. Figure 10 shows the gap as a function of $L, 1/L$ and $1/L^2$ in the D=1 case and is seen to scale

like $1/L$, consistent with gapless behaviour. We have extrapolated the data in the $L \to \infty$ limit by fitting to a function of the form $\Delta(L) = \Delta_0 + a/L + b/L^2$. The extrapolated gaps are shown in the table below and in figure 11 (b).

D	Δ
0.0	0.410(7)
0.1	0.347(7)
0.2	0.290(0)
0.3	0.237(2)
0.4	0.188(8)
0.5	0.145(9)
0.6	0.107(7)
0.7	0.059(4)
0.8	0.040(4)
1.0	0.01(6)

As can be seen, the gap appears to be approaching zero as $D \to 1$. It is not true to say that the DMRG gives a strict upper limit on the value of the gap, but we will now argue why this is probably the case.

It is certainly true that by systematically truncating the Hilbert space we are obtaining a variational approximation to the ground state energy. As we have block diagonalised the superblock Hamiltonian, the first excitation also corresponds to a lowest eigenvalue within a subspace of our Hilbert space and hence a variational principle also applies to this energy. We can therefore write

$$E_0' \geq E_0 \qquad E_1' \geq E_1 \tag{4.11}$$

where the primes indicate our DMRG results and the unprimed quantities are the real eigenvalues. We rewrite these expressions as

$$E_0' = E_0 + \delta_0 \quad E_1' = E_1 + \delta_1 \tag{4.12}$$

where δ_0 and δ_1 are both by definition positive quantities. Therefore the energy gap we calculate is given by

$$E_1' - E_0' = E_1 + \delta_1 - E_0 - \delta_0 \tag{4.13}$$

$$\Delta' = \Delta + (\delta_1 - \delta_0) \tag{4.14}$$

where Δ is the true gap. Obviously the relation between Δ and Δ' depends on the relative magnitudes of δ_1 and δ_0 . However, as we have seen, the convergence of the ground state energy is generally quicker and more accurate than that of the first excitation. Consequently we would expect $\delta_1 > \delta_0$, meaning that Δ' can generally be interpreted as an upper limit of the gap. In common with the S=1/2 results of the previous chapter, the results are most accurate when there is a substantial energy gap. Using the TMRG method, we have calculated the susceptibility and specific heat for varying *D/J*. It has been observed that χ can generally be obtained more accurately than C_V. The reason for this is that at low temperatures small oscillations occur in the internal energy, presumably as a result of accumulated truncation and round off errors in the calculation. This introduces larger errors when taking the derivative when calculating C_V. As χ does not involve taking a derivative, it does not suffer from this problem.

Considering first the susceptibility, figure 4.12 shows the zero field spin susceptibility per site in the range $0<D<0.7$. All curves show a broad maximum and exponential

behaviour at low temperature. Our results do not suffer from Curie-like divergences as a result of edge effects which are present in quantum Monte Carlo data. In this region, the ground state of the system is expected to be qualitatively similar to that of the isotropic system. We have therefore fitted the low temperature region of the data to curves of the form of equation (4.9) that is $\chi \sim \frac{1}{\sqrt{T}} \exp\left(-\frac{\Delta}{T}\right)$. By doing so we can obtain an estimate of the energy gap as a function of D. We show in the table below the results and a comparison with those of the T=0 DMRG results.

D	TMRG	DMRG
0.0	0.41(5)	0.4107
0.1	0.35(0)	0.3477
0.2	0.29(5)	0.2900
0.3	0.24(0)	0.2372
0.4	0.18(7)	0.1888
0.5	0.14(1)	0.1459
0.6	0.09(3)	0.1077
0.7	0.05(4)	0.0594

For $D < 0.5$ the agreement is very good suggesting that the chosen functional form for the susceptibility is accurate in this region. The discrepancy for larger D indicates the crossover to the gapless behaviour. Figure 4.13 shows the comparison of the data.

The compound $Ni(C_2H_8N_2)_2NO_2(ClO_4)$, usually referred to as NENP, is believed to be described by equation (4.10), with D lying in the region just discussed. The Ni ions form chains which are octahedrally coordinated giving rise to the anisotropy term. We have fitted susceptibility data by Takeuchi et al [14] with results from our TMRG

method with the parameters J=46K/k_B, D/J=0.25 and g=2.15 as shown in figure 4.13 (b). The fit is good over the whole temperature range.

In the region $0.8 \leq D \leq 1.2$ the TMRG method produces less accurate results and is unable to indicate whether the gap vanishes. At any given iteration of the calculation $T \sim 1/M$ where M is the Trotter number, hence the algorithm tends to T=0 asymptotically. As the number of iterations increases, so does the accumulated truncation and numerical errors. Therefore when the gap is reduced and the exponential behaviour of $\chi(T)$ is located in an ever decreasing region close to T=0, the results become less reliable. The susceptibility in this region is shown in figure 4.14. The specific heat calculated by this method is shown in figure 4.14 (b). The data below T~0.2J are not very accurate as discussed above.

We have also considered the properties of this system in the large D region. In the limit $D \to \infty$, the ground state would be that in which all the spins are in the $S^z = 0$ state, $\psi_0 = |000\cdots00\rangle$. In this case, the ground state energy density $\langle \psi_0 | H | \psi_0 \rangle / N$ tends to zero. We show in figure 4.15 the ground state per bond for large D and the expected asymptotic behaviour is observed. In this region a substantial energy gap is observed between the 0^+ and 1^- states. By perturbation theory [12] it can be shown that the gap behaves like $\Delta \approx D - 2 + O(1/D)$ as $D \to \infty$. In figure 4.15 (b) we show the DMRG results for the energy gap as a function of D and the expected asymptotic behaviour is observed. The thermodynamics of this system have been calculated. The susceptibility is shown in figure 4.16 (a). Due to the large gap the results are more accurate and show low temperature exponential behaviour. Fitting to a function of the form $\chi \sim \frac{1}{\sqrt{T}} \exp\left(-\frac{\Delta}{T}\right)$ can again be used to estimate the gap energy and the comparison

between these results and the DMRG results are shown in the table below and in figure 4.16 (b).

D	DMRG	TMRG
2.0	0.540	0.547
3.0	1.362	1.373
4.0	2.267	2.289
5.0	3.219	3.236

In figure 4.16 (c) we show the specific heat for D in this region. Gapped behaviour is demonstrated in the low temperature region.

In addition to positive single-ion anisotropy, we have considered the ground state properties for $D<0$. We show in figure 4.17 (a) the ground state energy density as a function of D. In the limit $D \to \infty$, we can consider the Neel state as an approximation to the true ground state. This gives the asymptotic behaviour of the energy as $e_0 \approx D - 1$. We show this in figure 4.17 (b). In this region the energy levels are ordered as shown below, alongside those of the isotropic case for comparison. The energy gap is seen to be between the ground state and the 1^+ state.

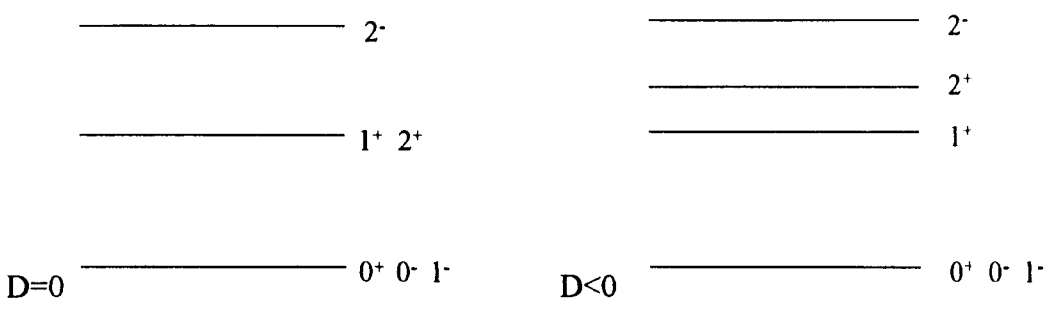

In figure 4.17 (c) we show the energy gap extrapolated in the limit $L \to \infty$. The gap appears to vanish at $D \approx -0.3$. This indicates that the Haldane phase is more unstable with respect to a transition to the Neel phase than to the X-Y phase which occurs at

$D \approx 1$. Finally, we show in figure 4.18 the ground state energy density and energy gap over the whole range $-1 \leq D \leq 2$.

4.5 Biquadratic Exchange

In Chapter 1 we showed how the application of second order perturbation theory to the one dimensional Hubbard model in the $U \to \infty$ limit led to an effective antiferromagnetic Heisenberg interaction. Fourth Order terms [15] contribute a term of the form

$$H_{bq} = -\frac{t^4}{U^3}\sum_i (\mathbf{S}_i \cdot \mathbf{S}_{i+1})^2 \tag{4.15}$$

which is referred to as the biquadratic exchange interaction. It was the inclusion of this term in equation (4.3) which leads to the formation of the VBS ground state in the AKLT model. The effect of this term has also been observed in real systems such as MnO [16]. The effect of biquadratic exchange on 1D Heisenberg systems has been studied by Xiang and Gehring [17] using a real space renormalisation method and by Bursill, Xiang and Gehring [18] using the DMRG.

We express the Hamiltonian incorporating biquadratic exchange as

$$H = \sum_i \cos\gamma \mathbf{S}_i \cdot \mathbf{S}_{i+1} + \sin\gamma (\mathbf{S}_i \cdot \mathbf{S}_{i+1})^2 \tag{4.16}$$

The system is exactly soluble at a number of points, namely

a) $\gamma = \pi/2$. At this point the system is ferromagnetic and hence its ground state wavefunction can be written down exactly. The excitation spectrum is gapless.

b) $\gamma = \pi/4$. The Lai-Sutherland point. Solution by the Bethe ansatz leads to a gapless, trimerised ground state.

c) $\gamma = \tan^{-1}(1/3)$. This is the Affleck point already discussed. The system is gapped and has a VBS ground state.

We have calculated the ground state energy and energy gap in the region $0 \leq \gamma \leq 0.8$ using the DMRG in order to show whether the isotropic chain is within the same part of the phase diagram as the Affleck point (i.e. does the energy gap disappear between these points?)

Considering first the ground state energy we show in figure 4.19 the ground state energy density as a function of L for varying γ. It is interesting to see the transition from a monotonically decreasing function of L to the period three staggering observed for $\gamma \geq 0.6$. It should be noted that as the DMRG algorithm increases the lattice by two sites at a time, the periodicity we observe is not the true periodicity of the system but the trimerisation (periodic in the lattice with period 3) aliased against the periodic increase of the lattice (period 2). In figure 4.19 (c) we show every third result from the DMRG calculation, which corresponds to an increase of the lattice by six sites from point to point. This is seen to be monotonically decreasing with L. Extrapolating to the thermodynamic limit we plot the ground state energy as a function of γ (figure 4.20 (a)).

We have also calculated the energy gap. Again evidence of trimerisation is observed for $\gamma \geq 0.6$ We see that the gap is finite up to and past the Affleck point indicating that the VBS and isotropic chain are part of the same phase. It then decreases with γ consistent with it vanishing at the Lai-Sutherland point at $\gamma \approx 0.785$. The gap is plotted as a function of γ in figure 4.20(b).

4.6 References

[1] Golinelli O, Jolicoeur T and Lacaze R, Phys. Rev. B, **50**, 3037 (1994)
[2] Jolicoeur T and Golinelli O, Phys. Rev. B, **50**, 9265 (1994)
[3] Renard J P, Verdaguer M, Regnault L P, Erkens W A C, Rossat-Mignod J and Sterling W G, Europhys. Lett., **3**, 945 (1987)
[4] Haldane F D M, Phys. Rev. Lett., **50**, 1153 (1983)
[5] Chang K, Affleck I, Hayden G and Soos Z, J. Phys. C, **1**, 153 (1989)
[6] White S R and Huse D A, Phys. Rev. B, **48**, 3844 (1993)
[7] Affleck I, Phys. Rev. B, **43**, 3215 (1991)
[8] Affleck I , Kennedy T, Lieb E H and Tasaki H, Ohys. Rev. Lett., **59**, 799 (1987)
[9] Affleck I , Kennedy T, Lieb E H and Tasaki H, Commun. Math. Phys., **115**, 477 (1988)
[10] Sorensen E S and Affleck I, Phys. Rev. Lett., **71**, 1633 (1993)
[11] Ito M, Mito M, Deguchi H and Takeda K, J. Phys. Soc. Japan, **63**, 1123 (1994)
[12] Golinelli O, Jolicoeur T and Lacaze R, Phys. Rev. B, **45**, 9798 (1992)
[13] Yamamoto S and Miyashita S, Phys. Rev. B, **50**, 6277 (1994)
[14] Takeuchi T, Ono M, Hori H, Yosida T, Yamagishi A and Date M, J. Phys. Soc. Japan, **61**, 3255 (1992)
[15] Yosida K, "Theory of Magnetism", Springer, Berlin (1996)
[16] Harris E A and Owen J, Phys. Rev. Lett., **11**, 9 (1963)
[17] Xiang T and Gehring G A, Phys. Rev. B, **48**, 303 (1993)
[18] Bursill R J, Xiang T and Gehring G A, J. Phys. A, **28**, 2109 (1995)

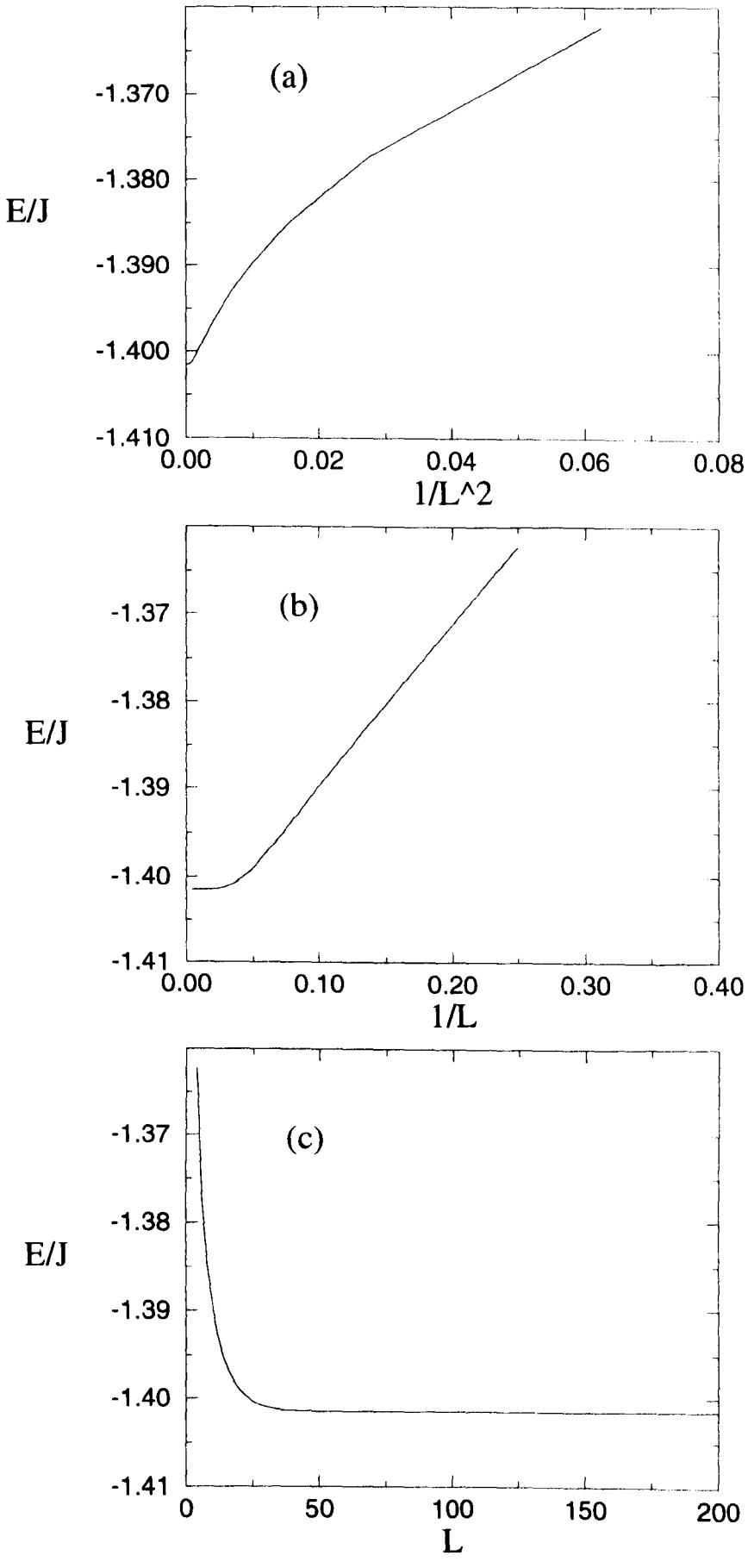

Fig 4.5 Ground state energy of S=1 Heisenberg model as a function of (a) 1/L^2 (b) 1/L (c) L.

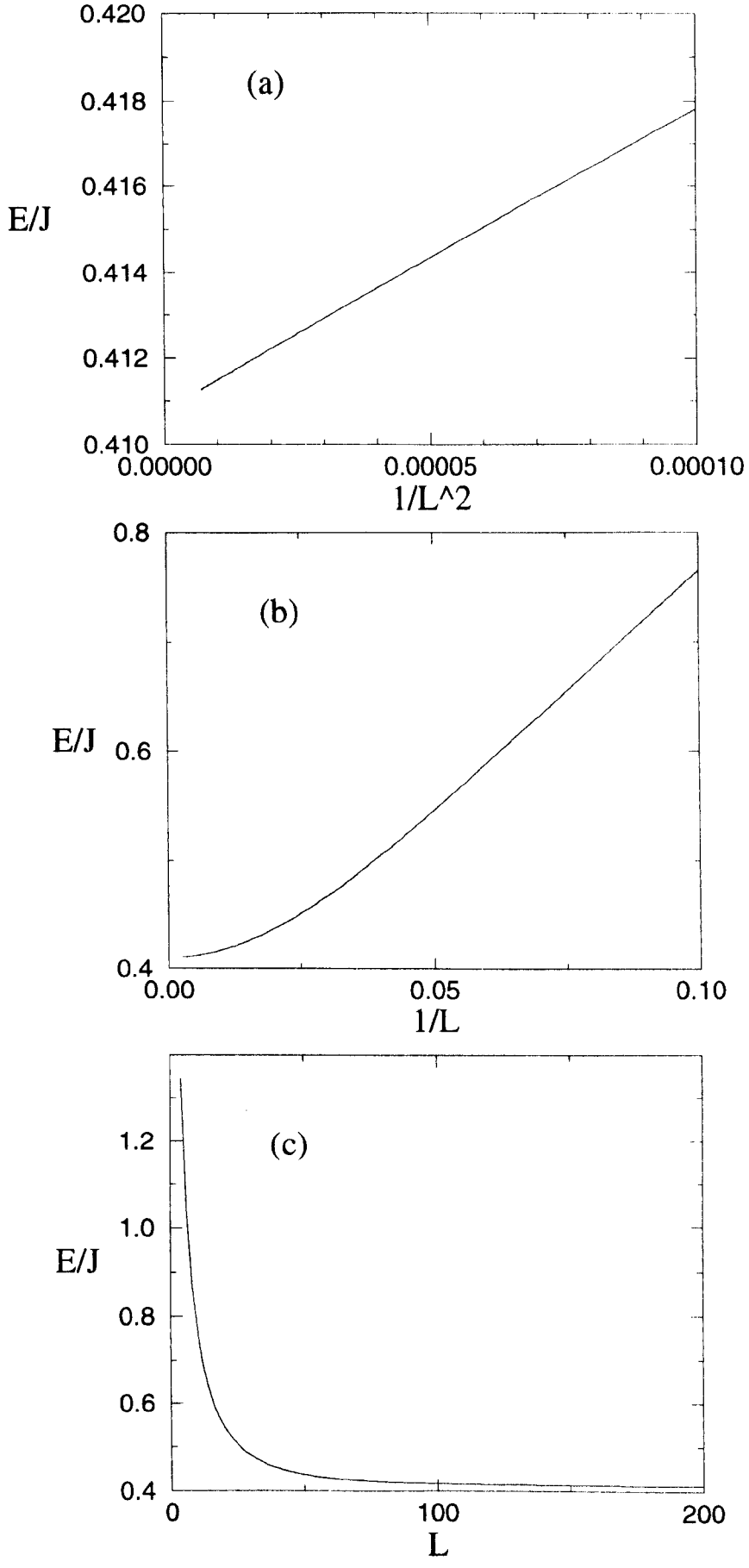

Fig 4.6 Haldane gap for S=1 Heisenberg model as a function of (a) 1/L^2 (b) 1/L (c) L.

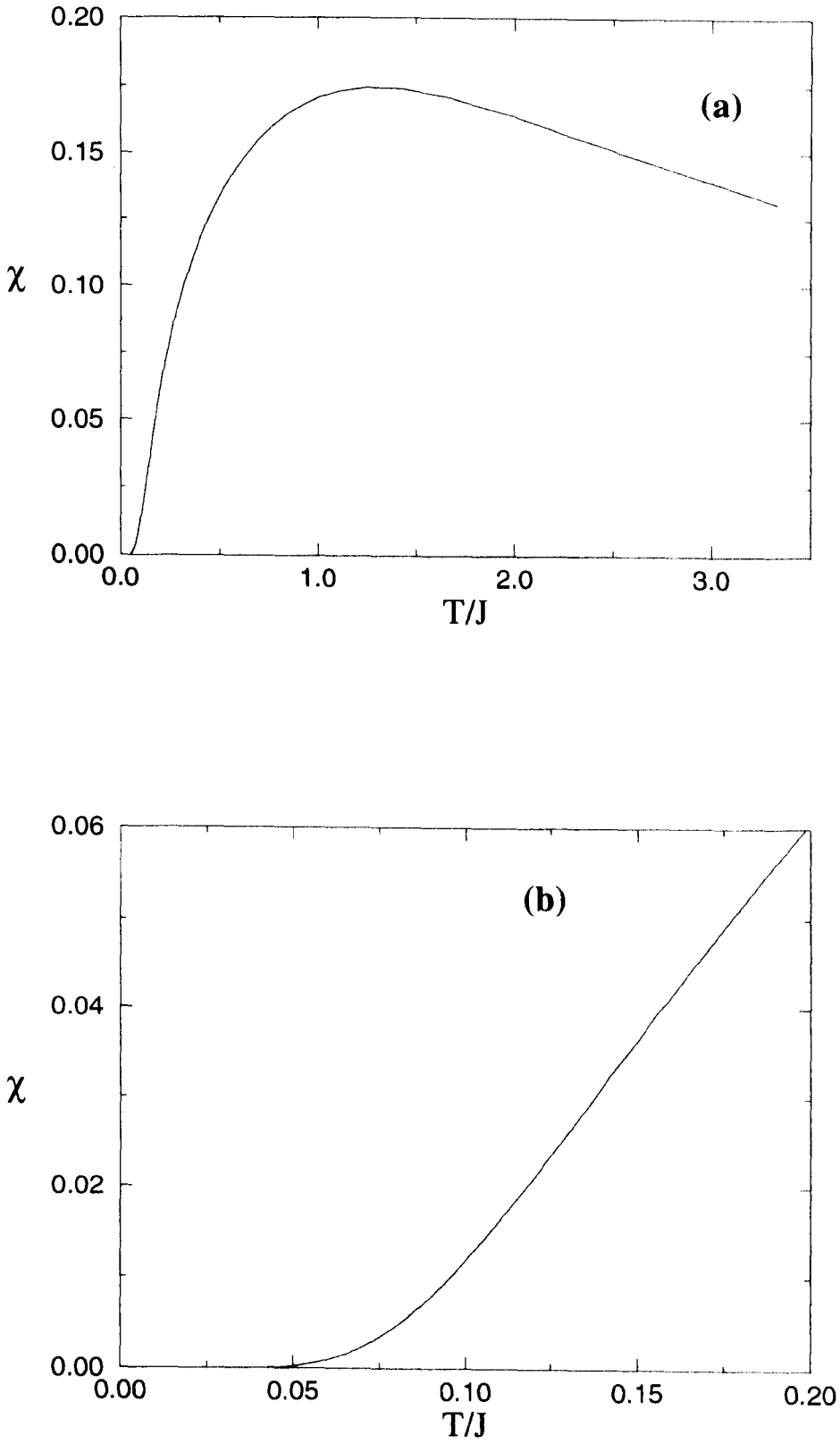

Fig 4.7 Temperature dependence of spin susceptibility for S=1 Heisenberg model.

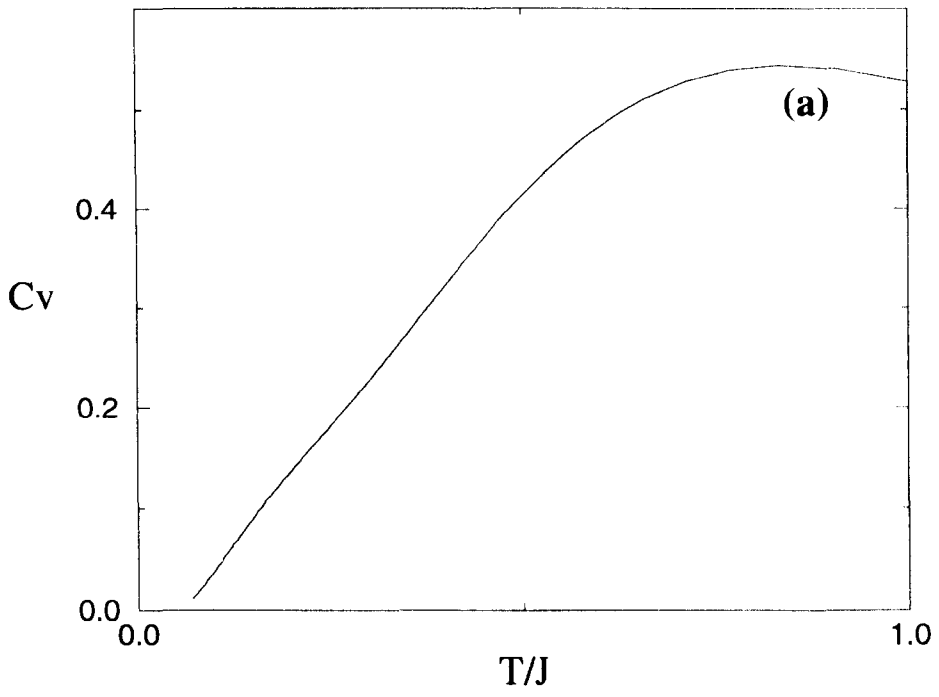

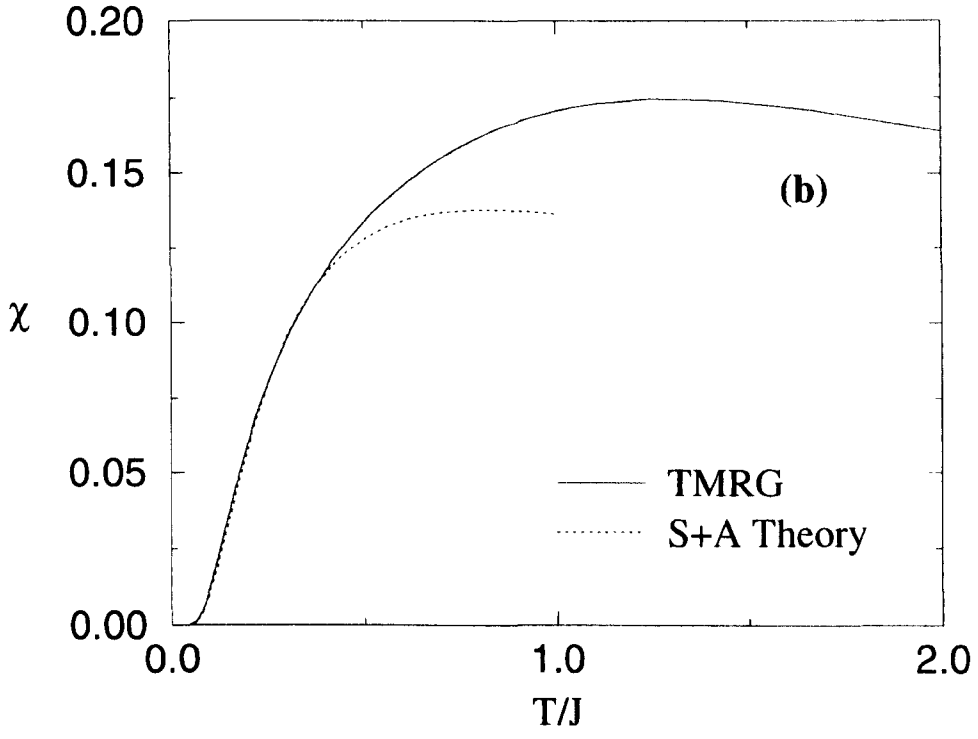

Fig 4.8 (a) Temperature dependence of specific heat for S=1 Heisenberg model. (b) Comparison of susceptibility calculated by TMRG and by Sorensen and Affleck theory.

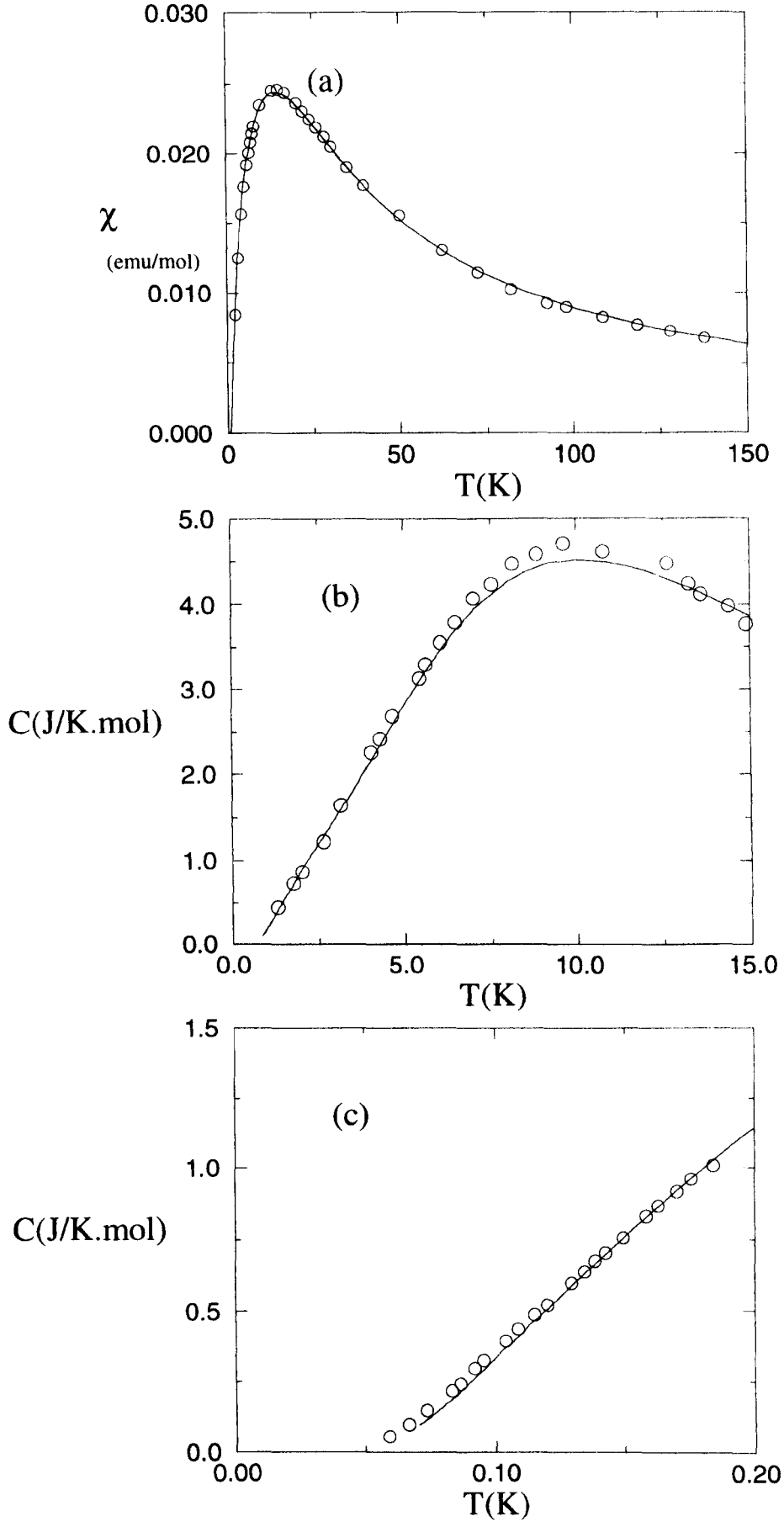

Fig 4.9 Comparison with experimental data for TMNIN (a) susceptibility (b) and (c) specific heat.

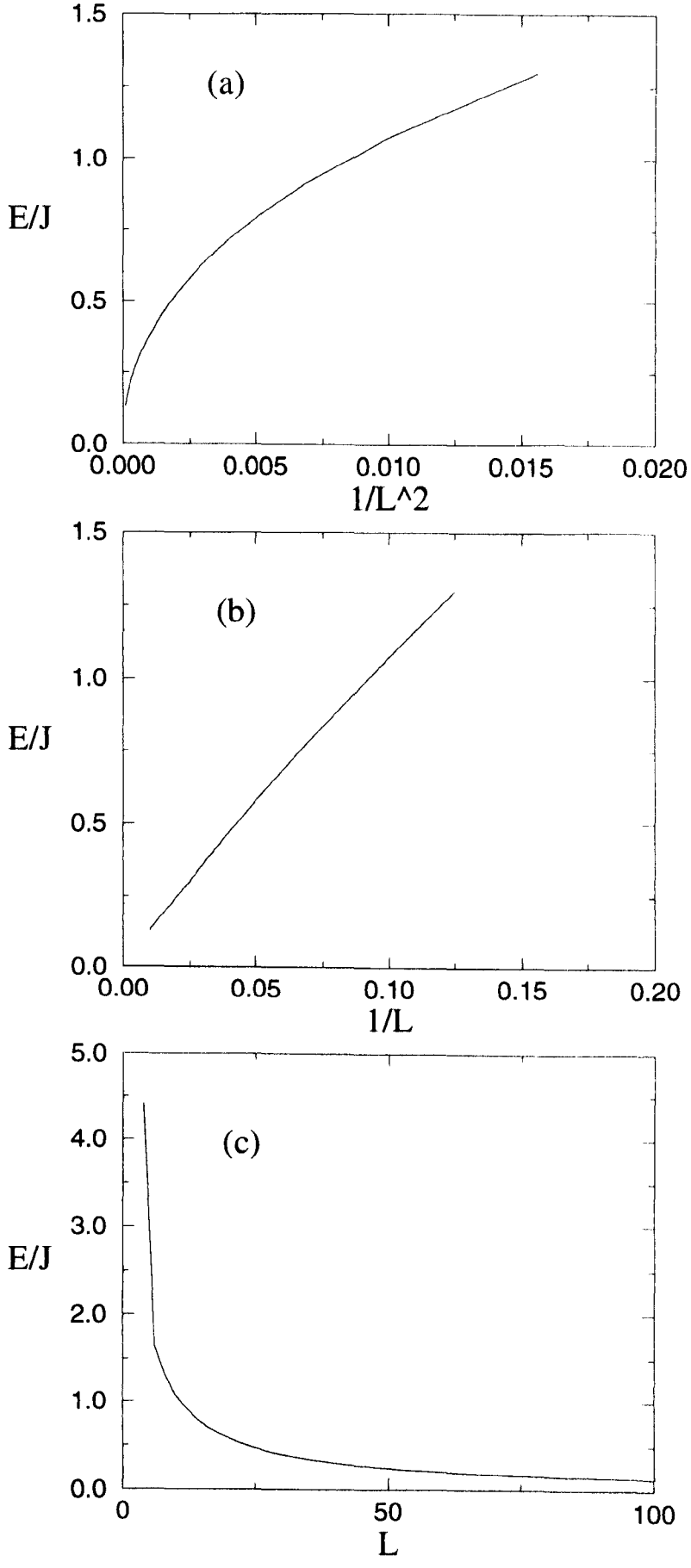

Fig 4.10 Haldane gap for D=1 case
as a function of (a) 1/L^2 (b) 1/L (c) L

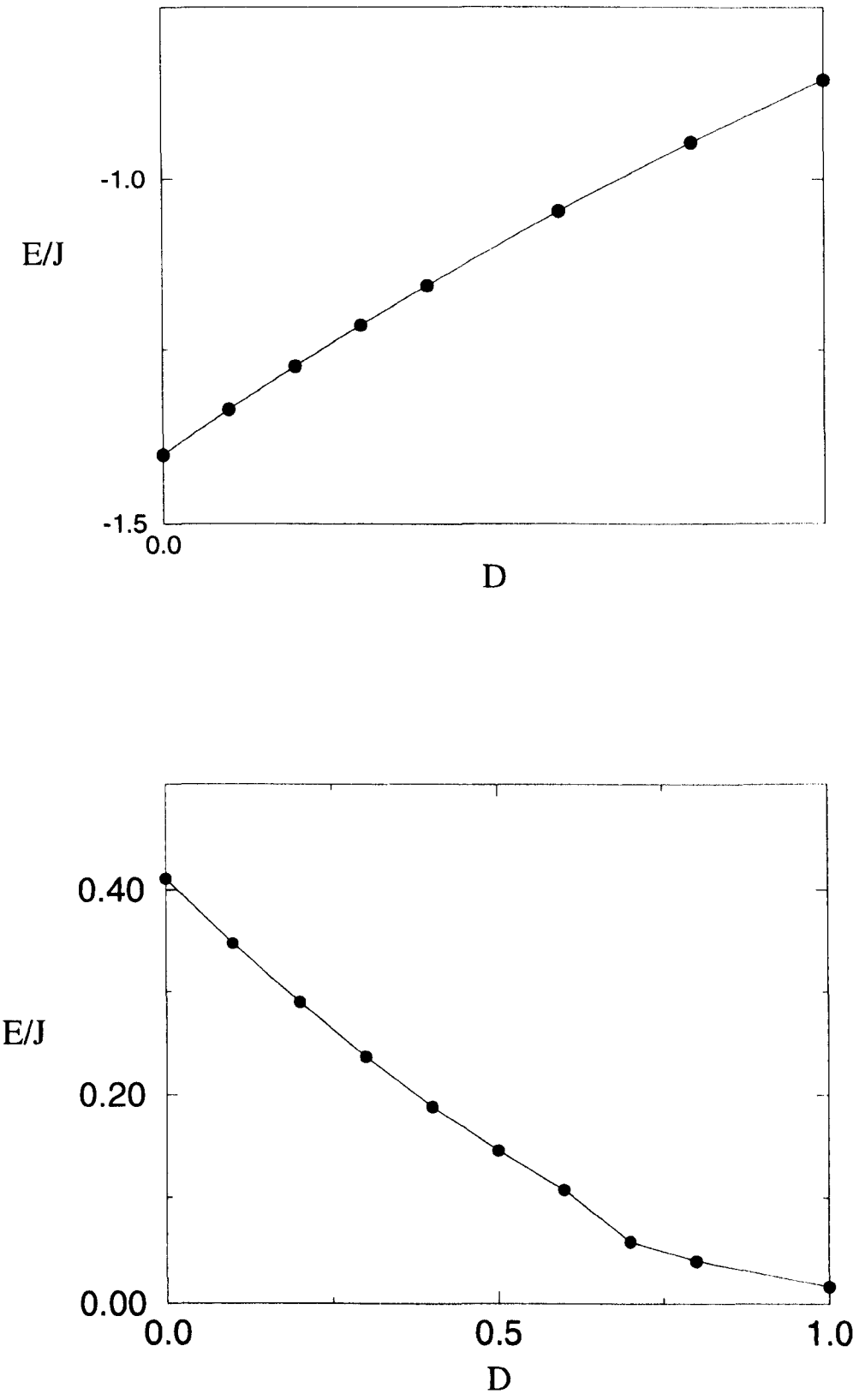

Fig 4.11 (a) Ground state energy per bond and (b) energy gap as function of D.

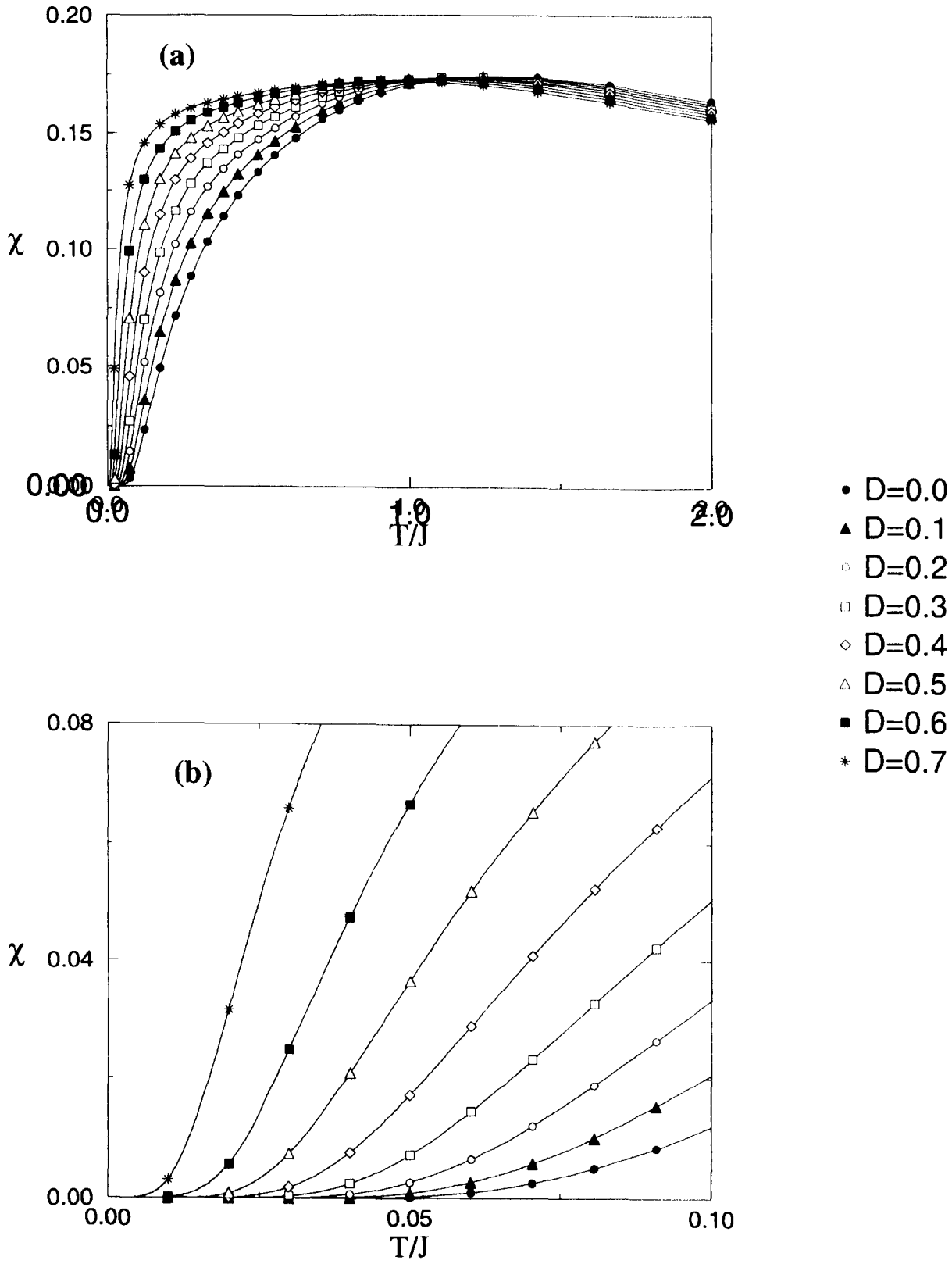

Fig 4.12 Susceptibility of S=1 chain for varying D

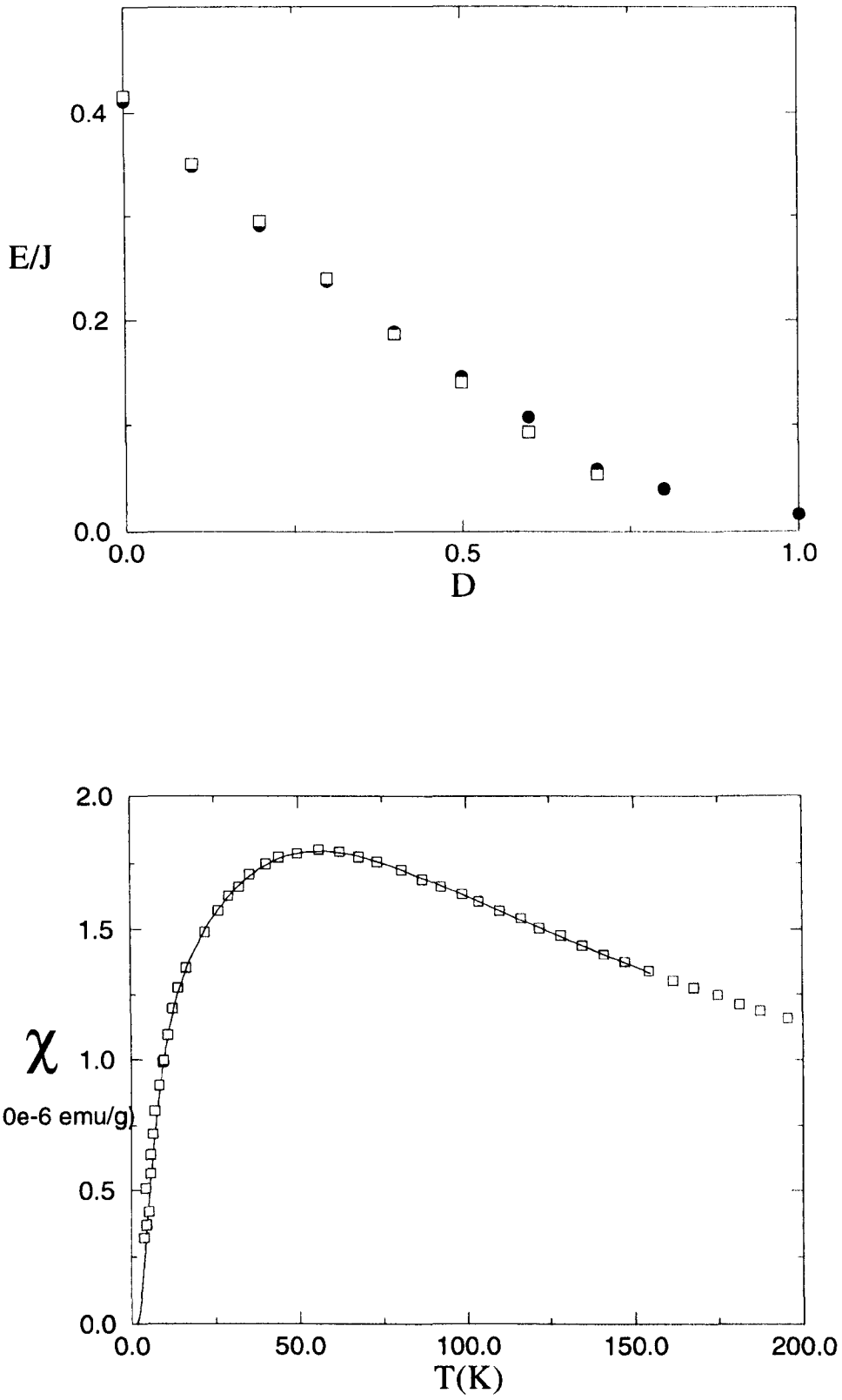

Fig 4.13 (a) Comparison of gap calculated by (a) DMRG and TMRG.(b) Comparison of susceptibility with that of NENP.

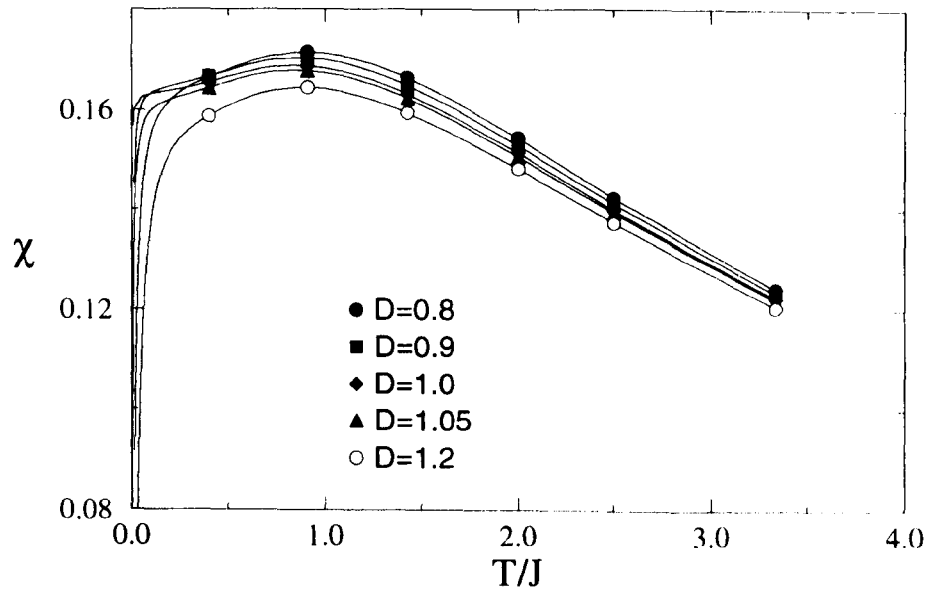

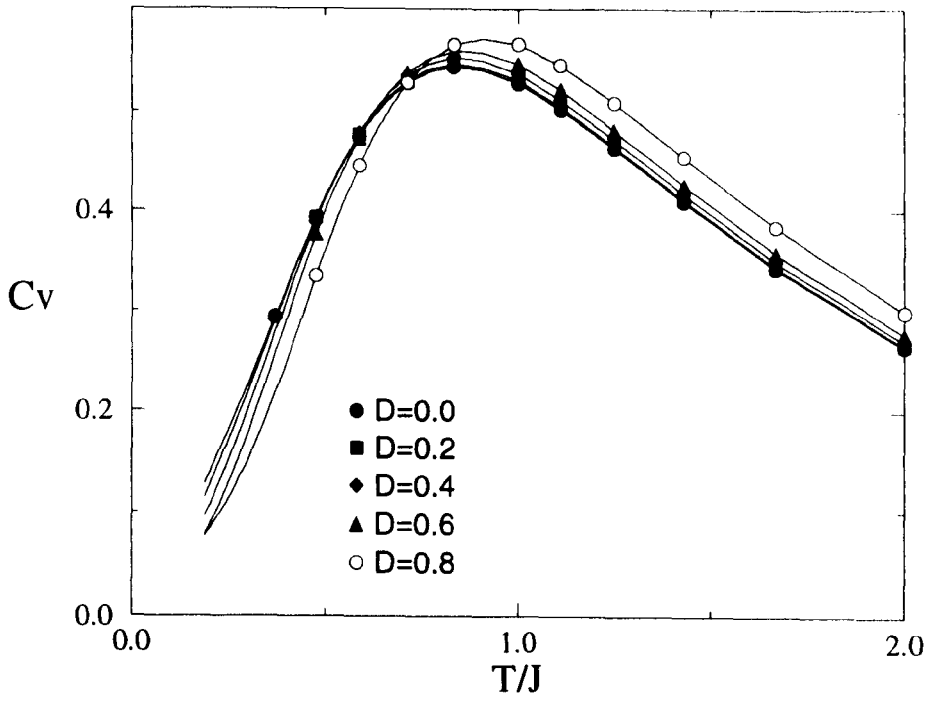

Fig 4.14 (a) Susceptibility and (b) Specific heat for varying D.

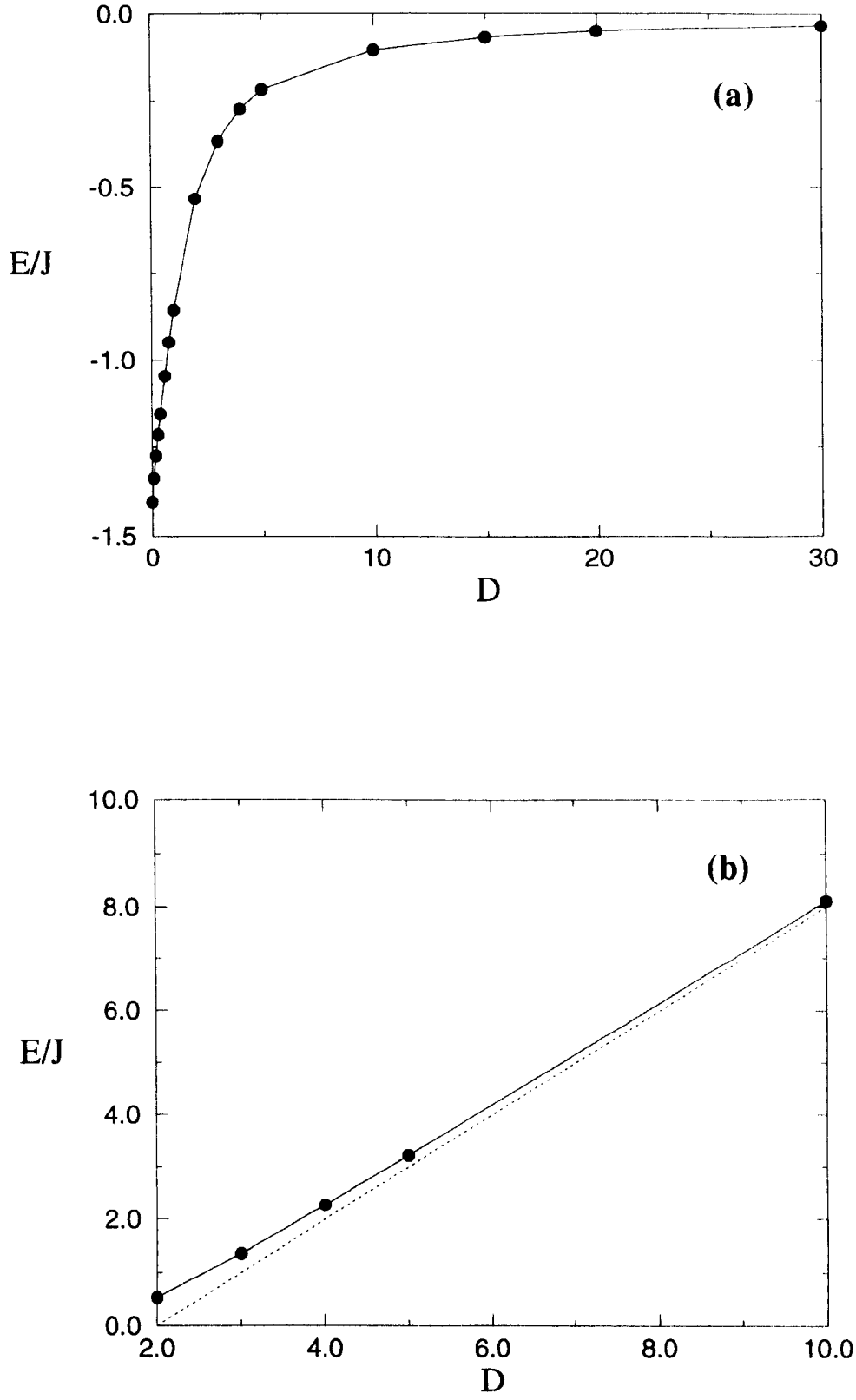

Fig 4.15 (a) Ground state energy and (b) energy gap for varying D.

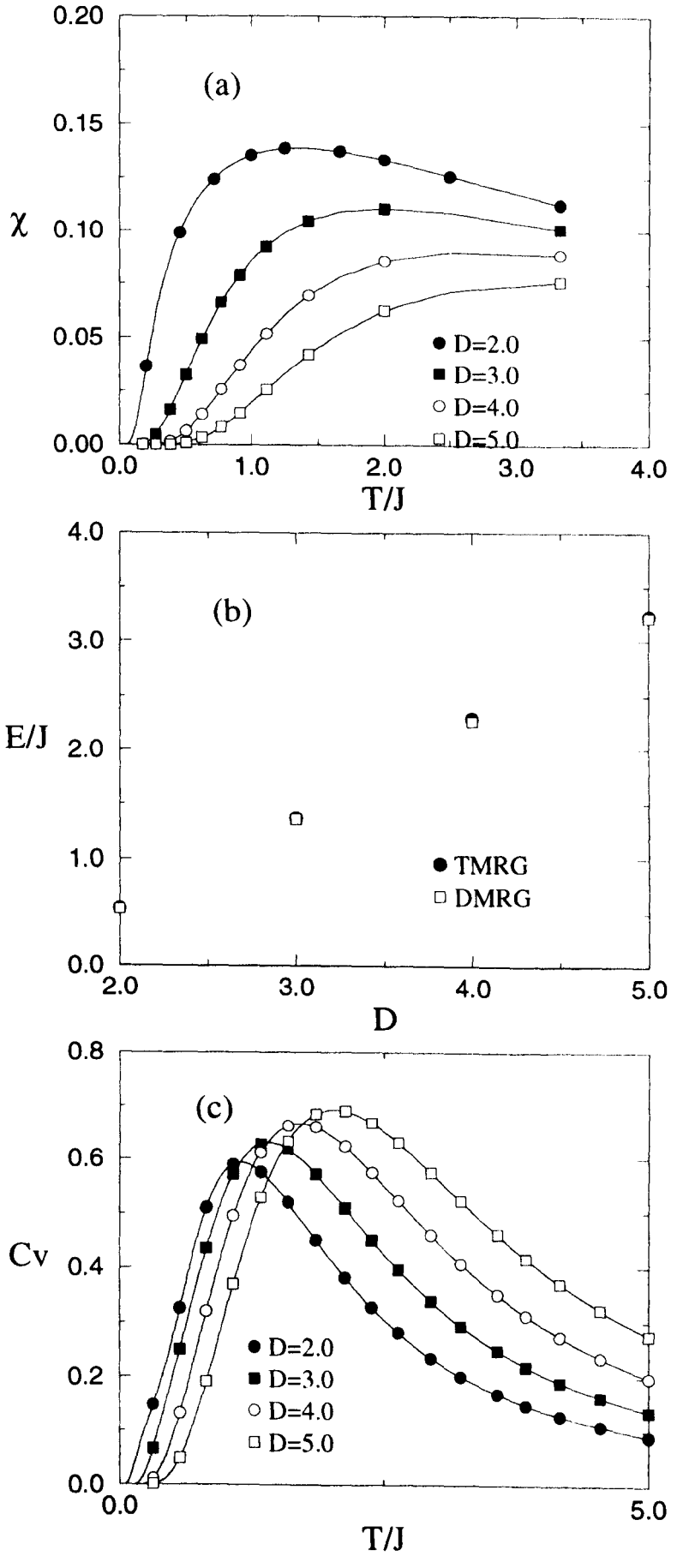

Fig 4.16 (a) Susceptibility for varying D (b) Comparison of gap calculated by TMRG and DMRG (c) Specific Heat for varying D.

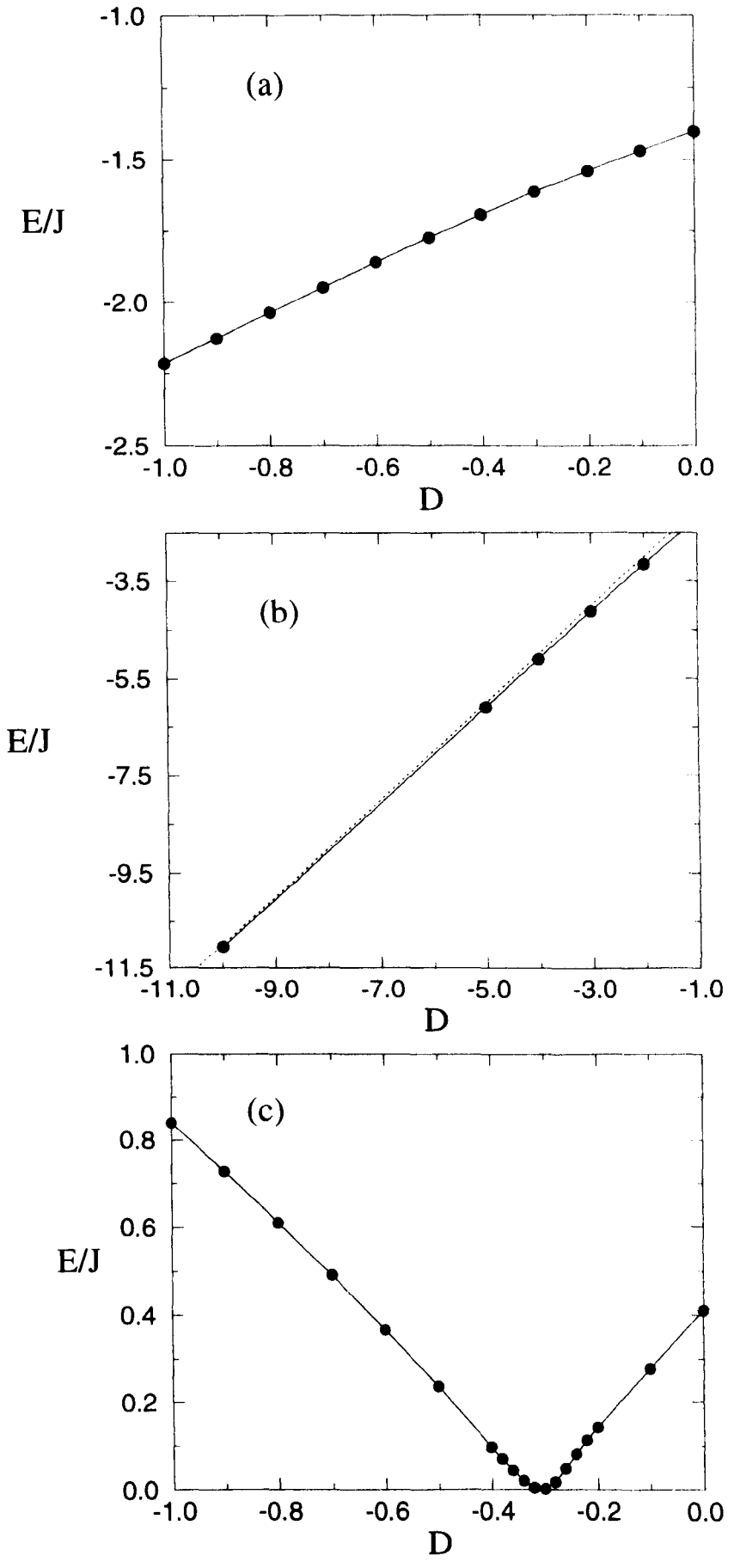

Fig 4.17 (a) and (b) Ground state energy and (c) energy gap for $D < 0$.

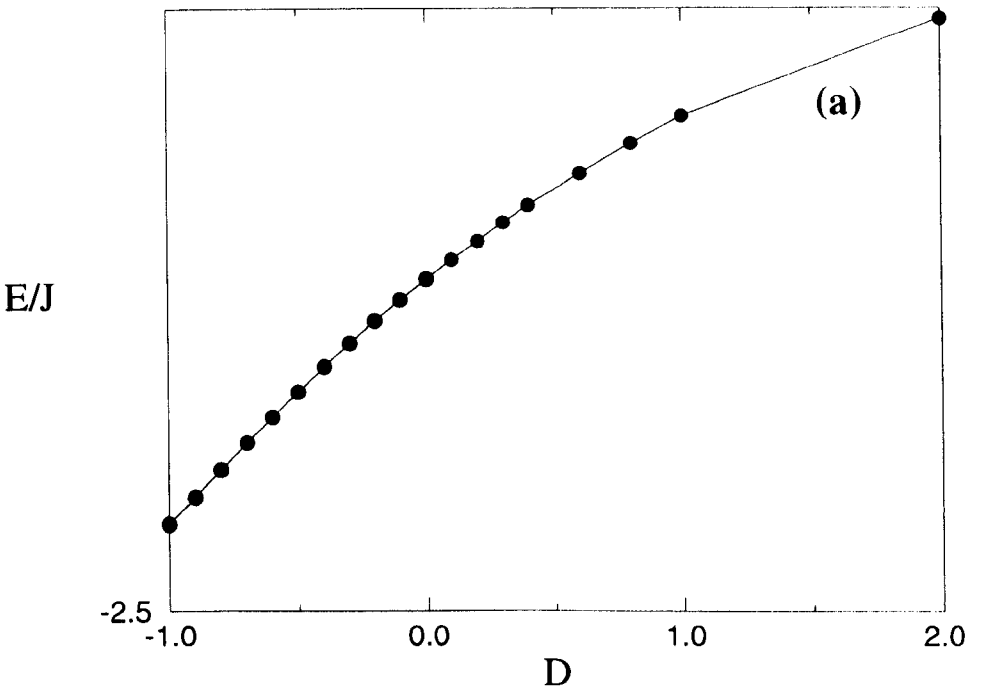

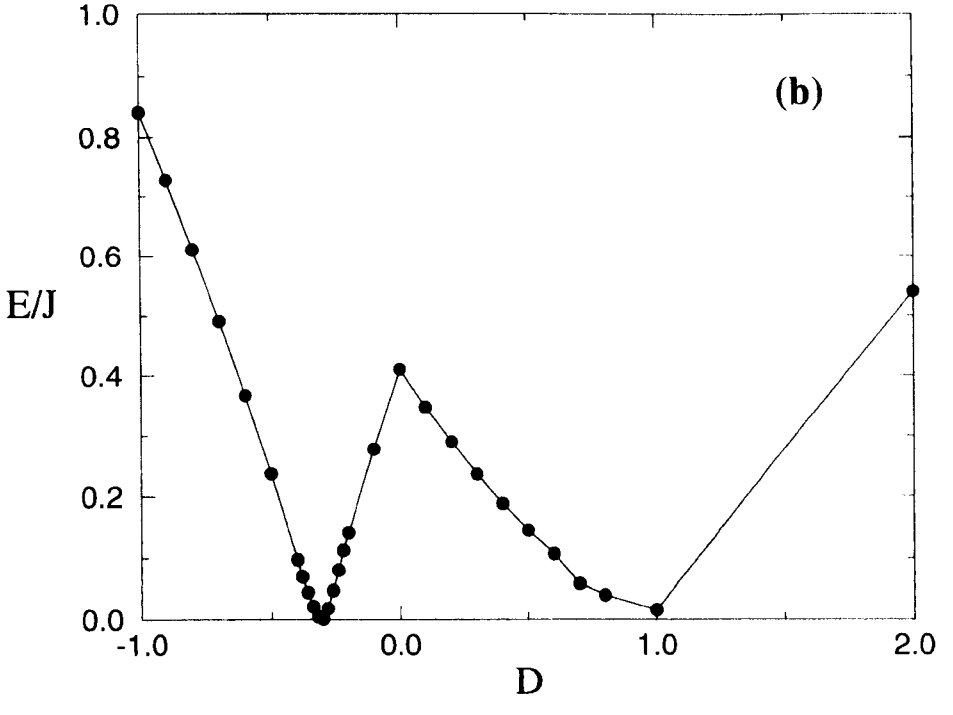

Fig 4.18 (a) Ground state energy and (b) energy gap for $-1 < D < 2$.

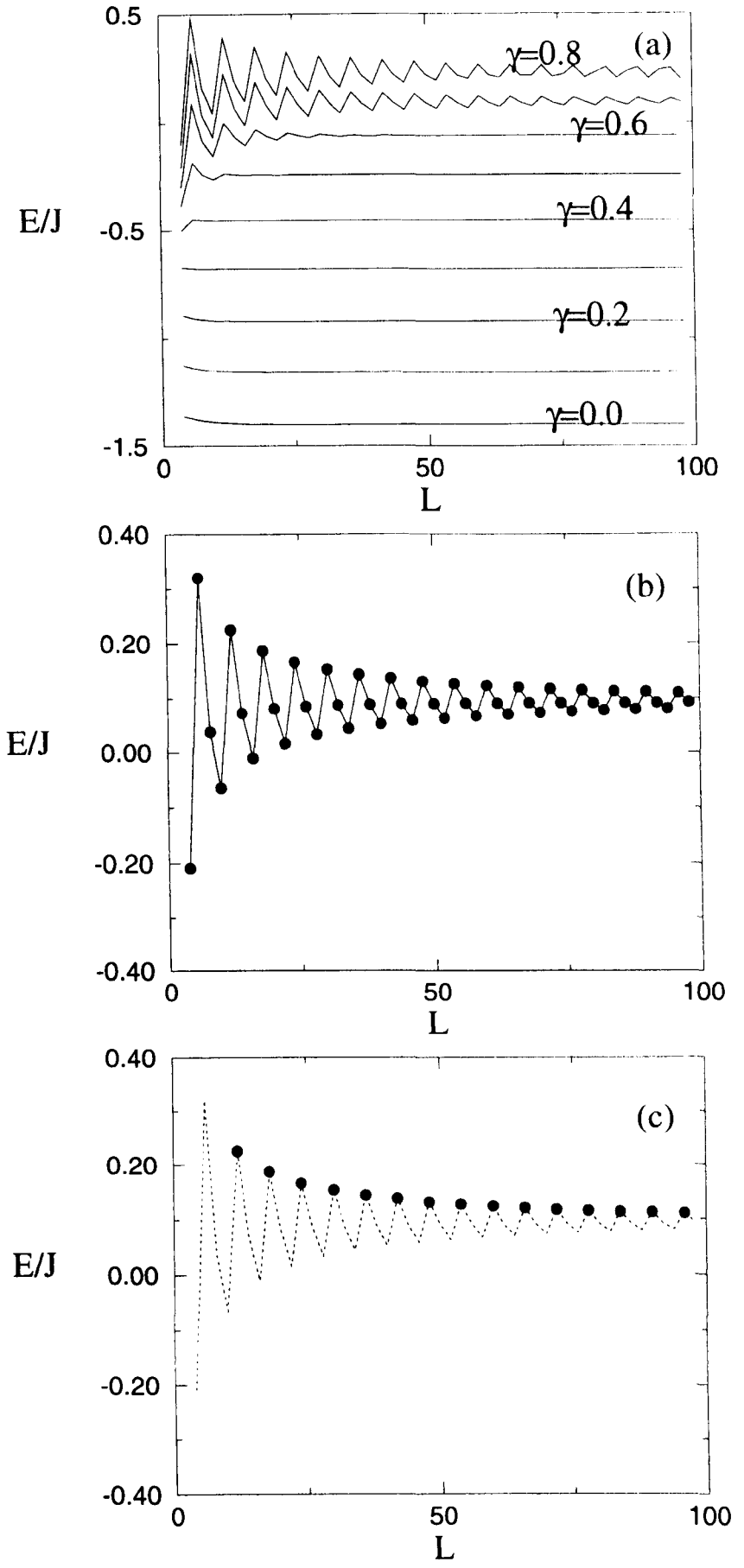

Fig 4.19 Ground state energy for (a) varying γ

(b) and (c) ground state for γ=0.6

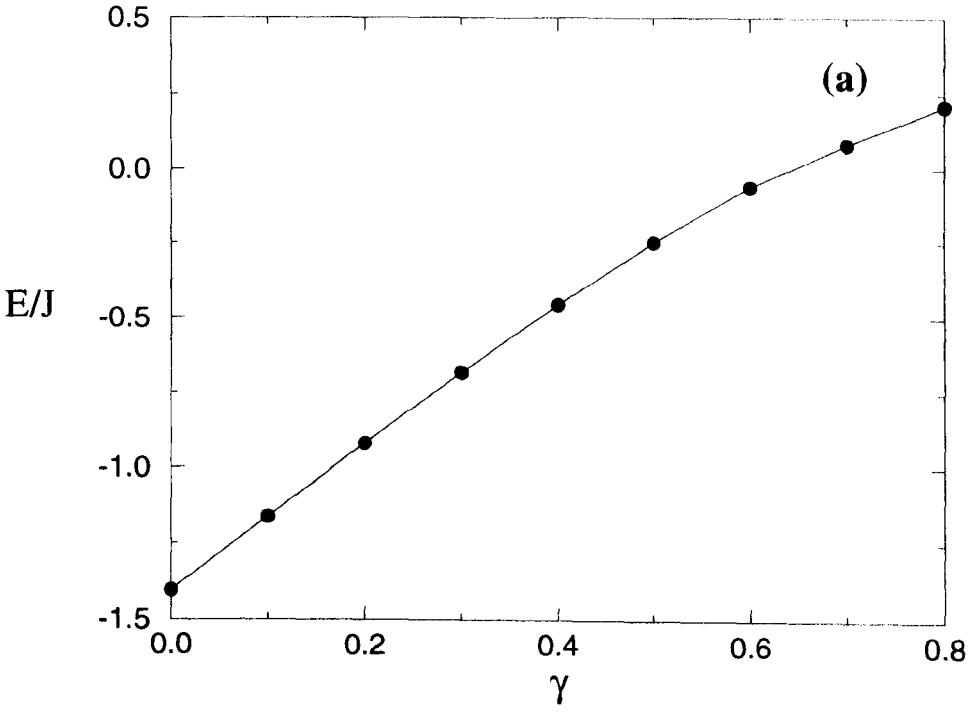

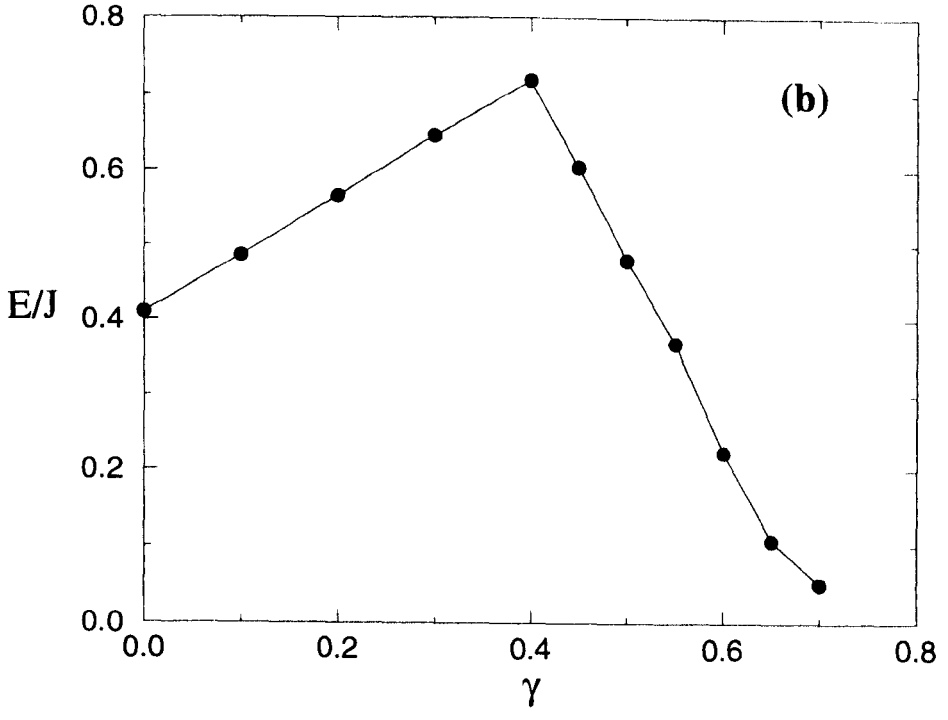

Fig 4.20 (a) Ground state energy and (b) energy gap for varying γ.

5. Electronic and Magnetic Properties of Mixed Valence Manganites.

The compounds $A_{1-x}B_xMnO_3$ (where A=La, Y, Pr, Nd and B=Ca, Sr, Ba, Pb) have been the subject of much attention due to the colossal negative magnetoresistance (CMR) [1] they exhibit. By this we mean the very large change in resistivity observed under application of a magnetic field. A great deal of theoretical and experimental effort has been made to understand the physical properties of these systems and to develop device applications [2].

In order to understand the magnetic properties of these compounds it is first necessary to consider their electronic structure. In the undoped parent compound (x=0), the manganese exists in the Mn^{3+} valence state. The octahedral symmetry of the ions causes the splitting of the *d*-band into the lower lying, triply degenerate t_{2g} orbitals and the higher, doubly degenerate e_g orbitals, each orbital being able to accommodate two electrons, one of each spin polarisation. There is also believed to be Jahn-Teller splitting of the e_g states. Due to Hund's rules, the four *d*-electrons are parallel and three occupy the t_{2g} state forming a core spin of $S = 3/2$ and one occupies the lower e_g orbital giving a total spin of $S = 2$. The lower e_g orbital effectively forms a filled conduction band and hence the compound is an insulator. A superexchange interaction causes antiferromagnetic (AF) alignment of the Mn ions as observed in neutron scattering experiments [2].

We now consider doping the compound with a divalent ion. The effect of this is to cause the manganese to exist in a mixed valent state, with a fraction x of the ions in the Mn^{4+} state and a fraction 1-x in the Mn^{3+}. The Mn^{4+} state is achieved by removing the e_g electron from the Mn^{3+}

ion. The net effect is therefore to dope the conduction band with holes at a concentration x. Now that the e_g band is not full, the electrons can become mobile. The effect of this electron mobility was extensively studied by Zener [3], de Gennes [4], Anderson and Hasegawa [5], and Kubo and Ohata [6]. Here we briefly review the main results of these investigations.

5.1 Double Exchange Ferromagnetism

We consider the case of a Mn^{3+} ion adjacent to a Mn^{4+} ion at an angle θ to each other where in figure 5.1 the solid arrows represent the core spin S = 3/2 and the open arrow the conduction electron spin of S =1/2.

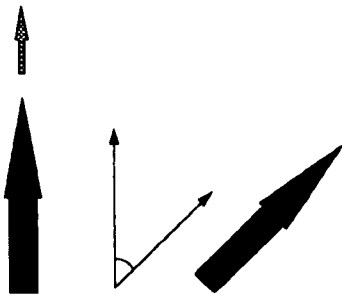

Figure 5.1

We now want to consider the process of hopping the conduction electron from one ion to another. Due to the on-site Hund's rule coupling, the electron must hop across into the e_g state parallel to the ion on the new site. We therefore need to be able to project an electron in an $\uparrow$ eigenstate in one basis onto an $\uparrow$ eigenstate in a basis rotated by θ. It was shown both classically [4] and quantum mechanically [5] that the transition matrix element for this process was of the form $t \sim \cos(\theta/2)$. This a maximum for $\theta = 0$ (parallel alignment of ions) and becomes zero for $\theta = \pi/2$ (antiparallel arrangement). The lowering of the kinetic energy due

to the mobility of the conduction electrons means that the hopping of the carrier mediates an effective ferromagnetic (FM) interaction between the ions, leading to competing AF/FM interactions. As the doping is increased above about x~0.1, the FM interaction dominates and the system is a so called 'Double Exchange Ferromagnet'. In this context, the CMR effects can be understood as applying a magnetic field will cause increased alignment of the ions and hence favour conduction. Above the Curie temperature, when the system is paramagnetic, the conduction obeys a thermally activated hopping behaviour.

Our work on these materials has been focused on two areas. One is the effect of correlations ~T_C and polaron formation, the other is the effect of an interface on the electronic and magnetic properties of the manganites with a view to investigating the feasibility of a particular device application being fabricated at Sheffield University.

5.2 Correlated Regions and Polaron Formation.

Above T_C there is evidence of short range magnetic order [7] and of course below T_C long range FM ordering occurs. We are interested in the growth of correlated magnetic regions as T_C is approached from above and the energy associated with them. The simplest correlated region is a pair of sites. We consider two sites, Mn^{3+} and Mn^{4+} with spins S=2 and S=3/2 respectively. The S=2 states may be written in terms of the core spin (3/2) and e_g spin (1/2) as follows:

$$|2;M\rangle = a_M|3/2;M-1/2\rangle|\uparrow\rangle + b_M|3/2;M+1/2\rangle|\downarrow\rangle \qquad (5.1)$$

The values of a_M and b_M are given below.

M	a_M	b_M
2	1	0
1	$\sqrt{3}/2$	$1/2$
0	$1/\sqrt{2}$	$1/\sqrt{2}$
-1	$1/2$	$\sqrt{3}/2$
-2	0	1

Thus when an electron is transferred off this site it will be left in state $|3/2; M - 1/2\rangle$ if the transfer was of an up spin electron and $|3/2; M + 1/2\rangle$ if a down spin electron was transferred.

The pair problem consists of sites S=3/2 and S=2 coupled in this way. The total spin of the pair may take values S_T = 7/2, 5/2, 3/2, 1/2 and these characterise the eigenstates. The values for the energies and degeneracies are shown below in terms of the hopping energy t_0. For reference the energy levels for a pair spins S=3/2 and S=2 coupled by a Heisenberg exchange interaction, $-J\mathbf{S}_1 \cdot \mathbf{S}_2$, is also given. It is seen that although the ordering of the energy states is the same the splittings between the states follow different patterns and there are also 'antibonding' states with positive energy in the polaron problem.

Total Spin	Degeneracy	Energy	Heisenberg Energy
7/2	8	$-t_0$	-3J
5/2	6	$-3t_0 / 4$	+J / 2
3/2	4	$-t_0 / 2$	+3J
1/2	2	$-t_0 / 4$	9J / 2
1/2	2	$t_0 / 4$	
3/2	4	$t_0 / 2$	
5/2	6	$3t_0 / 4$	
7/2	8	t_0	

This shows that there is a considerable lowering of energy if an e_g electron may delocalise between two Mn sites. This may account for the fact that an intermediate valence line is seen in the Mn NMR spectra over a wide range of concentrations [8].

This method may be extended to larger clusters. An obvious case to consider is that of a cluster of three sites consisting of two Mn^{3+} and one Mn^{4+} ions. This corresponds to the doping, x=1/3, which is required for optimum magnetoresistance. The state of lowest energy in this case corresponds to S_T = 11/2. The next step is to consider clusters of six sites containing four Mn^{3+} and two Mn^{4+} ions. We considered four arrangements, a loop, a starfish (five sites nearest neighbour of the central site) and a rectangle (six sites arranged in a block 2×3) and a cube of dimensions $3 \times 3 \times 3$ (figure 5.2). We treat only the case where the spins are fully aligned and so all the mobile electrons have the same spin. The system then becomes equivalent to a one spin band, non-interacting tight-binding model for which we calculate the one electron eigenstates and then fill up the lowest third to calculate the energy per hole. We have also considered the energy of the fully aligned lattice by a Monte Carlo *k*-space integration. The ground state energy per hole for these configurations is given in the table below and compared with that for the pair, the triple and a fully ordered lattice.

Number of sites	Number of holes	Cluster	Ground state energy per hole, E / t_0.
2	1	Pair	-1
3	1	Triple	-1.41
6	2	Starfish	-1.12

6	2	Loop	-1.5
6	2	Rectangle	-1.71
27	9	$3\times3\times3$	-2.20
Fermisea	33.3%	Cubic tight binding	-2.91

This demonstrates that the delocalisation of an e_g hole between a few Mn sites can lead to an energy lowering per hole which is a significant fraction of that achieved in the fully ordered state. This is achieved without significantly reducing the entropy and therefore without introducing a large positive entropic contribution to the free energy. This explains the large amount of short range magnetic order which is observed above T_c in these materials.

We will now consider the effect of correlated clusters on the paramagnetic susceptibility. If we have N ions in a crystal, each of spin S then the Curie paramagnetic susceptibility has the form

$$\chi_1 = \frac{Ng^2\mu_B^2 S(S+1)}{3k_B(T-T_C)} \tag{5.2}$$

whereas if we consider N ions arranged in correlated clusters each of m ions and with spin mS, then the susceptibility will be

$$\chi_m = \frac{\left(\frac{N}{m}\right)g^2\mu_B^2 mS(mS+1)}{3k_B(T-T_C)} \tag{5.3}$$

and we see that the effect of forming the clusters is that $\chi_m \approx m\chi_1$. This means that experimentally we may be able to see the formation of clusters as the temperature is lowered

towards T_C by plotting χ^{-1} as a function of temperature and look for changes in the gradient. This is what has been done by Amaral et al [9] and the predicted behaviour in the susceptibility is observed. They claim to see evidence for clusters of total S = 11, 22, 44 and 88 (corresponding to 6, 12, 24 and 48 sites containing 2, 4, 8, 16 holes respectively) at temperatures close to T_C. This is very strong evidence to suggest that our theory of small correlated cluster formation is a predominate mechanism in determining the magnetic order in these compounds.

5.3 Perturbation produced on manganites by a metallic interface

It would be highly desirable to be able to utilise the CMR effects exhibited by the mixed valent manganites in devices. However, the required field is usually prohibitively high (~5T). Being able to design device systems which require lower fields is therefore a technological priority. One possible method of inducing CMR at lower fields is to inject polarised electrons from a ferromagnet in to a manganite film and see if this induces ferromagnetic ordering in the film, hence changing the sample's conductivity. This has lead us to investigate the effect of a Ni interface on the electronic and magnetic properties of $La_{1-x}Ca_xMnO_3$ for x = 0.3

We have performed tight-binding calculations on an interface system consisting of $La_{1-x}CaMnO_3$ and Ni. We assume perfect epitaxy between the (100) surface of Ni and the simple cubic lattice formed by the Mn ions in the manganite. The basis states are the *d*-band electrons of Ni and the e_g electrons of Mn. The tight-binding parameters for Ni were obtained from reference [10], the Mn hopping parameter was fitted to give the correct band width in bulk

$La_{1-x}CaMnO_3$ [2] and the interface hopping was calculated using a root-mean-square interpolation [11].

We utilised the Haydock recursion scheme to calculate diagonal elements of the on site Green's function from which we have obtained the density of state for Mn e_g orbitals near the interface.

5.3.1 Haydock Recursion Scheme

The Haydock Recursion Scheme [12] (HRS) is mathematically equivalent to the Lanczos Method discussed in Appendix 1. It constructs a tridiagonal basis by repeated application of the Hamiltonian. However, the HRS is geared towards calculating local properties of the system which is done by choosing the initial state to be localised in the region of interest (generally a single orbital). Successive applications of the Hamiltonian on this state therefore produce linear combinations of 1st, 2nd 3rd etc. nearest neighbour orbitals. It is reasonable to expect that for systems with short range interactions and localised electron states, that the effect of these new states decreases with distance from the initial site. The Hamiltonian in the tridiagonal basis is used to construct the Greenian operator $(E-H)^{-1}$ in terms of the Lanczos parameters $\{a_i, b_i\}$. The diagonal element of this operator on the initial state can be written as a continued fraction of the form

$$G_0(E) = \cfrac{1}{E - a_1 - \cfrac{b_2^2}{E - a_2 - \cfrac{b_3^2}{E - a_3 - \cfrac{b_4^2}{E - a_4 - \cdots}}}} \tag{5.4}$$

By including an infinitesimal imaginary part to the energy $E \to E + i\delta$, we can use the property of Green functions that the density of states $\rho(E)$ is related to the Greens function by [13]

$$\rho(E) = \lim_{\delta \to 0} -\frac{1}{\pi} \mathrm{Im}\left[G_0(E + i\delta)\right] \tag{5.5}$$

In order to actually use this to make calculations we must be able to terminate the continued fraction expression for the Green's function. It can be shown that for a continuous band, the parameters a_i and b_i tend to a limit as $i \to \infty$. In this case, the continued fraction can be exactly terminated by a square-root termination.

Figures 5.3 and 5.4 shows the density of states for the Mn e_g band for the first three planes near to the interface for the two situations where the conduction band in the manganite is parallel to the majority or minority band of the Ni. The electron occupation on each site is shown in Figure 5.5. As can be seen, the occupation reaches it's bulk value of 0.7 electrons per site within ~5 lattice spacings.

The difference in integrated energy between the two spin situations gives a measure of the magnetic interaction between the two materials. Using this as an input parameter, mean field simulations have been carried out to estimate the magnetisation profile in the manganite as a function of distance from the interface. However, it was seen that the desired effect i.e. an enhanced magnetisation near the interface only penetrated about ten lattice planes into the manganite which would suggest that this may not be a suitable method for obtaining CMR at low applied fields.

5.4 References

[1] von Helmolt R, Wecker J, Holzapfel B, Schultz L and Samwer K, Phys. Rev. Lett., **71**, 2331 (1993)

[2] Coey J M D, Viret M and von Molnar S, *to be published*

[3] Zener C, Phys. Rev., **82,** 403 (1951)

[4] Anderson PW and Hasegawa H, Phys. Rev., **100**, 675 (1955)

[5] deGennes PG, Phys. Rev., **118,** 141 (1960)

[6] Kubo K and Ohata N, J. Phys. Soc. Japan, **33**, 21 (1972)

[7] De Teresa et al, Nature, **386**, 256 (1997)

[8] Kapusta_C, *to be published*

[9] Amaral et al, *to be published in J. Appl. Physics*

[10] Bonnelle C, Cyrot-Lackman F, Jonnard P, Julien J P, Mayou D and Vergand F, Physica Scripta, **38**, 100 (1988)

[11] Shiba H, Prog. Theor. Phys., **46**, 77 (1971)

[12] Haydock R, Solid State Physics, **35**, 216 (1980)

[13] Rickayzen G, "Green's Functions and Condensed Matter", Academic Press, London (1980)

triple

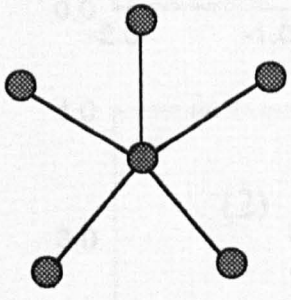

starfish

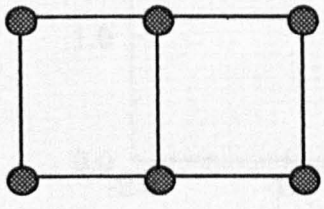

rectangle

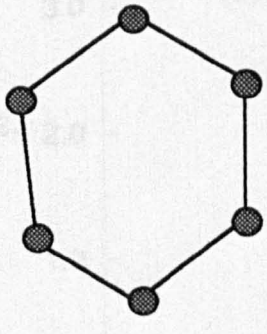

loop

Fig 5.2

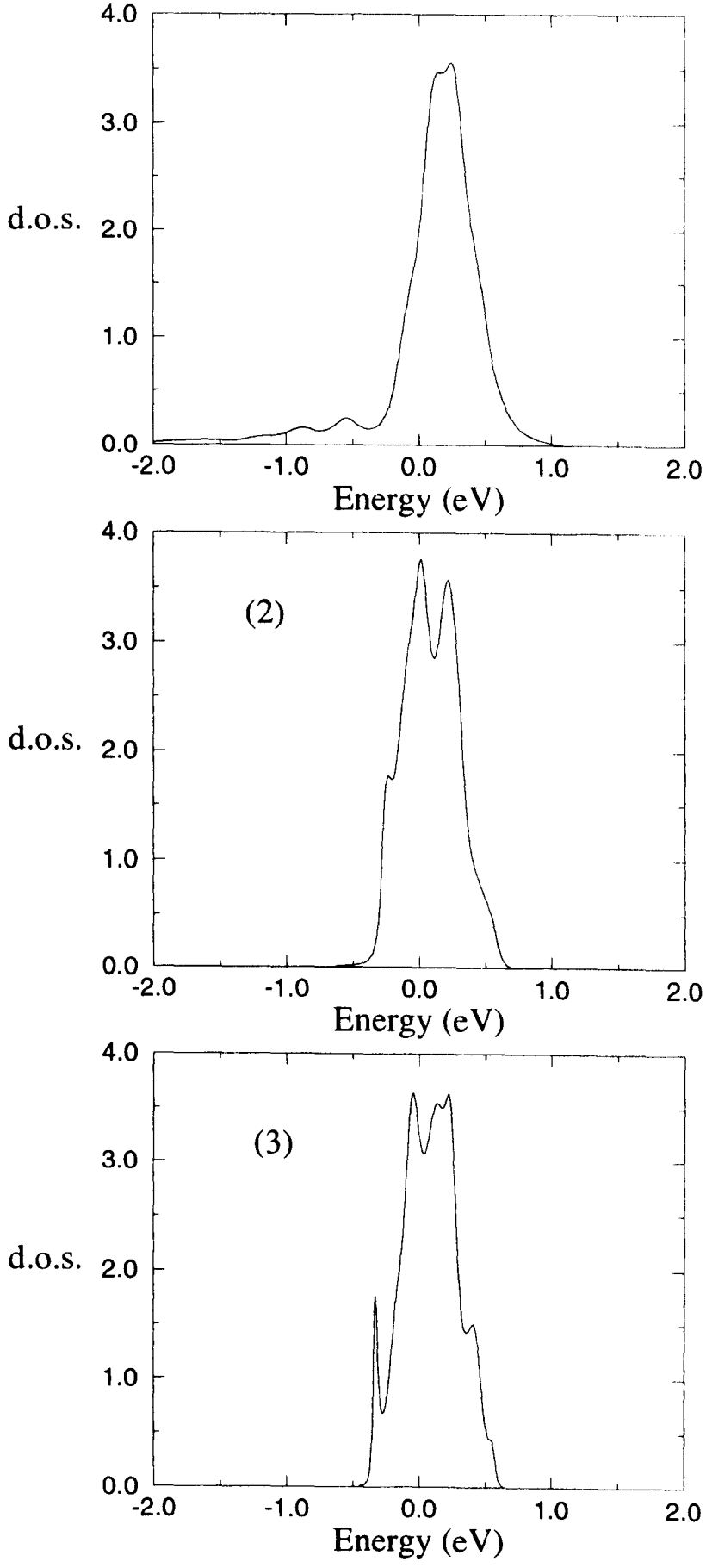

Fig 5.3 Local density of states for first three lattice planes away from interface for carriers parallel to Ni majority band

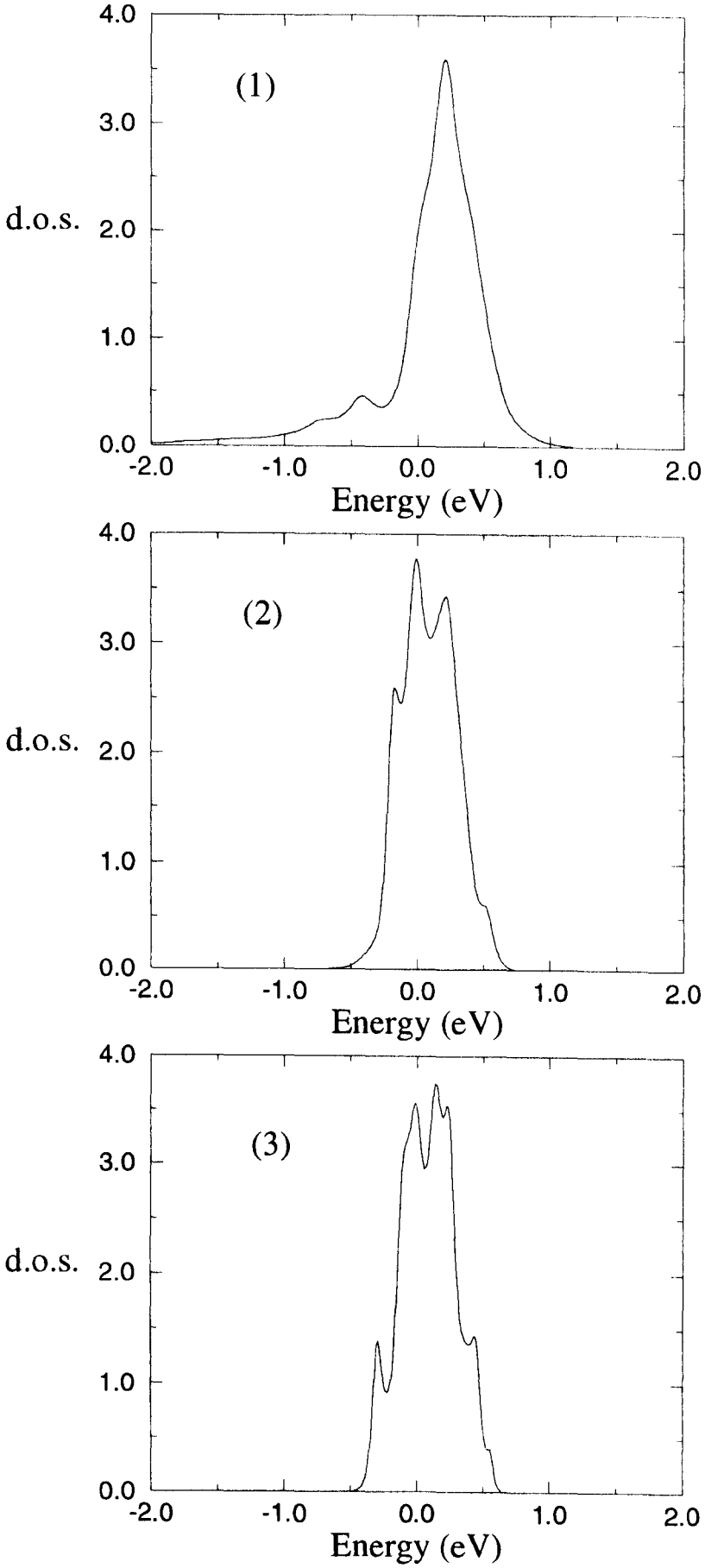

Fig 5.4 Local density of states for first three lattice planes away from interface for carriers parallel to Ni minority band

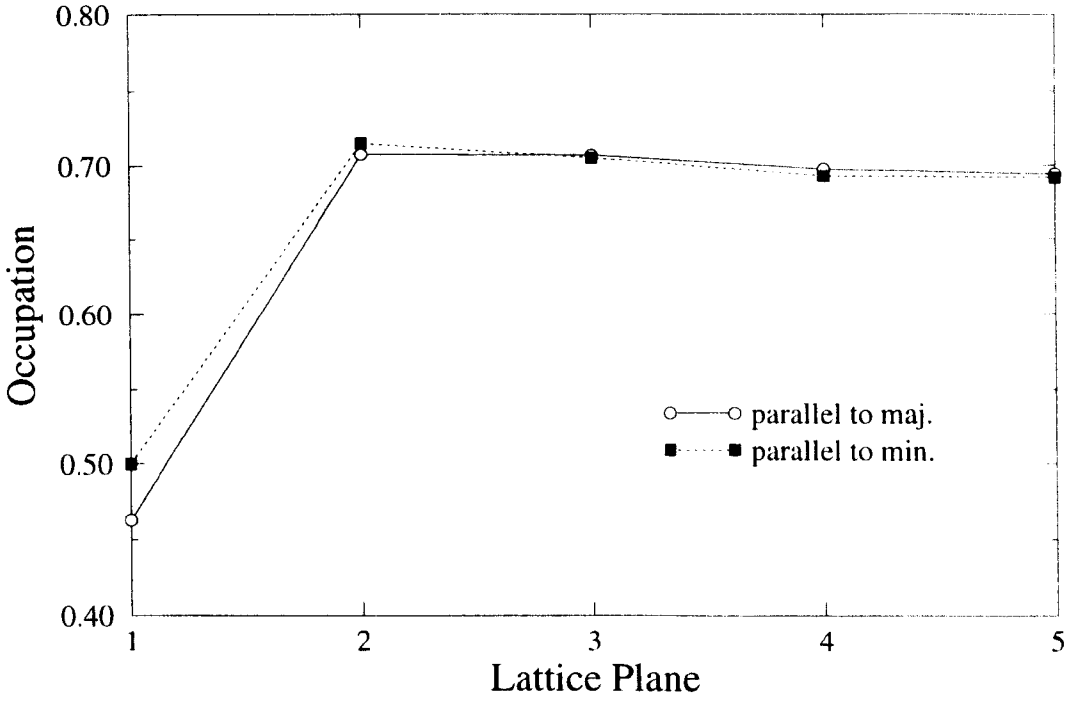

Fig 5.5 Occupation as a function of lattice plane for carriers parallel to majority and minority Ni bands.

Appendix 1 - Matrix Methods

When one wants to find the eigenvalues and eigenvectors of a matrix a number of methods are available, the choice of which will depend upon factors such as

a) How many eigenvalues/eigenvectors are required?

b) The size and sparsity of the matrix.

c) Are there any symmetries of the matrix which can be exploited?

If the whole matrix is to be diagonalised, then most methods rely on being able to cast the matrix into a particular form through a series of similarity transformations which is then easier to deal with. Examples of this are reduction of a symmetric matrix to tridiagonal form or of an asymmetric matrix to Hessenberg form. Alternatively, factorisation methods such as the QR and QL algorithms can be employed [1].

In condensed matter physics, we are often interested in extrema of a matrix's eigenvalue spectrum. This may be the ground state of some Hamiltonian or the maximum eigenvalue of a transfer matrix. In addition there may be certain symmetries of the system reflected in the form of the Hamiltonian which lead to the matrix being relatively sparse. We would like to exploit these facts and this we have done by using a number of sparse matrix algorithms in our DMRG and TMRG code.

The Lanczos Algorithm

The standard Lanczos algorithm [2] provides a method of transforming a Hamiltonian in some known basis, into a new basis in which it is tridiagonal. This is done by choosing a starting state $|\psi_1\rangle$ and repeatedly operating with the Hamiltonian, H, to generate new states which are linked by the recursion formula:

$$H|\psi_n\rangle = a_n|\psi_n\rangle + b_n|\psi_{n-1}\rangle + b_{n+1}|\psi_{n+1}\rangle \tag{A1.1}$$

where $b_1 = 0$ and $|\psi_{n-1}\rangle = 0$. This leads to a tridiagonal matrix of the form

$$\begin{pmatrix} a_1 & b_2 & 0 & 0 \\ b_2 & a_2 & b_3 & 0 \\ 0 & b_3 & a_3 & b_4 \\ 0 & 0 & b_4 & a_4 \end{pmatrix} \tag{A1.2}$$

If the rank of H is N, then N-1 applications of the formula generates a tridiagonal basis which completely spans the Hilbert space of the Hamiltonian. At each stage, however, the Lanczos algorithm provides a truncated basis and the lowest energy eigenvalue of H in this basis gives a variational approximation to the true ground state. The power of the Lanczos method lies in the fact that the approximation to the true ground state converges, generally, in much less than N iterations provided that the initial trial state has non-zero overlap with the true ground state. This is due to the repeated action of H on the trial state.

Modified Lanczos Algorithm

A modification of the above method, aimed specifically at finding the ground state energy alone, is the so called modified Lanczos algorithm [3]. In this method, a trial state $|\psi_1\rangle$ is

chosen, which is a first approximation to the true ground state of H, and is operated upon with H. In general this will give a component in the direction of $|\psi_1\rangle$ and a component orthogonal to it. We write this as

$$H|\psi_1\rangle = a_1|\psi_1\rangle + b_1|\psi_2\rangle \tag{A1.3}$$

Similarly we can write

$$H|\psi_2\rangle = a_2|\psi_2\rangle + b^*_1|\psi_1\rangle \tag{A1.4}$$

This give a 2×2 matrix representation of H in the space spanned by $|\psi_1\rangle$ and $|\psi_2\rangle$

$$H' = \begin{pmatrix} a_1 & b_1 \\ b^*_1 & a_2 \end{pmatrix} \tag{A1.5}$$

This matrix is easily diagonalised and its lower eigenvalue and eigenvector the new approximation to the ground state. This state then becomes the new trial state and replaces $|\psi_1\rangle$ in equation (A1.3). The process continues iteratively until the ground state is found to the required accuracy.

Conjugate Gradient Method

A related approach to finding the lowest eigenvalue and eigenvector of H is the conjugate gradient method [3]. Like the Modified Lanczos Method, the CG method creates successive approximations to the ground state, but uses extra information about the gradient of these vectors to choose a more direct sequence towards the true ground state. The CG method effectively lifts the orthogonality requirement of the MLM between successive states. It is this

method which we have found to be most reliable in converging quickly and accurately to the ground state.

Asymmetric Matrices

When dealing with the quantum transfer matrix as discussed in chapter 2, we are faced with the problem of finding the maximal eigenvalue of a large, sparse asymmetric matrix. One quite simple minded way of proceeding is the power method. This involves choosing a trial state $|\psi\rangle$ and by repeated action of the matrix we are studying, the trial state is transformed into the state with maximum eigenvalue. To see how this works consider the matrix T with right eigenvectors $|\phi_1\rangle,|\phi_2\rangle\cdots|\phi_N\rangle$ and corresponding eigenvalues $\lambda_1,\lambda_2\cdots\lambda_N$ such that $\lambda_1 > \lambda_2 > \cdots > \lambda_N$. Now consider the trial state $|\psi\rangle$ expanded in the eigenstates of T.

$$|\psi\rangle = \sum_i a_i|\phi_i\rangle \tag{A1.6}$$

Acting upon this state with T gives

$$T|\psi\rangle = \sum_i a_i\lambda_i|\phi_i\rangle \tag{A1.7}$$

We consider the effect of repeated action giving

$$T^M|\psi\rangle = \sum_i a_i\lambda_i^M|\phi_i\rangle = \lambda_1^M\left[a_1\phi_1 + \sum_{i=2}^{N} a_i\phi_i\frac{\lambda_i^M}{\lambda_1^M}\right] \tag{A1.8}$$

and

$$T^{M+1}|\psi\rangle = \sum_i a_i \lambda_i^{M+1} |\phi_i\rangle = \lambda_1^{M+1} \left[a_1 \phi_1 + \sum_{i=2}^{N} a_i \phi_i \frac{\lambda_i^{M+1}}{\lambda_1^{M+1}} \right] \qquad \text{(A1.9)}$$

Hence as M is increased, the ratio of the squared norm of successive states generated tends to λ_1^2 and the states tend towards $|\phi_1\rangle$. An analogous method is used to generate the left eigenvector.

Arnoldi Algorithm

A generalisation of the Lanczos algorithm to asymmetric matrices was made by Arnoldi [4]. This is a much more complicated method to understand ands to program. As a consequence of this we have made use of commercially available 'black box' routines supplied in the ARPACK library [5], which is available as a shareware package. This provides a comprehensive set of reliable routines for various matrix operations. Reference [6] gives a detailed review of the theory behind Arnoldi methods and their computational implementation.

References

[1] Press W H, Flannery B P, Teukolsky S A and Vetterling W T, "Numerical Recipes: The Art of Scientific Computing", Cambridge University Press, New York (1986)

[2] Lanczos C, Res. Nat. Bur. Stand., **45**, 255 (1950)

[3] Nightingale M P, Viswanath V S and Muller G, Phys. Rev. B, **48**, 7696 (1993)

[4] Arnoldi W E, Quart. J. Applied Mathematics, **9**, 17 (1951)

[5] http://www.caam.rice.edu/software/ARPACK/

[6] Lehoucq R, "Analysis and Implementation of an Implicitly Restarted Arnoldi Iteration", Ph.D Thesis, (1995)

Appendix 2: Fitting Procedures

In order to compare our theoretical susceptibility and specific heat curves to those of experiment we have to determine how the parameters in our calculations correspond to real quantities. Considering first the susceptibility, we will use the alternating chain Heisenberg Hamiltonian as an example given by

$$H = \sum_{i=1}^{N/2} \left(\mathbf{S}_{2i-1} \cdot \mathbf{S}_{2i} + \alpha \mathbf{S}_{2i} \cdot \mathbf{S}_{2i+1} \right) + h \sum_{i=1}^{N} S_i^z \tag{A2.1}$$

where we have set the exchange integral J equal to 1. The theoretical susceptibility we have calculated is given by

$$\chi_{th} = \langle s^z \rangle / h \tag{A2.2}$$

We now need to compare this with the Hamiltonian of the real system which is given by

$$H = \sum_{i=1}^{N/2} J \left(\mathbf{S}_{2i-1} \cdot \mathbf{S}_{2i} + \alpha \mathbf{S}_{2i} \cdot \mathbf{S}_{2i+1} \right) + g\mu_B B \sum_{i=1}^{N} S_i^z \tag{A2.3}$$

which we write as

$$H = J\{ \sum_{i=1}^{N/2} \left(\mathbf{S}_{2i-1} \cdot \mathbf{S}_{2i} + \alpha \mathbf{S}_{2i} \cdot \mathbf{S}_{2i+1} \right) + \frac{g\mu_B B}{J} \sum_{i=1}^{N} S_i^z \ \} \tag{A2.4}$$

We therefore identify our parameter h as representing $\frac{g\mu_B B}{J}$. In MKS units the volume susceptibility is given by

$$\chi_{MKS} = \frac{M}{H} \tag{A2.5}$$

where M is the magnetic moment per unit volume. If N is the number of magnetic ions per unit volume then we can write

$$\chi_{MKS} = \frac{Ng\mu_B \langle s^z \rangle \mu_0}{B} = \frac{\mu_0 N g^2 \mu_B^2 \chi_{th}}{J} \tag{A2.6}$$

where all the quantities are in MKS units. We can express the mass susceptibility in terms of the volume susceptibility by dividing by the density

$$\chi_{MKS}^{mass} = \frac{\mu_0 N g^2 \mu_B^2 \chi_{th}}{\rho J} \tag{A2.7}$$

which we can write in terms of Avogadro's number N_A and the mass of one mole of the particular compound we are considering, W as

$$\chi_{MKS}^{mass} = \frac{\mu_0 N_A g^2 \mu_B^2 \chi_{th}}{WJ} \tag{A2.8}$$

Many magnetic measurements are expressed in terms of emu units. We can make the conversion by dividing by $4\pi \times 10^{-3}$, where the 10^{-3} takes into account the different mass units in the two systems [1]. We can therefore now write

$$\chi_{emu}^{mass} = \frac{10^{-4} N_A g^2 \mu_B^2 \chi_{th}}{WJ} \tag{A2.9}$$

The temperature which is measured in units of T/J must also be rescaled to correspond the true experimental temperature. This expression can now be used to compare our results with those of experiment.

In the case of the specific heat, we consider the above Hamiltonian without the field term. If J is the real exchange energy, the calculated internal energy E and the experimental internal energy E^* are related by $E^* = JE$, while the theoretical temperature $T$and the experimental temperature are related by $T^* = JT$. Hence, the experimental specific heat $\partial E^*/\partial T^*$ is related to the theoretical value, $\partial E/\partial T$ by

$$\frac{\partial E^*}{\partial T^*} = \frac{\partial E^*}{\partial E}\frac{\partial E}{\partial T}\frac{\partial T}{\partial T^*} = J\frac{\partial E}{\partial T}\frac{1}{J} = \frac{\partial E}{\partial T} \tag{A2.10}$$

Hence the specific is the same of that of the theoretical model with the temperature rescaled.

References

[1] Bleaney B I and Bleaney B, "Electricity and Magnetism", Oxford University Press, London (1965)

Appendix 3: Implementation of Spin Symmetries.

In this appendix I will explain the implementation of the spin symmetries used in the DMRG and TMRG calculations. All the Hamiltonians considered conserve the value of the component of spin in the direction of the axis of quantisation (taken to be the Z-axis), that is $\left[H, S^z\right] = 0$. In addition S^2 is also conserved, however we did not utilise this symmetry. This means that the action of the Hamiltonian on a state with a particular value of S^z will in general be a linear combination of states also with the same value of S^z. The consequence of this is that the Hamiltonian matrix may be block diagonalised according to this quantum number. The transfer matrix is block diagonalised according to pseudo-spin as described in chapter 3. The block diagonalisation greatly speeds up the application of sparse matrix eigenvalue/vector calculation.

In the calculations we have carried out, the values of S^z for each superblock and system and environment block states are stored as integer numbers of spin quanta. The density matrix is also block diagonal in S^z if it is constructed from a single target state or from a combination of target states originating from the same symmetry sector. Although the density matrix diagonalisation takes only a small fraction of the time of the calculation as a whole, I will now demonstrate why it is necessary to block diagonalise it and calculate the eigenstates of each block separately when targeting the singlet ground state wavefunction.

Consider a density matrix eigenstate having z-component of spin σ and eigenvalue ε. We will denote this state by $|\sigma\rangle$ and the following equation are satisfied

$$\rho|\sigma\rangle = \varepsilon|\sigma\rangle$$

$$S^z|\sigma\rangle = \sigma|\sigma\rangle$$

However, in the absence of a magnetic field this state will be degenerate with a state with all the spins reversed i.e. $\sigma \rightarrow -\sigma$. We denote this state by $|-\sigma\rangle$ and the following equations are satisfied

$$\rho|-\sigma\rangle = \varepsilon|-\sigma\rangle$$

$$S^z|-\sigma\rangle = -\sigma|\sigma\rangle$$

If we do not block diagonalise ρ before we calculate its eigenspectrum, then a typical diagonalisation method will have no reason to differentiate between these two eigenstates and will in general produce some linear combination of them as an eigenstate

$$|\phi\rangle = a|\sigma\rangle + b|-\sigma\rangle$$

It is clear that $|\phi\rangle$ is not an eigenstate of S^z and hence our system of labelling states according to integer numbers of spin quanta is destroyed. For this reason the density matrix was always block diagonalised before the eigenstates were determined.